Alma Mater Studiorum – Università di Bologna

DOTTORATO DI RICERCA IN SCIENZE CHIMICHE

Ciclo XXI

Settore scientifico disciplinari di afferenza: CHIM/03

MACROMOLECULAR CRYSTALLOGRAPHY: CRYSTALLISATION AND STRUCTURAL DETERMINATION.

Presentata da: Dr.ssa Giovanna Tosi

Coordinatore Dottorato

Chiar.mo Prof. Giuliano Longoni

Relatore

Chiar.mo Prof. Norberto Roveri

Co-relatore

Dott.ssa Simona Fermani

Bologna 2009

ABSTRACT

Macromolecular Crystallography: Crystallisation and Structural Determination.

This thesis explores the protein crystallography in its crucial steps: from the crystallisation process to the resolution of the crystalline structure. The first chapter is a general introduction to macromolecular crystallography and crystallisation processes of, the parameters affecting it, are described with together the most used crystallisation techniques. The following three chapters report the research themes object of this PhD thesis to three themes strongly correlated to the crystallography of biological macromolecules: (1) The design and developing of engineered surfaces and tools to favor the crystallisation of biological macromolecules; (2) The three-dimensional structure determination of toxins belonging to the RIPs family to be able to correlate their molecular structures to the biological activities; (3) The structural characterisation of adducts between model proteins and platinum-based anticancer drugs or, generally, metal ions.

1. The success of structural analyses of biological macromolecules by X-ray crystallography depends on the availability of suitable single crystals. The second chapter illustrates the research on functionalised surfaces as protein nucleator. To crystallise model proteins, we have used two functionalised surfaces exposing ionisable groups: sulphonated polystyrene films and silanised mica. The results showed that for some proteins, those functionalised surfaces decreased the median waiting time and the starting protein concentration necessary to obtain crystals, with respect to the siliconised glass cover slips (reference) (Tosi *et al.*, 2008).
In order to compare the effect of the different surfaces, experiments must be done under similar conditions. We have tested the functionalised surfaces with together a modified essicator, the Crystallisation Mushroom (Triana S&T), to perform vapour diffusion experiments that allows the equilibration of more than 12 drops against a unique reservoir. Also in this case, the obtained results highlight the influence of ionisable groups, linked to the surfaces, on the nucleation and growth of protein crystals, confirming that functionalised surfaces decrease the nucleation induction-time with respect to the siliconised glass cover slips (Tosi *et al*., submitted).

2. In the third chapter, the crystallisation studies on several toxins belonging to the family of RIPs (Ribosome Inactivating Proteins) are presented. In particular, the results obtained for two of them,

bouganin and lychnin, are discussed. The resolution of the three-dimensional structure of those two RIPs has allowed to compare them with other known RIPs (Fermani *et al.*, submitted). It is showed that he overall structure of bouganin and lychnin is similar to the other considered RIPs and the typical RIP fold is conserved. The superimpositioning of their C_α atoms highlights some differences in the N-terminal and C-terminal domains. The studies of their structures has been carried out in parallel to the study of their adenine polynucleotide glycosylase activity and the comparison. It has been hypothesised that two conditions are needed to be present at the same time in a RIP to guarantee an efficient interaction with the substrate and an efficient catalysis. They are a negative electrostatic surface potential at the active site and several exposed positively charged residues in the region around that site.

3. The fourth chapter explores the interactions between model proteins and platinum-based anticancer drugs or, generally, metal ions. The study of Pt-protein adducts is important both for drug's activity and undesired side effects. The characterisation of protein-cisplatin adducts can give valuable information for designing new and better anticancer drugs and possibly overcome cisplatin resistance. As model of study, four proteins have been chosen: human ubiquitin and superoxide dismutase (SOD) for their biological relevance and their full characterisation in the native state, while Hah1 and CopC because they are proteins naturally involved in copper homeostasis and responsible for platinum drugs transport. Crystals of protein and cisplatin or other metal ions such as Cd, Cu, Hg, and Zn have been prepared by co-crystallisation or soaking of already formed native crystals. The crystallographic structures of ubiquitin with Cd, Zn, or Hg have confirmed that the protein has highly affinity for metal ions and have revealed which residues have greater propensity to bind metal ions and, likely, also cisplatin (Falini *et al.*, 2008).

Keywords:

Protein crystallisation, heterogeneous nucleation, functionalised surfaces, crystallisation mushroom, RIPs (Ribosome Inactivating Proteins), Bouganin, Lychnin, metal-protein adducts, cisplatin, Ubiquitin.

REFERENCE

- Falini, G., Fermani, S., Tosi, G., Arnesano, F., Natile, G. Structural probing of Zn(II), Cd(II) and Hg(II) binding to human ubiquitin. (2008) *Chem. Commun.*, 5960-5962.
- Fermani, F., Tosi, G., Farini, V., Polito, L., Falini, G., Ripamonti, A., Barbieri, L., Chambery, A., Bolognesi, A. Structure/function studies on two type 1 ribosome inactivating proteins: bouganin and lychnin. (2009) *J. Struct. Biol.* Submitted.
- Tosi, G., Fermani, S., Falini, G., Gavira Gallardo, J.A., Garcia Ruiz, J.M. Crystallisation of proteins on functionalised surfaces. (2008) *Acta Cryst. D* **64(10)**, 1054-1061.
- Tosi, G., Fermani, S., Falini, G., Gavira Gallardo, J.A., Garcia Ruiz, J.M. "Merging strategies in proteins crystallisation: functionalised surfaces in the crystallisation mushroom". (2009) *Cryst. Growth Des.* Submitted.

INDEX

CHAPTER 1: THE PROTEIN CRYSTALLISATION

CHAPTER 2: HETEROGENEOUS CRYSTALLISATION

CHAPTER 1: THE PROTEIN CRYSTALLISATION

1.1 INTRODUCTION

The first protein crystals were grown from haemoglobin over 150 years ago in a laboratory in Germany and this was immediately recognised as an exceptional and valuable discovery. Their appearance signified purity, uniqueness and a connection between the living and the inanimate world from which life emerged (though evolution was not suspected). Since then protein crystals have evolved from objects of wonder, speculation and demonstration of molecular purity to essential intermediates in the discovery of macromolecular structure. Parallely, methods of crystallisation developed as well from empirical, trial and error approaches to the more rational, direct and physically characterised concepts of the past several years.

The success of Human Genomics and the need of rational drug design have substantially accelerated protein structure investigations. Completion of the Human Genome Project offers the possibility to identify a host of genetic disorders and design therapies to treat them. Genes encode proteins, which are the targets of drugs. The function of proteins is determined by their three-dimensional structure; thus, a detailed knowledge of protein structure becomes essential to develop therapeutic treatments and engineer proteins with improved properties. If the active site structure of a salient enzyme in a metabolic or regulatory pathway is known, then chemical compounds, such as drugs, can be rationally designed to inhibit or otherwise affect the behaviour of that enzyme.

The secret of life is hidden in the structure of proteins and in the 1930s it was become to perceive that the technique, that would be able to unlock it, was X-ray crystallography. The work that firmly and finally established the value of protein crystallisation came with the early experiments of Crowfoot, Bernal and Fankuchen who applied X-ray diffraction to protein crystals.

Max Perutz, the giant of the age, made indelible the extraordinary powder of X-ray crystallography through his classic investigation of haemoglobin crystals (Fig. 1). No technological advance has so revolutionised a field as X-ray crystallography has molecular and structural biology.

Indeed, with X-ray crystallography it has been possible to study macromolecular assemblies as large as a nucleosome (Luger *et al.*, 1997), viruses (Kim *et al.*, 1989) or ribosome (Yonath *et al.*, 1980); while NMR application, despite having the advantage of being performed in solution, is limited to the study of proteins and polypeptides with molecular weight lower than 30 kDa. On the other hand, X-ray crystallography is totally dependent on the need for highly quality diffraction crystals and the obtainment of such crystals is the rate-limiting step to structure determination. The

crystal becomes the keystone element of the entire process and the ultimate determinant of its success. The quality of the final structural image is directly determined by the perfection, size and physical properties of the crystalline specimen. To obtain good structural data, crystals need to be single and have dimension of at least 10 μm^3, preferably much larger (Chayen, 2004). It is said amongst crystallographers that crystallisation is an art, crystallography a science.

Figure 1. Max Perutz (left) with his model of haemoglobin and John Kendrew (right) with his model of myoglobin.

1.2 THE CRYSTALLISATION PROCESS

Although comparable in their morphologies and appearance, there are substantial differences between crystals of low-molecular-mass compounds and crystals of proteins and nucleic acids. Crystals of conventional molecules are characterised by firm lattice forces, are relatively highly ordered, generally physically hard and brittle, easy to manipulate, can be usually exposed to air, have strong optical properties and diffract X-rays intensely. Macromolecular crystals are by comparison usually more limited in size, very soft and crush easily, disintegrate if allowed to dehydrate, exhibit weak optical properties and diffract X-rays poorly (McPherson, 2004). They are temperature sensitive and undergo extensive damage after prolonged exposure to radiation. The extent of the diffraction pattern from a crystal is directly correlate with its degree of internal order. The most vast the pattern, or the higher the resolution to which it extends, the more structurally uniform the molecules are in the crystal and the more precise their periodic arrangement is. The level of detail to which atomic positions can be determined by crystal structure analysis corresponds closely with the degree of crystalline order. Protein crystals contain very high solvent content (20-70%) of the cell volume. The crystal can be considered as an ordered gel with big interstitial spaces through which the solvent and other small molecules can freely diffuse. This contributes in producing weak interactions and destabilising the crystal lattice. The interaction involved in the crystal packing can be specific (hydrogen bonds, electrostatic interactions and Van der Walls interactions) or non-specific (hydrophobic interactions).

Crystallisation is a phase transition phenomenon involving different steps: nucleation, nuclei growth and cessation of growth (Kam *et al.*, 1978). Nucleation is the key of crystallisation and it can be homogeneous in the bulk of the solution, or heterogeneous, which is caused by a foreign agent to the crystallisation solution (Chayen *et al.*, 2008). Nucleation is the most difficult problem to address theoretically and experimentally because it represents a first order phase transition by which molecules pass from a wholly disordered state to an ordered one. Presumably this occurs through the formation of partially ordered or paracrystalline intermediates (McPherson, 2004). During the nucleation phase ordered nuclei are formed in solution as result of fluctuation of matter. Nuclei which exceed the critical size start to growth. The crystallisation of macromolecules in solution is a process influenced by the physical-chemical properties of the solvent, the solute and the solute-solvent interaction. It requires that a supersaturated state is achieved.

The crystallisation process can be illustrated by a phase diagram, which indicates the stable state (liquid, crystalline or amorphous solid, i.e. precipitate) under a variety of crystallisation parameters (Fig. 2). The saturation limit line separate the undersaturated from the saturated region. Crystals

dissolve in the undersaturated region, where the protein concentration in solution is below the protein solubility curve, while they can grow in the saturated region. In principle, crystals will grow from an aqueous protein solution when the solution is brought into supersaturation and the protein concentration exceeds the solubility. In practice, crystals hardly form unless the concentration exceeds the solubility by a factor of at least three (Asherie, 2004). The large supersaturation is required to overcome the activation energy barrier that represents the free energy required to create the small microcluster of proteins, known as a nucleus, from which the crystal will eventually grow (Fig. 3). The crystallisation of molecules from solution is an equilibrium phenomenon and the specific kinetic and thermodynamic parameters depend on the chemical and physical properties of the solvent and solute involved. Under condition of supersaturation the system is driven toward an equilibrium state in which the solute is partitioned between a soluble and solid phase. Although the individual molecules lose rotational and translational freedom, thereby lowering the entropy of the system, they, at the same time, form many new, stable bonds which maximise the number of attractive interactions and minimise those dispersive or repulsive. This reduces the potential or free energy of the system and provides the driving force for the ordering process. The impetus for macromolecules to crystallise is the minimisation of free energy that occurs when the number of attractive interactions are maximised and the dispersive or repulsive interactions are minimised. For biological macromolecules, which exist predominantly in an aqueous environment, one free energy minimum is represented when they are fully solvated. In extremely concentrated solutions in which there is insufficient water to maintain hydration, the molecules may crystallise or they may aggregate as an amorphous precipitate. The supersaturation region can be divided in three zones: metastabile, labile and precipitation zone. In the labile zone the supersaturation is large enough that spontaneous nucleation is observable. If the supersaturation is too large, then disordered structures (such as aggregates, spherulites or precipitates) may form. An amorphous precipitate corresponds to one local energy minimum and frequently occurs when aggregation proceeds too rapidly. If the energy minimum is sufficiently deep, the molecules remain in that state. The precipitation zone is unfavourable for crystal formation, however, occasionally the energy barrier is small and, waiting for sufficient time, crystals may grow from the amorphous material. In the metastabile zone crystals can growth but being the supersaturation too small, no nuclei can form for any period of time.

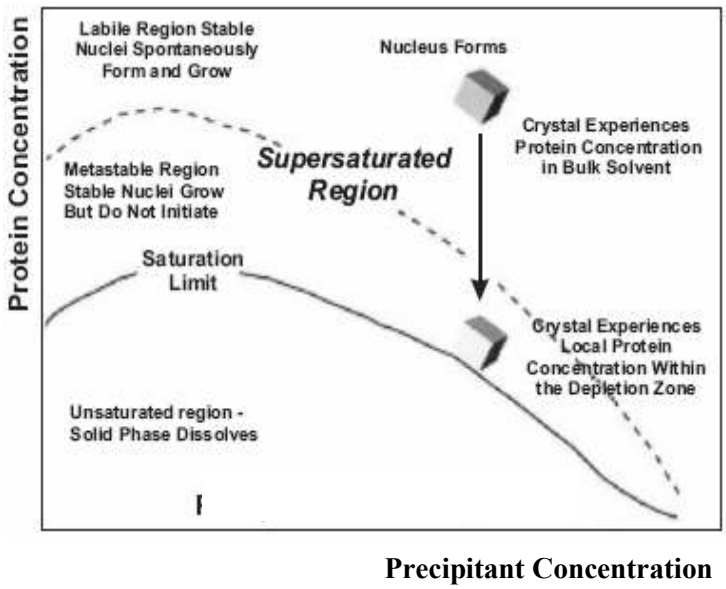

Figure 2. Schematic phase diagrams showing the solubility of a protein as a function of the concentration of the precipitant and the protein present in solution.

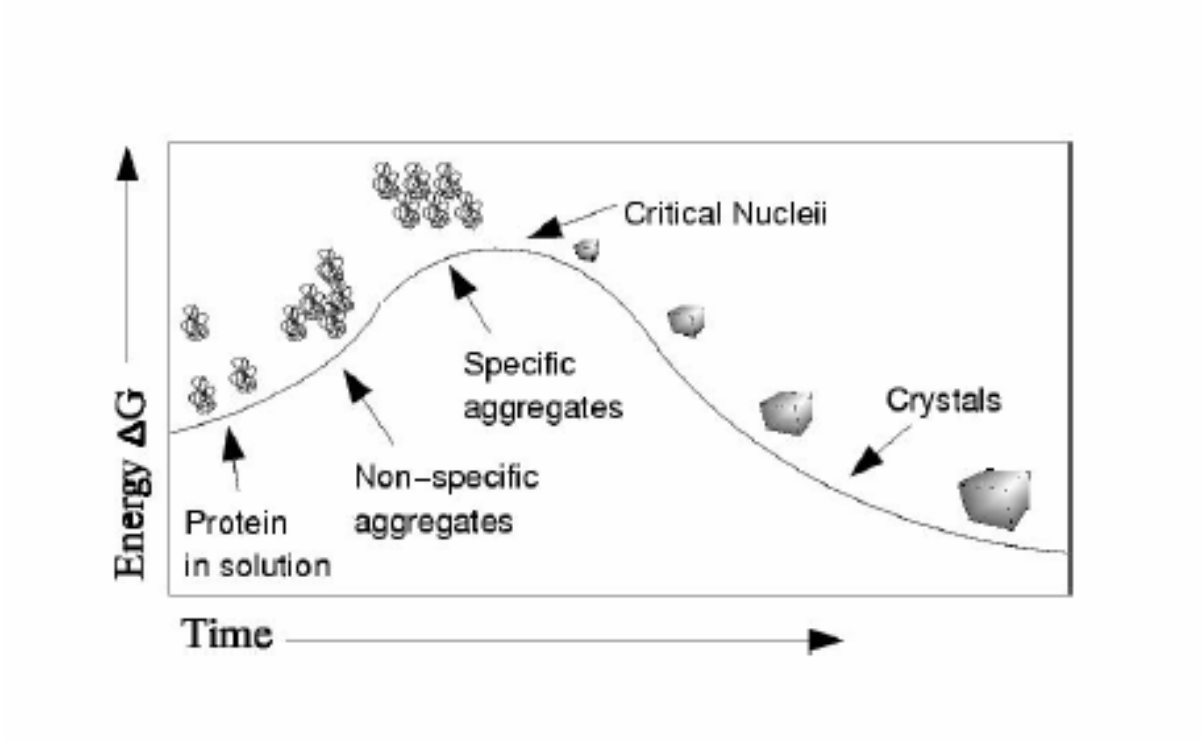

Figure 3. Schematic phase diagram showing the free-energy profile during the crystallisation process.

In an ideal experiment, once nuclei have formed, the concentration of protein in the solute will drop, thereby leading the system from the labile into the metastable zone, where few crystals will grow. More often, either no crystals forms at all or excess nucleation occurs, whereby numerous clusters of tiny crystals are formed instead of a few sizeable ones. An additional frustrating problem is the formation of large single crystals that do not diffract.

To induce macromolecular crystallisation and obtain crystals of high quality suitable for X-ray diffraction, it is necessary to bring the system very slowly toward a state of minimum solubility and thus achieve a limited degree of supersaturation by varying the concentration of precipitant, protein and additives, pH, temperature and other parameters (Table 1). It is well known that protein crystal formation requires interactions that are selective, highly directional and arranged in geometry that is appropriate for producing three-dimensional (or in some cases two dimensional) crystal lattice. If the transformation process from the liquid to the solid state proceeds too fast, the molecules have no time to order themselves properly.

The protein crystallisation process is influenced by a large number of factors (Table 1) but far the most important is the property of the protein sample. Important requirements for a successful crystallisation are purity, homogeneity and stability. The higher the purity, the easier the crystallisation is. Even at 100% of chemical purity, the molecules can exist in different conformation states or in interchange between two or more conformational equilibrium states, that interfere with the formation of a highly ordered crystal (Durbin *et al.*, 1996). The protein should usually be at least 97% pure to guarantee sufficient homogeneity of the sample. The failure to achieve crystals, the growth of poor diffracting crystals or low reproducibility usually suggest the impurity. Possible sources of impurity include:

- variation in primary structure (genetic)
- post-translation modifications (glycosylation)
- variation in secondary structure (misfolding, denaturation)
- variation in tertiary structure (conformers, dynamic changes)
- variation in quaternary structure (mixed oligomeric states)
- partial binding of ligands or ions
- mixed oxidation states of Cys residues, ligands or metals
- fragmentation (proteolysis).

The solubility in a generic solution of a molecule of any type depends on the interactions of the molecule with the solvent molecules.

There are hydrophobic and hydrophilic amino acids in protein molecules. After protein folding in aqueous solution, hydrophobic amino acids usually form unexposed hydrophobic areas while

hydrophilic amino acid interact with the surrounding solvent molecules through hydrogen bonds. If a sufficient portion of the protein surface is hydrophilic, the protein can be dissolved in aqueous solutions. The protein solubility strongly depends on the ionic strength: at very low ionic strength a phenomenon called "salting in" takes place, i.e. in the presence of small amount of electrolyte proteins are more soluble then in pure water because of the interactions between the charged residues and the ions. The "salting in" effect does not depend on the nature of ions, but only on the ionic concentration. As the ionic strength is increased the protein solubility raises to a maximum and then decreases when the ionic concentration is such that the ions begin to compete with the solute (protein) for the surrounding water. The salt ions are more easily hydrated than macromolecules. This causes the removal of ions essential to satisfy the electrostatic requirements of protein molecules, which will try to balance their charge through interactions among themselves. Proteins molecules start to interact and aggregate. This process is known as "salting out". Different ions will affect the solubility of the protein in different ways. Small highly charged ions are more effective than large low charged ions in salting out.

Along with ionic strength, pH is one of the most important variables influencing the solubility of proteins

The solubility minimum corresponds to the isoelectric point of the protein, at which the net surface charge is zero and the solubility drops down. Below the isoelectric point proteins carry a net positive charge, above it a net negative charge. The isoelectric point is of significance in protein purification because it is the pH at which mobility in an electrofocusing system is zero (and therefore the point at which the protein will accumulate).

Also the distribution of the charges, the dipole moment of the protein, its conformation and in many cases its aggregation state depend on the pH. The pH is also the most useful variable to investigate the growth of polymorph crystals with different habits or unit cell.

The precipitant agents play an important role during the crystallisation process. They can be divided in four categories based on their mechanisms for promoting crystallisation: (1) salt, (2) organic solvents, (3) long chain polymers and (4) low molecular weight polymers and non-volatile organic compounds (Table 2) (McPherson, 2004).

Table 1. Parameters affecting the proteins crystallisation process.

1- Ionic strength
2- pH and buffer
3- Concentration and nature of precipitant
4- Temperature and temperature fluctuations
5- Concentration of macromolecule
6- Purity of macromolecules
7- Additives, effectors and ligands
8- Organism source of macromolecule
9- Substrates, coenzymes, inhibitors
10- Reducing or oxidising environment
11- Metal and other specific ions
12- Equilibration and growth rate
13- Surfactants or detergents
14-Gravity convection and sedimentation
15- Vibrations and sound
16- Volume of crystallisation sample
17- Presence of amorphous or particulate sample
18- Surfaces of crystallisation vessels
19- Proteolysis
20- Contaminations by microbes
21- Pressure
22- Electric and magnetic fields
23- Handling by investigator and cleanliness
24- Viscosity and mother liquor
25- Heterogeneous or epitaxial nucleating agents

Salts influence the solubility of a protein through the salting out effect. Organic solvents bind water to themselves just as salt ions do and also significantly reduce the dielectric constant of the medium. The first of these effects decreases the capacity of the system to fully solvate the macromolecules while the second one reduces the effective electrostatic shielding between individual macromolecules. Ethanol is the most commonly used precipitant but acetone is often advantageous as it is somewhat milder. However, the high volatility of these solvents makes them difficult to handle and less volatile solvents, which are miscible with water, are preferable. Amongst these, 2-methyl-2,4-pentanediol (MPD) has proved useful. MPD is a small polyalcohol which has properties midway between those of low molecular weight PEGs and organic solvents. MPD works as a precipitant by a combination of effects, including competition for water, hydrophobic exclusion of protein solutes, lowering of the solution's dielectric constant, and detergent-like effects. It is generally used in excess or in a concentration of 40% (v/v).

Organic solvents often denature proteins and this should be minimized by working at low temperature. Polymers such as polyethylene glycols are very efficient and, unlike proteins, have no

consistent conformation, writhe and twist randomly in solution, occupy more space than they otherwise deserve. This results in less solvent available space for the other macromolecules which then segregate, aggregate, and ultimately form a solid phase, often crystals. Many protein structures have been solved using crystals grown from polyethylene glycols. Because of the larger molecular weight, polyethylene glycols probably do not even enter the crystals and therefore do not directly contact the interior molecules. Solutions of polyethylene glycols have mean electron densities roughly equivalent to water and do not generally interact in a deleterious manner with heavy atom compounds, thus making them particularly well suited for macromolecular crystallisation. PEG's with molecular weights less than 1000 are typically liquids and are generally used at concentrations above 40% v/v. PEG's with molecular weights above 1000 are generally solids and are used in the 5-50% w/v concentration range. All PEG solutions should be made with the inclusion of ~0.l% Na azide (which, incidentally, is also highly toxic to humans) to prevent bacterial growth. PEG sizes from MW=400 to 20,000 Da are used but the most useful are the ones in the range of 2000-8000Da.

Table 2. Precipitant used in macromolecular crystallisation.

Salts	Volatile organic solvents	Polymers	Non-Volatile organic solvents
Ammonium phosphate sulphate	Ethanol	Poly(ethylene glycol) 1000, 1450, 3350, 4000, 6000, 8000, 20.000	2-Methyl-2,4-pentanediol
Lithium sulphate	Propanol and isopropanol	Polyamine	2,5-Hexandediol
Sodium or ammonium citrate	1,3-Propanediol	Jeffamine T, Jeffamine M	Ethylene glycol 400
Sodium or potassium phosphate	Methanol		
Sodium or potassium or ammonium chloride	Dioxane		
Sodium or ammonium acetate	Acetone		
Magnesium or calcium sulphate	Butanol		
Calcium chloride	Acetonitrile		
Ammonium or sodium nitrate	Dimethyl sulfoxide		
Sodium or magnesium formate			
Sodium or potassium tartrate			
Cadmium sulphate			

Most proteins vary in solubility as a function of temperature, and some are very sensitive. The dielectric constant decreases with increase of temperature and the entropy terms in the free energy of solution tend to dominate the enthalpy terms. Temperature coefficient of solubility varies from protein to protein and with the condition such as ionic strength and the presence of organic solvents. Crystallisation experiments are usually carried out at 4 °C or room temperature (25 °C). Several protein will denaturate at temperatures above 40 °C so temperature can be varied over only a

limited region (i.e. 0-40 °C) (Wiencek, 1999). Low temperatures tend to limit degradation problems as well as bacterial growth. The solubility of proteins in salt solutions tends to increase at low temperatures, whereas in PEG and MPD solutions, protein solubility generally decreases with decreasing temperature. By increasing or decreasing precipitant or protein concentration, crystallisation should, at least in theory, be possible at either room temperature or 4 °C, although the kinetics of crystallisation can be expected to vary in accord with temperature.

The protein concentration should be as high as possible. Crystals have been reported grown at concentrations from one to several hundred milligrams per millilitre, although the most common range seems to be from 5 to 30 mg/mL.

Other parameters may be less important but often play crucial roles. It can not be predicted which variables may be of importance for a particular macromolecule. The methodology employed to find the experimental conditions that will lead a protein to crystallise is a strict empirical "trial and error" procedure. Once the crystallisation conditions have been identified, the second step involves their optimisation. This process refines the chemical and physical parameters identified during screening to produce crystals of as higher as possible quality that are suitable for X-ray analysis. Optimisation builds directly upon the success of the screening experiments. In the first step of optimisation the initial crystallisation conditions are taken and the concentration of the macromolecule or precipitant, or pH, or the growth temperature are varied.

One of the paradoxes in crystallisation is that the optimal solution conditions for nucleation of the crystals are not the ideal ones to support their subsequent growth. This is because spontaneous nucleation is quite simply more likely to occur when the levels of supersaturation are high, whereas slow, ordered growth of large crystals is favoured by lower levels. The ideal experiment therefore must somehow uncouple nucleation from growth to satisfy the distinctly different requirements of the two events. Seeding (See page 25) is only one of many possible optimisation methods. Some alternatives to separate nucleation from growth, or to slow down the growth after nucleation has occurred, are presented in Table 3 (Bergfords, 2003).

Table 3. Easy optimisation strategies.

Method	Comments	Reference
Filter the protein	It removes dust, precipitated protein, particles that could be unintentional nucleation sites	Blow *et al.* (1994)
Cover the reservoir with oil (vapour diffusion)	It slows the rate of equilibration	Chayen *et al.* (1997)
Evaporative dialysis	Useful for proteins with a narrow metastable zone	Bunick *et al.* (2000)
Temperature shifts	It can work for proteins that exhibit temperature-sensitive solubility	Blow *et al.* (1994)
"Backing off" (vapour diffusion)	After nucleation has occurred, the cover slip is moved to a different reservoir for equilibration at metastable conditions	Saridakis *et al.* (2000)

1.3 CRYSTALLISATION TECHNIQUES

The methods used in macromolecular crystal-growth are continually being refined. Here the most used microtechniques which have been developed for use with small amounts of protein will be reported.

1. <u>MICROBATCH METHOD</u>: This is the classical method described for early enzyme crystallisation (Blundel *et al.*, 1976). The primary disadvantage of this method is the relatively large amount of material required and the difficulty in modifying conditions once vials are prepared. For this reason, since 1972 with the crystallisation of phycocyanin, the batch method has been adapted to the use of microliter quantities of material (Dobler *et al.*, 1972). The micro-batch method is a variation of the simple batch crystallisation technique, in which the concentrated protein solution is mixed with concentrated precipitant in a closed vessel to produce a final supersaturated condition, which may eventually lead to crystallisation. The components are at their final concentration at the start of experiment. The objective of microbatch technique is to reduce the consumption of sample by generating crystallisation trials in very small volumes (Chayen, 1998). The protein is dissolved at low ionic strength so as to have a highly concentrated solution. The precipitating agent (salt or organic solvent) is then added to bring the solution to a state of low supersaturation. The protein sample and precipitant solution are dispensed into the well of a plate and the well is covered with paraffin oil or low-density oil to prevent evaporation, contamination and physical shock (Fig. 4). During the incubation period, the concentration of a precipitant agent remains constant since evaporation is limited and, therefore, the volume of the drop remains the same during the experiment. On the other hand, the concentration of the protein changes on formation of either crystals or amorphous precipitant. If the concentration of precipitant agent is chosen in such a way that the solution is in an undersaturated state, crystallisation will never occur. On the other hand, a turbidity or opalescence in the solution probably indicates that the point of low supersaturation has been passed. Nevertheless quite often an amorphous precipitate will redisolve and crystals will slowly form. This technique was used very successfully for the production of large crystals of lysozyme, ribonuclease and enzymes of the trypsin family, but it offers very few possibilities of crystal growth control. The main disadvantage of this method is that the equilibration occurs very rapidly, thus affecting the rate of crystal growth and consequently the quality of the obtained crystals. It is only useful for proteins whose nucleation and growth velocities are extremely low even at high supersaturation or for those ones which give well ordered crystals at even high growth rates. The second disadvantage is that the manipulation of the crystals from the drop covered by oil

is very difficult. However, since the use of very small volumes of protein solution can be made, the micro-batch technique is quite useful as an initial screening method.

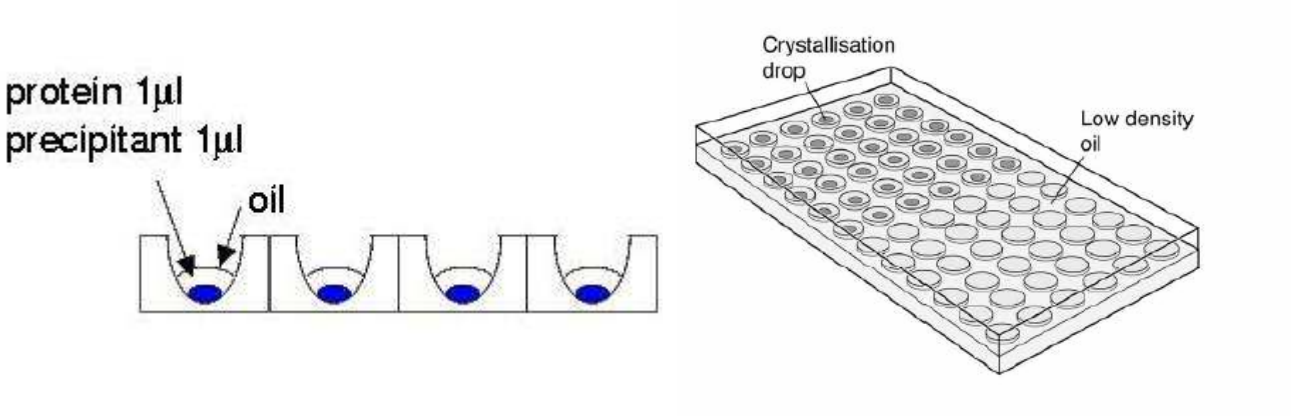

Figure 4. Microbatch method: A small drop of the sample combined with the crystallisation reagent is pipetted under a layer of oil**.**

2. <u>VAPOR DIFFUSION</u>: This method uses the evaporation and diffusion of water between solutions of different concentrations as a means of approaching and achieving supersaturation of protein macromolecules. Different techniques based on the same principle can be used (Fig. 5):

- hanging drop
- sitting drop
-sandwich drop.

Simply, the hanging drop method differs from the sitting drop method for the geometry of the system. It is important to mention that both methods require a closed system. The system must be sealed off from the outside using an airtight container or high-vacuum grease between glass surfaces. In sandwich drop method, the sample solution mixed with the precipitant is placed in the middle of two siliconized glass cover slides.

Typically, in vapour diffusion experiments the protein solution is mixed in a 1:1 ratio with a solution containing the precipitant agent at the concentration that needs to be achieved after vapour equilibration has occurred. The drop is then suspended and sealed over the well solution, which contains the precipitant solution at the target concentration, as either a hanging or sitting drop. The difference in precipitant concentration between the drop and the well solution is the driving force which causes water to evaporate from the drop until the concentration of the precipitant in the drop equals that of the well solution. Since the volume of the well solution is much larger than that of the drop (1-3 ml as compared to 1 - 15 µl), its dilution by water vapour leaving the drop is insignificant.

The volume of a hanging drop is limited to about 8 - 10 μl, since bigger volumes might cause the drop to fall out of the cover slip. This limitation is overcome in the sitting drop technique in which the drop sits on a pedestal (e.g. microbridge) above the reservoir solution. In the hanging drop technique the microdroplet is suspended from the underside of a microscope cover slip which is then placed over a small well containing the precipitating solution (Fig. 5). The cover slips must be thoroughly and carefully coated with nonwetting silicone to ensure proper drop formation and prevent spreading (McPherson, 1982).

During a vapour-diffusion experiment, the protein will start to concentrate from an unsaturated state to reach a supersaturated state. As the first crystals appear, the concentration of protein will decrease. The crystal will then grow until the concentration of the protein in the drop reaches the solubility curve.

Vapour-diffusion is the optimal technique for screening a large number of conditions. Furthermore, this method can be used to increase or decrease the concentration of protein in the equilibrated state, varying the ratio between protein and well solutions when the drop is initially set up.

In the case of salt precipitating and non volatile organic solvents as MPD and PEG, the droplet of mother liquor must initially contain precipitant at a concentration lower than that one of the reservoir. The equilibrium occurs by distilling water out of the droplet and into the reservoir. In case of volatile organic precipitants, nothing has to be added initially to the droplet, as the distillation and equilibration proceed in the opposite direction.

The rate of vapour-diffusion can also be controlled, to a certain extent; it greatly depends on the surface area of the drop. By reducing the surface area it is possible to slow the equilibration process dramatically. This can be achieved by means of the so-called 'sandwich drop' technique. A major advantage of the vapour diffusion method is the possibility of affecting the equilibrium rate of the trials and thus approaches the saturation more slowly, by varying the distance between the drop and the reservoir (Luft *et al.*, 1994; Luft *at al.*, 1996). The larger the distance which separate them, the slower the droplet equilibrates with the reservoir. The variation of the equilibrium rate with the distance droplet-reservoir is not linear. The rate is more sensitive to variations in the droplet-reservoir separation at short distance.

A further advantage of the vapour diffusion method is the possibility of altering the composition and/or the concentration of the components in the trial without touching the drop, by concentrating or diluting the reservoir (Yonath *et al.*, 1982; Pryzbylska, M., 1989) or just transferring the cover slip with the drop from one reservoir to another (Chayen *et al.*, 1989). A combination between the microbatch and water vapour diffusion methods is accomplished by placing a layer of a low density oil or a mixture of oils on the reservoir solution which will act as a barrier through which the vapour

phase will diffuse slowly (Chayen *et al.*, 1997). The type of oil and the thickness of the oil layer situated above the reservoir will dictate the rate of vapour diffusion and consequently the speed of crystallisation. This can reduce the number of grown crystals and increase their size.

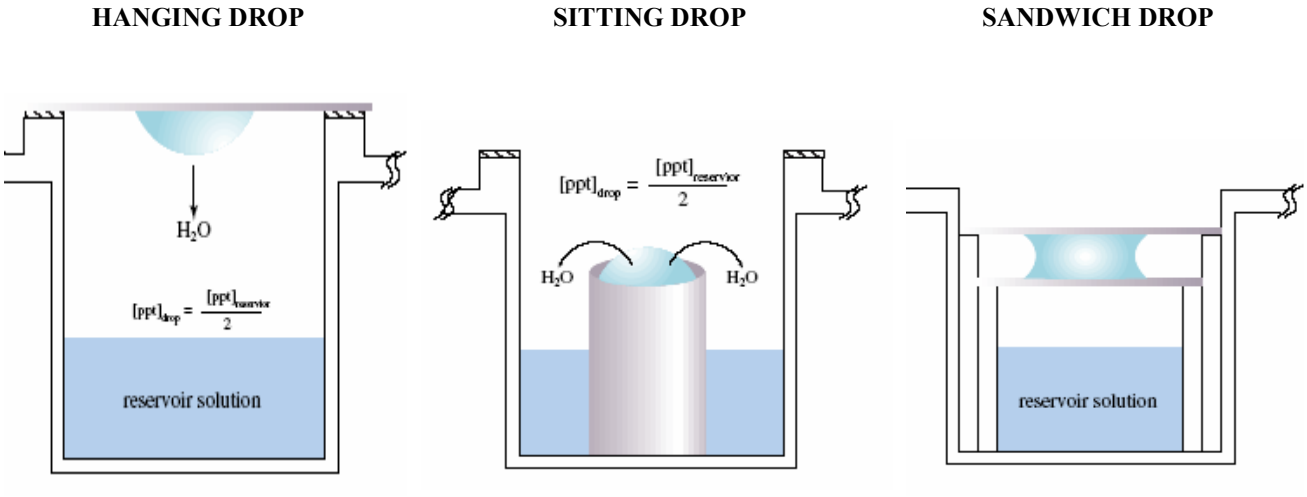

Figure 5. Vapour diffusion method: In hanging drop technique, the drops is suspended over the well solution (left), in sitting drop technique it sits on a pedestal (center), in sandwich drop technique it is placed in the middle of two siliconized glass cover (right).

3. <u>DYALISIS METHOD</u>: This technique was first described by Theorell (1932) and used in the crystallisation of haemoglobin (Boyes-Watson *et al.*, 1947). Dialysis techniques utilise diffusion and equilibration of small precipitant molecules through a semipermeable membrane as a means of slowly approaching the concentration at which the macromolecule solute crystallises. Initially, the protein solution is contained within the dialysis membrane, which is then equilibrated against a precipitant solution. Equilibration against the precipitant in the surrounding solvent slowly achieves supersaturation for the solute within the dialysis membrane, eventually resulting in crystallisation. A dialysis membrane can be used to cover the opening of a dialysis button, allowing diffusion of the surrounding solvent into the solute through the dialysis membrane (Fig. 6). Dialysis buttons themselves come in a variety of sizes from 7 µl to 200 µl. The protein solution at the start of the dialysis experiment is in an undersaturated state. The concentration of the precipitant agent slowly increases as its diffusion through the membrane takes place.

The advantage of dialysis over other methods is that the precipitating solution can be varied, simply by moving the entire dialysis button or sack from one condition to another. Thus, the protein

solution can be continuously recycled until the correct conditions for crystallisation are found. This technique has been adapted to small amounts of material becoming a microtechnique in which no more than 5-50 µl are used in each trial. The microdialysis method first used in the crystallisation of alcohol dehydrogenase has been introduced by Zeppeneuer (Zeppeneuer *et al.*, 1967; Zeppeneuer *et al.*, 1968; Zeppeneuer *et al.*, 1971). Samples of protein or nucleic acid solution are injected into glass short capillaries or tubes (McPherson, 1982). The capillaries have a piece of dialysis membrane stretched over one end that is held in place by a collar of PVC or surgical rubber tubing cut so as to provide support legs as well. The other end is sealed by a plug of dental wax or simply with a piece of parafilm. The entire system is then submerged in a test tube or other vessel containing the solution. Slow equilibration takes place across the membrane and crystallisation frequently occurs.

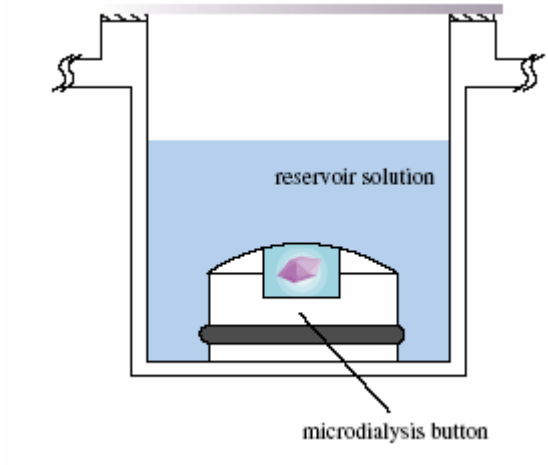

Figure 6. Dialysis method: The protein is placed in a Dialysis Button which is sealed with a dialysis membrane and placed into a suitable container holding the precipitant or crystallisation media.

4. <u>BULK CRYSTALLISATION METHOD</u>: A solid salt or a saturated solution of the salt is added to the solution containing the purified protein or nucleic acid until a visible opalescence is developed. Two of the first animal proteins crystallised, ovalbumin (Hopkins *et al*., 1898) and horse serum albumin (McMeekin *et al*., 1939) were obtained by this method. The solution is then centrifuged and the supernatant is stored for few days or weeks. Highly concentrated protein solutions (in a range from 10 to 100 mg/mL) are essential.

5. <u>FREE INTERFACE DIFFUSION</u>: If a macromolecule is differently soluble in two solvents and if one solution containing the dissolved sample can be layered carefully atop the other, transient conditions of supersaturation will be established in the region of the interface (Fig.7). As the two layers diffuse into one another toward equilibrium, nuclei are formed. This technique has been adapted to milligram quantities of starting material using small glass capillary (Salemme *et al.*, 1972; Weber *at al.*, 1970). With this method applicable to either salt solutions or organic solvents, it is recommended that the protein or nucleic solutions are highly concentrated (50 mg/mL) and great care is taken to eliminate dust and debris from the system. The concentration of the precipitant solution has to be so that only a detectable turbidity forms at the interface. If a flocculent precipitate forms, that means that the concentration is too high. This technique is less frequently used than the sitting and hanging drop vapour diffusion but is one of the methods used by NASA (National Aeronautics and Space Administration) to perform protein crystallisation experiments in microgravity. The technique allows to screen a gradient of sample precipitant concentration combinations.

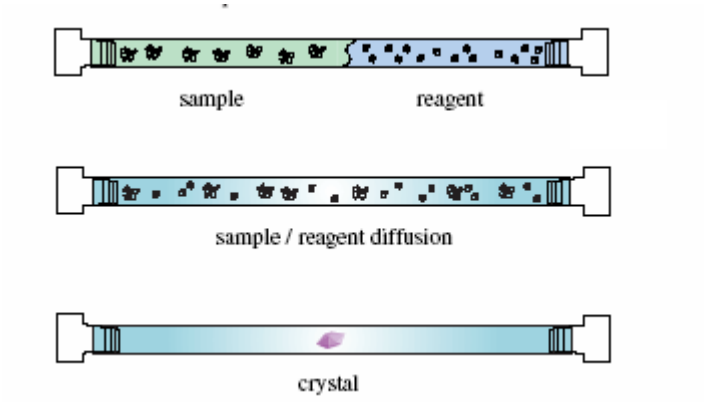

Figure 7. The free interface diffusion technique as applied to microliter samples in small capillaries.

6. <u>LIQUID BRIDGE METHOD</u>: This method is a variant of the previous one (McPherson, 1982). A microdrop of mother liquor and a drop of the precipitating solution are placed in close proximity on a glass slide. A fine needle is used to draw a thin liquid bridge connecting the two drop so that free diffusion can occur between them. The slides and droplets are then sealed from the air to prevent evaporation. By direct liquid diffusion across the bridge into the mother liquor, the precipitant induces crystallisation.

7. <u>COUNTER DIFFUSION METHOD</u>: Counterdiffusion (CD) techniques have been well investigated and explained for over 100 years since the first description of periodic precipitation pattern formation in gelled medium (Liesegang, 1897). In counter diffusion experiments, the interacting precipitating agent and protein solutions either contacts one another directly or is separated by an intermediate chamber working as a physical buffer (NG *et al.*, 2003; Garcia Ruiz, 2003) (Fig. 8).

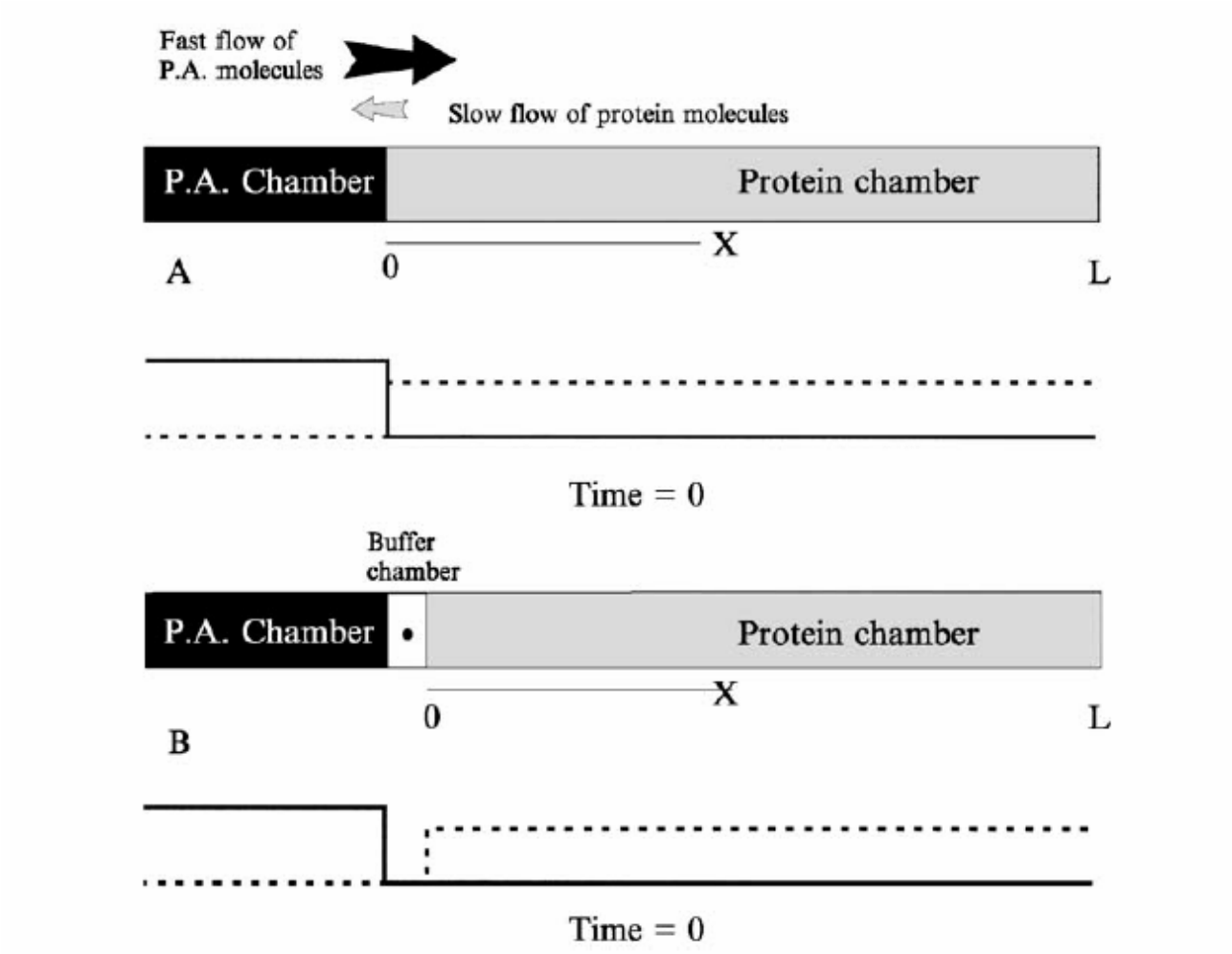

Figure 8. Geometry of a counter diffusion experiment showing the phenomenology of the technique with (a) or without (b) a buffer chamber. PA indicates precipitating agent.

As soon as the two solutions come in contact, they will interact according to the solubility dependence of the protein on the precipitating agent concentration. The two processes working in the experiment, mass transport and precipitation, are consecutive. In the case of macromolecules, upon starting the experiment, the molecules of protein diffuse toward the left (in the geometry of Fig. 8) while the salt will diffuse toward the right 10 to 100 times faster than the protein molecules toward the left, invading the protein chamber. As the precipitant diffuses into the protein, it will

provoke the precipitation of the protein according to the solubility of protein. Once the salt ions run into the protein chamber, the system moves deep into the labile region provoking the immediate precipitation of an amorphous phase at the location $x = x_0$ (Fig. 9). The precipitation of the protein occurs because its solubility varies with, for instance, the concentration of salt. In the diagram showed in figure 9 the starting protein concentration is indicated as 0_M and the concentration of the salt as 0_P. When these solutions come into contact, the system moves toward point E_1 in the phase diagram. The supersaturation is very high. Therefore, the first precipitate could be an amorphous phase forming at x_0. Its formation depletes the concentration of protein in the neighboring zones. As the salt continues to diffuse into the protein chamber, a new precipitation event takes place, this time at lower supersaturation eventually producing microcrystals (location x_1 in the phase diagram). Iteration of this process provokes the precipitation at lower supersaturation as the precipitation front moves far from the precipitant chamber toward the protein chamber (x_2, x_3, … x_e). This yields precipitation zones of fewer crystals of larger size and higher quality. Contrasting the classic drop and batch methods, the counterdiffusion technique explores a large number of crystallisation conditions in a single experiment.

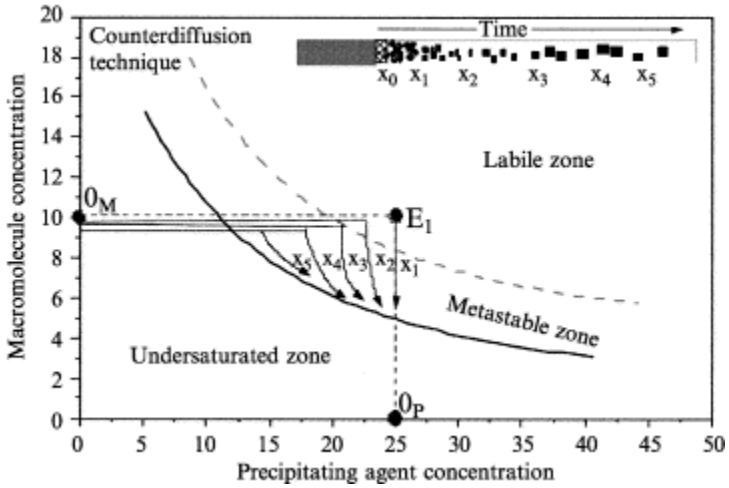

Figure 9. The solubility diagram showing how CD (Counter Diffusion) crystallisation works.

From this phenomenological description, it is clear that the mechanism initiating pattern formation differs in counter diffusion from that in other crystallisation techniques. The counterdiffusion technique is an out of equilibrium precipitation system moving spontaneously toward equilibrium. One counter diffusion experiment is therefore equivalent to a large number of hanging drop or batch experiments across the phase diagram. The counterdiffusion crystallisation procedure is able to compose a continuous supersaturation gradient. During the diffusion process a supersaturation state

with respect to the protein can be attained in the labile region, while crystal growth can occur in a continuous range in the metastable area of the phase diagram. Hence, crystal formation is caused by the progression of a nucleation front resulting from the nonlinear interplay among mass transport, protein crystal nucleation and growth.

García-Ruiz proposed applying the counterdiffusion techniques in gelled medium to the crystallisation of biological macromolecules as an alternative method to carry out a wide screening of experimental crystallisation conditions in a single experiment (Garcia-Ruiz, 1991). In 1993, García-Ruiz and collaborators developed the gel acupuncture method (GAME), in which the protein solution is confined in a capillary punched in a gel layer and the precipitating agent is poured on the gel layer (Fig. 10) (Garcia-Ruiz *et al.*, 1993). The capillary acts as a long protein chamber and removes convection from the system. When the precipitating system contacts the protein solution, a wave of supersaturation is triggered. This wave travels along the protein chamber and screens different crystallisation conditions of progressively lower supersaturation values as it moves further from the lower end of the capillary. Unlike traditional methods, one of the main advantages of GAME is its ability to yield crystals obtained under different nucleation and growth conditions in every experiment. This implies that a single GAME experiment is equivalent to many experiments with traditional methods. GAME is the only technique that produces crystals that fill the capillary diameter and do not slip, allowing data collection at room temperature from the same capillary in which the crystals were grown. The use of capillaries is even more advantageous as it has been proven that crystals can be frozen into capillaries for cryocrystallography studies after diffusion of an appropriate cryoprotectant (NG *et al.*, 2003). Additionally, the use of very thin capillaries of 0.1 mm in diameter reduces the consumption of protein solution for screening purposes.

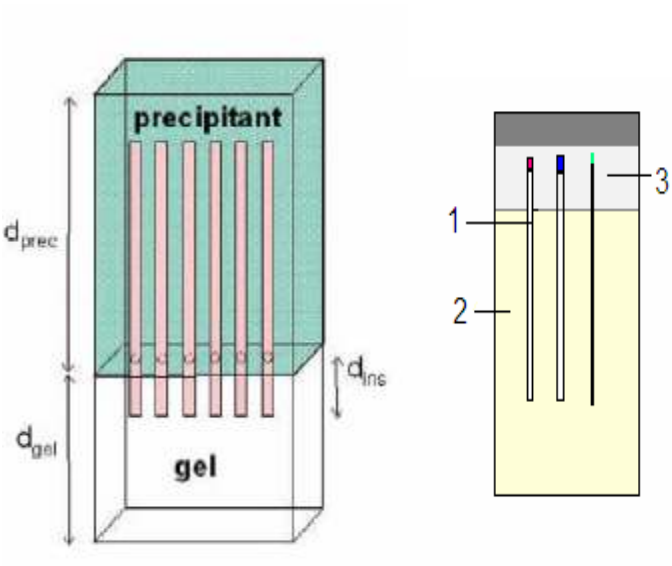

Figure 10. The gel acupuncture method (GAME) with capillaries of different diameters. In the image on left 1 is the capillary, 2 the precipitant, 3 the agarose gel.

The crystallisation by counter diffusion is a very efficient technique for obtaining high quality crystals. A prerequisite for the use of counter diffusion techniques is that mass transport must be controlled by diffusion alone. Sedimentation and convection can be avoided either by working in gelled systems or in the absence of gravity (Snell *et al.*, 2005; Zegers *et al.*, 2006). Since the early eighties, several thousands of crystallisation experiments were performed in space on board NASA's Shuttle, on board automatic platforms like the European Retrievable Carrier (EURECA) platform, or on board the Russian Mir Space Station (Kundrot *et al.*, 2001). The crystallisation experiments performed on the ISS (International Space Station) have allowed to visualise the growth of crystals in capillary counter diffusion investigating the microgravity effect. Crystal perfection has been shown to be higher for crystals grown in non-convective environments compared with that one of crystals grown in convective environments.

8. **HIGH-THROUGHPUT PROTEIN CRYSTALLISATION**: Several projects have recently been initiated to construct automated systems able to rapidly performing a large number of crystallisation trials, with the intent of 'industrializing' protein crystallisation (Yon *et al.*, 2003; Huia *et al.*, 2003). Technical advances have been made in crystallisation and an increasing number of robotic systems have been described that allow hundreds or thousands of crystallisation experiments to be carried out (Khun *et al*., 2002). Commercially available systems include IMPAX and Oryx robots from Douglas instruments (http://www.douglas.co.uk) (Fig. 11), Cyberlab from Gilson (http://www.gilson.com) and those from Cartesian (Fig. 12) (http://www.cartesiantech.com). Higher-density formats have become common for sitting drops with the marketing of microplates for 96-well sitting drops (Hampton Research, http://www.hamptonresearch.com). Microbatch crystallisation under oil is being practiced at high-throughput. The Hauptmann–Woodward group has developed a system based on 1536-well plates and a customized 384-channel Hydra liquid-handling robot from Robbins Scientific (Luft *et al*., 1999). The robot sets up the following experiment in each well: 200 nl of protein and 200 nl of screening solution are independently dispensed into 5 µl of paraffin oil. Low-speed centrifugation ensures mixing of the protein and buffers and settlement of the mixed drops onto the bottoms of the wells.

Also the biotechnology company Syrrx (http://www.syrrx.com) and the Genomics Institute of the Novartis Research Foundation (http://web.gnf.org) have pioneered the use of automation to set up nanolitre-scale crystallisation drops (20–100 nl) (Stevens, 2000; Goodwill *et al.*, 2001). Nanolitre crystallisation has the significant advantages of allowing extensive crystallographic screens to be performed with much less protein (making the task of protein production easier) and of reducing crystallisation times. The practical limitation of this approach is the resulting crystal size-up to 50

μm. In September 2003, at the EMBL (European Molecular Biology Laboratory) of ESRF (European Synchrotron Radiation Facility) of Grenoble, a high-throughput crystallisation platform, the HTX Lab, has been set up with the aim to increase the success rate and speed up the process of crystal structure determination. In this platform the whole process of crystallisation screening is automated through the introduction of liquid handling, crystallisation and crystal imaging robots. It allows to perform experiments using extremely low volumes of sample, which makes it possible to perform extensive screening even when the amount of sample is limited. Screens of large numbers of crystallisation conditions can now be rapidly carried out, analysed and, if required, followed up with fine screening to optimise conditions. With sufficient investment in robotics like the systems mentioned above, preparing crystal trials is not a problem; however, every crystallisation experiment has to be inspected to score the drops, to determine the optimisation strategy, and to capture the time at which a crystal appears optimal. Increased numbers of crystallisation experiments have driven the development of systems to store crystallisation trays and capture and analyse images of the crystallisation wells (e.g. the Robomicroscope II from Robodesign and the CrystalScore™ imaging system developed by Diversified Scientific Inc.). Most labs rely on human inspection, but there have been advances in imaging that promise to alleviate the challenge and tedium of inspecting thousands of protein drops every week. Automated image capture offers various advantages over human inspection, namely ergonomics and throughput. With an image capture system, most protein drops can be examined on a computer with the microscope. Using automated methods, the drops can be inspected more frequently and each observation time-stamped precisely. Moreover, digitised images of protein drops can be analyzed using a myriad of artificial intelligence techniques which, though not yet competitive with human expertise, can be trained to recognise patterns not obvious to the human eye.

Figure 11. Oryx robot of Douglas instrument to perform microbatch and vapour diffusion experiments.

Figure 12. Cartesian instrument, Honeybee 961, a dedicated sitting drop system that fills reservoirs as well as shelves.

8. **SEEDING TECHNIQUE**: Seeding is a powerful tool for the separation of nucleation and growth (Bergfors *et al.*, 2003). In this technique, previously nucleated crystals are used as seeds and introduced into new drops equilibrated at lower levels of supersaturation. Seeding techniques can be classified into two categories based on the size of the seeds:

• Microseeding—transfer of submicroscopic seeds, too small to be distinguished individually.

• Macroseeding—transfer of a single crystal, usually 5–50 μm.

Microseeding is an easy method and therefore the type of seeding to try first. Macroseeding (also called seed transfer) is much more labour intensive. It requires tedious transfers of the parent crystal through multiple washes, although the effort can be worth it, especially in terms of increasing the size of the crystal. However, in most seeding situations, a whole seed is not required; microseeds will suffice. The disadvantage to microseeding is that it is difficult to control the number of seeds that are transferred. Microseeds can be made and introduced into the new drop in many different ways. Foe example, the crystals can be pulverized (smashed) into crystalline particles by tissue homogenizers, sonication, vortexing, seed beads, glass rods, or other utensils.

Not all precipitates are equal: it is important to distinguish the precipitates of denatured protein from amorphous and non-amorphous precipitates and recognize submicroscopic crystals which look like amorphous precipitate. One quick assay for microcrystallinity of precipitates is streak-seeding (Stura, E. *et al.*, 1991). In this method, the precipitate is streak-seeded into a new drop and the results are examined after 2–7 days. Amorphous precipitates will generate only more precipitate along the streak line, whereas crystalline precipitates will generate microcrystals. Sometimes the seeds generated along the streak line are large enough to use without further refinements.

Seeding can be used in conjunction with other optimisation measures such as fine-tuning the precipitant and protein concentrations, adjusting the pH, and screening additives. This approach is usually applied when crystals of inadequate quality or crystalline precipitate have been obtained from initial crystallisation trials. The advent of microfocusing synchrotron beams now makes it possible to collect data from crystals of less than 100 μm but the need for large crystals still exists. Seeding can be used to grow larger crystals or get them to grow singly, improve their diffraction quality, save protein, reduce long waits for spontaneous nucleation, and cross-seed other proteins. If no crystals or microcrystals are forthcoming in the initial crystallisation screening, seeding can be attempted with any solid phase that has resulted. It is obvious that spherulites represent some kind of semiordered aggregation, but even oils and precipitates can exhibit short-range order and therefore act as nuclei (ordered aggregates) for further crystal growth (Stura *et al*., 1991). For these solid states of the protein, streak-seeding is the method of transfer.

The main difficulty is to find a suitable fibre to use, cat's whiskers are excellent. A parent crystal is stroked to pick up invisible seeds. Then the seeds are introduced into a fresh drop by stroking the fibre in a straight line through the drop. Crystals will grow along the streakline. Sometimes new self nucleated crystals in parts of the drops farther away from the streakline will appear (Fig. 13) .

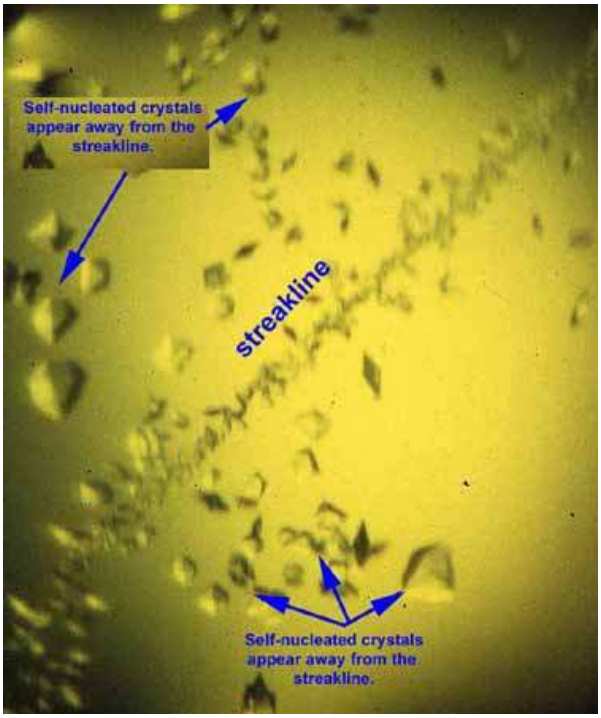

Figure 13. Crystals grown in a drop in which streak-seeding has been carried out using a cat whisker.

1.4 REFERENCES

- Asherie, N. Protein crystallisation and phase diagram. (2004) *Methods* **34**, 266-272.
- Bergfors, T. Seeds to crystals. (2003) *J. Struct. Biol*. **142**, 66-76.
- Boyes-Watson, J., Davidson, E., Perutz, M.F. An X-ray study of horse methaemoglobin. (1947) *Proc. Roy. Soc. Ser.* **A 191(1024)**, 83-132.
- Blow, D.M., Chayen, N.E., Lloyd, L.F., Saridakis, E. Control of nucleation of protein crystals. (1994) *Protein Sci.* **3**, 1638-1643.
- Blundel, T.L., Johnson, L.N. Protein crystallography. (1976) Academics Press Inc., New York, London, San Francisco.
- Bunick, C., North, A., Stubbs, G. Evaporative microdialysis: an effective improvement in an established method of protein crystallisation. (2000) *Acta Crystallogr.* ***D*** **56**, 1430-1431.
- Chayen, N.E., Lloyd, L.F., Collyer, C.A., Blow, D.M. Trigonal crystals of glucose isomerase require thymol for their growth and stability. (1989) *J. Cryst. Growth* **97**, 367-374.
- Chayen, N.E. A novel technique to control the rate of vapour diffusion, giving larger protein crystals. (1997) *J. Appl. Cryst.* **30**, 198-202.
- Chayen, N.E. Comparative studies of protein crystallisation by vapour-diffusion and microbatch techniques. (1998) *Acta Cryst.* **D54**, 8-15.
- Chayen, N.E. Turning protein crystallisation from art into a science. (2004) *Curr. Opin. Struct. Biol.* **14**, 577-583.
- Chayen, N.E., Saridakis, E. Protein crystallisation: from purified protein to diffraction-quality crystal (2008) *Nature Methods* **5**, 147-153.
- Dobler, M., Dover, S.D., Laves, K., Binder, A., Zuber, H. Crystallisation and preliminary crystal data of C-phycocyanin. (1972) *J. Mol. Biol.* **71(3)**, 785-787.
- Durbin, S.D., Feher, G. Protein crystallisation. (1996) *Annu. Rev. Phys. Chem.* **47**, 171-204.
- Garcia-Ruiz, J.M. Uses of crystal growth in gels and other diffusing-reacting systems. (1991) *Key Eng. Mater.* **88**, 87-106.
- Garcia-Ruiz, J.M., Moreno, A., Viedma, C., Coll, M. Crystal quality of lysozyme single crystals grown by the gel acupuncture method. (1993) *Mater. Res. Bull.* **28**, 541-546.
- Garcia-Ruiz, J.M. Counter-diffusion methods for macromolecular crystallisation. (2003) *Methods Enzym.* **36**, 130-154.
- Goodwill, K.E., Tennanta, M.G., Stevens, R.C. High-throughput X-ray crystallography for structure-based drug design. (2001) *Drug Discovery Today* **6**, S111-S118.
- Huia, R., Edwards, A. High-throughput protein crystallisation. (2003) *J. Struct. Biol.***142(1)**, 154-161.
- Hopkins, F.G., Pinkus, S.N. Observations on the crystallisation of animal proteins. (1898) *J. Physiol.* **23(1-2)**, 130-136.

- Kam, Z., Shore, H.B., Feher, G. On the crystallisation of proteins. (1978) *J. Mol. Biol.* **123(4)**, 539-555.
- Kim, S.S., Smith, T.J., Chapman, M.S., Rossmann, M.C., Pevear, D.C., Dutko, F.J., Felock, P.J., Diana, G.D., McKinlay, M.A. Crystal structure of human rhinovirus serotype 1A (HRV1A). (1989) *J. Mol. Biol.* **210(1)**, 91-111.
- Kuhn, P., Wilson, K., Patch, M.G., Stevens, R.C. The genesis of high-throughput structure-based drug discovery using protein crystallography. (2002) *Curr. Opin. Chem. Biol.* **6**, 704-710.
- Kundrot, C.E., Judge, R.A., Pusey, M.L, Snell, E.H. Microgravity and macromolecular crystallography. (2001) *Cryst. Growth Des.* **1(1)**, 87-99.
- Liesegang, R. Chemische Fernwirkung. (1897) *Photographisches Arch.* **800**, 305-309.
- Luft, J.R., Arakali, S.V., Kirisits, M.J., Kalenik, J., Wawrzak, I., Cody, V., Pangborn, W.A., DeTitta, G.T. A macromolecular crystallisation procedure employing diffusion cells of varying depths as reservoirs to tailor the time course of equilibration in hanging and sitting drop vapor diffusion and microdialysis experiments. (1994) *J. Appl. Cryst*. **27**, 443-452.
- Luft, J.R., Albright, D.T., Baird, J.K., DeTitta, G.T. The rate of water equilibration in vapour-diffusion crystallisations: Dependence on the distance from the droplet to the reservoir. (1996) *Acta Cryst.* **D52**, 1098-1106.
- Luft, J.R., Rak, D.M., DeTitta, G.T. Microbatch macromolecular crystallisation on a thermal gradient. (1999) *J. Cryst. Growth* **196**, 447-449.
- Luger, K., Mäder, A., Richmond, R.K., Sargent D.F., Richmond, T.J. Structure of the nucleosome core particle at 2.8Å resolution. (1997) *Nature* **389**, 251-260.
- McMeekin, T.L. The preparation and properties of crystalline horse serum albumin of constant solubility. (1939) *J. Am. Chem. Soc.* **61**, 2884-2890.
- McPherson, A. Preparation and analysis of protein crystals. (1982) Krieger publishing company, Malabar, Florida.
- McPherson, A. Introduction to protein crystallisation. (2004) *Methods* **34**, 254-265.
- Ng, J.D., Gavira, J.A., García-Ruíz, J.M. Protein crystallisation by capillary counterdiffusion for applied crystallographic structure determination. (2003) *J. Struct. Biol*. **142(1)**, 218-231.
- Przybylska, M. A double cell for controlling nucleation and growth of protein crystals. (1989) *J. Appl. Cryst.* **22**, 115-118.
- Salemme, F.R. A free interface diffusion technique for the crystallisation of proteins for x-ray crystallography. (1972) *Arch. Biochem. Biophys.* **151(2),** 533-539.
- Saridakis, E., Chayen, N. Improving protein crystal quality by decoupling nucleation and growth in vapor diffusion. (2000) *Protein Sci.* **9**, 755-757.
- Snell, E.H., Helliwell, J.R. Macromolecular crystallisation in microgravity (2005) *Rep. Prog. Phys.* **68**, 799-853.
- Stevens, R.C. High-throughput protein crystallisation. (2000) *Curr. Opin. Struct. Biol*. **10**, 558-563.

- Stura, E., Wilson, I. Applications of the streak seeding technique in protein crystallisation. (1991) *J. Cryst. Growth* **110**, 270-282.
- Zegers, I., Carotenuto, L., Evrard, C., Garcia-Ruiz, J.M., De Gieter, P., Gonzales-Ramires, L., Istasse, E., Legros, J.C., Martia, J., Minetti, C., Otalora, F., Queeckers, P., Schockaert, C., VandeWeerdt, C., Willaert, R., Wyns, L., Yourassowsky, C., Dubois, F. Counterdiffusion protein crystallisation in microgravity and its observation with PromISS (protein microscope for the international space station). (2006) *Microgravity - Science and Technology* **18 (3-4)**, 165-169.
- Zeppenzauer, M., Soderberg, B.O., Branden, C.I. Crystallisation of horse liver alcohol dehydrogenase complexes from alcohol solutions. (1967) *Acta Chem. Scand.* **21**, 1099-1101.
- Zeppenzauer, M.H., Eklund, E., Zeppenzauer, E. Microdiffusion cells for the growth of single protein crystals by means of equilibrium dialysis. (1968) *Arch. Biochem. Biophys.* **126**, 564-573.
- Zeppenzauer, M. Formation of large crystals. (1971) *Methods Enzymol.* **22**, 253-266.
- Weber, B.H., Goodkin, P.E. A modified microdiffusion procedure for the growth of single protein. (1970) *Archives Biochem. Biophys.* **141(2)**, 489-498.
- Wiencek, J.M. New strategies for protein crystal growth. (1999) *Annu. Rev. Biomed. Eng.*, 505-534.
- Yonath, A., Mussig, J., Tesche, B., Lorenz, S., Erdmann, V.A., Wittmann, H.G. Crystallisation of the large ribosomal subunits from Bacillus stearothermophilus. (1980) *Biochem. Int.* **1**, 428-435.
- Yonath, A., Müssig, J., Wittmann, H.G. Parameters for crystal growth of ribosomal subunits. (1982) *J. Cell. Biochem.* **19(2)**, 145-155.
- Yon, J., Jhoti, H. High-throughput structural genomics and proteomics: where are we now? (2003) *Targets* **2(5)**, 201-207.

CHAPTER 2: HETEROGENEOUS CRYSTALLISATION

2.1 INTRODUCTION

In proteins crystallisation, either getting no crystals at all, or even more frustrating, getting crystals that are not of high enough quality to allow structure determination is a real problem. The ultimate means to obtain good crystals is to control their conception stage, i.e. the nucleation stage which is the first step that determines the entire crystallisation process. This is not an easy task, hence, the holy grail is to find a 'universal' nucleant, a substrate that would induce crystallisation of any protein. Anecdotally, protein crystals have been often observed to grow on the surface of fortuitous impurities in the drop, such as dust particles and fibres. This has led to more systematic studies of the benefits of including heterogeneous nucleation agents in protein crystallisation. Heterogeneous nucleation involves the introduction of a solid material termed the heterogeneous nucleating agent, nucleant or seed. It is the formation of critical nuclei on particles or surfaces that facilitate the process by attracting the molecules electrostatically, hydrophobically or via more specific interactions, reducing the critical nuclear size or inducing crystalline order through epitaxy. Heterogeneous nucleation can therefore take place at metastable conditions. In fact, nucleation occurs on the surface of the nucleant material, which creates a higher local concentration of macromolecules, lowers the energy barrier for nucleation and bypasses the high kinetic barrier of spontaneous nucleation. A lower level of supersaturation is required under such circumstances for the nucleation step to occur, compared to homogenous nucleation (Chayen *et al.*, 2006). Recent notions on protein crystal nucleation have stressed this idea known for long time ago (Nanev, 2007). A search for a "universal nucleant" for biological macromolecules has been ongoing for 2 decades (Saridakis *et al.*, 2008) and the main lines of research have involved studies of epitaxic nucleants (McPherson *et al.*, 1987; McPherson *et al.*, 1988), lipid layers (Edwards *et al.*, 2004; Hemming *et al.*, 1995) and a lot of natural materials.

The most obvious way to attract molecules to each other is through electrostatic interactions. Charged nucleation-promoting surfaces have been therefore engineered for the purpose of facilitating nucleation. For example, a silicon substrate with microlithographically etched alternate stripes of n- and p-doping was able to promote nucleation only on those surface regions that were oppositely charged to the protein of interest and nucleation elsewhere was suppressed. A p-doped silicon (p-Si) surface in contact with an electrolyte at pH<7 will accumulate positive charge, whereas it will be neutral when in contact with an electrolyte at pH>7. Conversely, the n-Si surface

potential will be almost zero at pH<7 and negative at pH>7. Experiments performed with lysozyme on such patterned surfaces, as well as on unpatterned SiO_2, Si_3N_4 and Al_2O_3 surfaces, showed that they were able to induce nucleation, which depended on the surface potential of the material and the charge of the protein at a given condition of pH, buffer concentration and ionic strength (Sanjoh *et al.*, 1999; Sanjoh *et al.*, 2001).

Polymeric films containing ionisable groups, such as sulfonated polystyrene, cross-linked gelatin films with adsorbed poly-l-lysine or entrapped poly-l-aspartate and silk fibroin with entrapped poly-L-lysine or poly-L-aspartate, have been tested as heterogeneous nucleant surfaces for crystallising concanavalin A and chicken egg-white lysozyme (Fermani *et al.*, 2001). It was found that the crystallisation of concanavalin A by the vapour diffusion technique was strongly influenced by the presence of ionisable groups on the film surface. Both the induction time and protein concentration necessary for the crystal nucleation decreased whereas the nucleation density increased on going from the reference siliconised cover slip to the uncharged polymeric surfaces and even more to the charged ones. The authors proposed that non-specific attractive and local interactions between the protein and the film surface might promote molecular collisions and the clustering with the due symmetry for the formation of the crystal nuclei. Moreover, chemically modified mica sheets, a natural mineral that can be cleaved to present atomically flat surfaces, have been tested as heterogeneous nucleant surfaces for lysozyme, concanavalin A and thaumatin (Falini *et al.*, 2002). They have shown be able to promote nucleation not only through non-specific electrostatic attraction but also through local interactions between exposed charged residues of the protein and ionisable groups attached to the mica surface. These local interactions can become more important than the net-charge effect of the whole protein molecule. Chemical modifications of mica by silanisation reactions could not only change the density of charged groups on its surface but also somewhat modify its wettability and roughness. An increase of the wettability and the roughness of the sheet surface has been also suggested to contribute to the observed enhanced nucleation-inducing properties. Furthermore, Nanev's group has reported that glass coated with positively charged poly-L-lysine promoted the nucleation of crystals of ferritin, which, at the given crystallisation conditions, is negatively charged, whereas the glass suppressed the nucleation of crystals of the positively charged lysozyme (Nanev, 2007; Nanev, 2007; Tsekova *et al.*, 2002).

For crystallising proteins, favourable protein–protein interactions involving precisely defined areas (‘patches’) on the surface of the protein molecules are needed. A surface made of the protein to be crystallised itself is therefore a good candidate for a heterogenenous nucleant. Pechkova and Nicolini have pioneered protein-crystal growth on so-called Langmuir-Blodgett (LB) protein thin films (Pechkova *et al.*, 2004). Microcrystals of two previously uncrystallisable proteins, the human

protein kinase CK2 catalytic α subunit and bovine cytochrome P450scc, were obtained on those LB thin films. Two possible mechanisms have been proposed for such a nucleation induction by LB films. The first explanation assumes that a high electrostatic potential is induced at the film surface, which is caused because the charged protein molecules are oriented in the same way in the thin film. The film therefore attracts the molecules from solution and orients them in a way that favours protein–protein attractive electrostatic interactions. The second mechanism involves the migration of film fragments, which constitute tightly packed ordered molecules of the protein to be crystallised, into solution, in which they have the role of seeds (Nicolini *et al.*, 2004).

Porous materials have been designed that have greater universality in their nucleation-inducing effects (Chayen *et al.*, 2008). Two materials of different chemical composition, but sharing a wide distribution of pore sizes on the same order of magnitude as protein molecules, have proven successful: porous silicon with pore sizes of 5–10 nm (Chayen *et al.*, 2001) (that has been shown experimentally to be an effective nucleation-inducing material for protein crystals: five of six tested proteins crystallised from metastable solutions in its presence) and mesoporous bioactive gel-glass material ('bioglass') with pore sizes of 2–10 nm (Chayen *et al.*, 2006). Both have been successful in producing crystals with reduced mosaicity as well as producing single diffracting crystals under conditions in which spontaneous nucleation yielded only useless crystals.

Other porous materials, such as Sephadex beads of various sizes, carbon powder, alumino-silicates (Davis *et al*., 1989), mesoporous molecular sieves (Chen *et al.*, 1993) and zeolites of various mesh sizes were generally unsuccessful (Chayen *et al.* 2001). In contrast to porous silicon, these materials exhibit minimal variation of pore size and shape. Cacciuto *et al.* studied, by numerical simulation, the nucleation of the hard-sphere model of colloids (Cacciuto *et al.*, 2004). They observed that the model colloid crystallised on curved surfaces, including concave surfaces that may be considered as models for part of a pore. The concave surface acted as a nucleant, and its ability to do so depended on its curvature.

The mechanism of heterogeneous nucleation is complex, but the nucleation potential is mainly defined by the surface properties and chemical composition of the nucleating agent. Hair, especially horsehair, has been used successfully for many years in macromolecular crystallisation, however, not as a nucleant *per se*, but in order to transfer crystal seeds (i.e. post-critical nuclei) into metastable solutions. The sharp microstructure of hair with its overlapping cuticles, which are particularly present in horse hair, is ideal for trapping the microfragments of a crystal (Bergfors *et al.*, 2003).

Recently, heterogeneous nucleation on fragments of human hair has been visualized by confocal fluorescent microscopy and atomic force microscopy, and the chemical and morphological

properties of the nucleant surface have been investigated by treatment with chemicals (Georgieva *et al.*, 2007). The presence of keratin, but not lipids, was found to be essential for nucleation**.** Fragments of human hair combine most of the properties of the foreign substances used in the last thirty years as nucleant agents. They match important criteria required to an agent to be considered nucleant: surface ordered at the molecular level, ionisable groups, lipid layers, local concentration cavities, nano and mesoscopic structure. They have allowed to obtain macrocrystals and showers of tiny crystals under conditions that did not produce crystals in the absence of the nucleating substrate, not only in the case of model proteins but, more interesting, in the case of a polysaccarid-specific Fab fragment and potato protease inhibitor. Moreover, Thakur *et al*. have shown how also others materials, such as dried seaweed, horse hair, cellulose and hydroxyapatite, can be used as nucleating substrates, able to increase the crystallisation success of several model proteins, especially when a combination with each other are used (Thakur *et al*., 2007). A number of different fibrous materials (rat whiskers, horse hair and dried seaweed) were successfully tested with glucose isomerase, lysozyme and trypsin (D'Arcy *et al.*, 2003).

Two kinds of layer silicate, semi-synthetic micromica and natural chlorite, have been tested as heterogeneous nucleant material (Takehara *et al.*, 2008). Added as powder to a hanging drop, they were able to aid protein crystallisation. In particular, micromica powder has shown the potential to be used as universal nucleant for many proteins in the absence of precipitants. Micromica is a non-swellable clay, originating from modification of a natural precursor-layered mineral (Utracki *et al.*, 2007). Natural chlorite, another nanostructured material, suppressed nucleation in six out of the ten proteins tested, whereas it slightly increased the speed of crystallisation for two proteins and had no effect on the remaining two. Although the authors did not propose a detailed mechanism for the induction of nucleation by layered nanostructured material, such as these phyllosilicates, it can be speculated that this particular structure might promote nonspecific protein absorption. The differences in nanostructure between the two materials might explain their different effects.

Also microporous synthetic zeolite Molecular Sieves have turned out to be candidates for universal hetero-epitaxic nucleant able to selectively facilitate new crystal forms which did not grow spontaneously from solution, acting as a crystallisation catalyst (Sugahara *et al.*, 2008). Zeolite-mediated crystallisation also improved the crystal quality in almost all of tested proteins (5 of 6). In these molecule sieves, the pores are much smaller than a single protein molecule, which led the authors to propose that nucleation followed an epitaxial growth mechanism that requires a regular arrangement of pores, such as those present on the zeolite surface.

Poly vinylidene fluoride membranes with pore sizes of 400 nm have successfully used as heterogeneous nucleant surfaces: they promoted the growth of perfect lysozyme crystals allowing

to obtain two distinct forms (Zhanga *et al.*, 2008) . Nucleation of lysozyme crystals have been promoted also by using glass slide surfaces chemically modified with (3-aminopropyl)triethoxysilane, poly(2-hydroxyethylmethacrylate) and poly-L-glutamic acid (Liu *et al.*, 2007). Moreover, polymer-induced nucleation has been used for production of high-quality lysozyme crystals and to induce selectively nucleation of multiple macromolecule crystal forms (Grzesiak *et al*., 2008).

The most recent studies have tested the effect, both in screening and as an additive for known crystallisation conditions, of polystyrene nanospheres on protein crystallisation with three commercial proteins, lysozyme, xylanase, xylose isomerase and with five research target proteins (Kallio *et al.*, 2009). In screening, the addition of an aqueous solution of nanosphere to the crystallisation drop had a significant positive effect on crystallisation success in comparison to the control screen. As an additive, the nanospheres altered the crystal packing.

The progression from the mineral crystals as nucleant agents that promote epitaxial nucleation in a highly specific manner, through the use of charged surfaces, towards a greater universality offered by porous and other natural or engineered microstructured materials has been explored. In addition to the already well known effects of epitaxy and electrostatic interactions, a rough and irregular structural pattern of terraces, hillocks, cuticles or pores on a solid substrate can enhance nucleation-promoting properties, thus providing a new paradigm for the design of protein-crystal nucleants.

In this contest, one topic of the thesis has been focalised on the development of crystallisation techniques able to promote and ease protein nucleation using functionalised surfaces. The aim is to evaluate the nucleant capacity of surfaces exposing chemical ionisable groups and understand the mechanism by which the surfaces control the protein crystallisation.

2.2 FUNCTIONALISED SURFACES

Two surface have been used in the crystallisation experiments: Polystyrene films and mica sheets. Polystyrene films have been functionalised through a sulphonation reaction and are negatively charged, while mica sheets have been positively charged by a silanisation reaction in vapour diffusion (Tosi *et al.*,2008).

2.2.1 Preparation and functionalisation of polystyrene films: Polystyrene films were prepared by dissolving polymer granules in 7% (w/v) 1,2-dichloroethane and 9 ml of the obtained solution was poured into a glass Petri dish (5.5 cm diameter) and left overnight under a chemical hood. The films were formed by solvent evaporation at room temperature, which was completed by incubating the films at 333K for about 12 h. Successively, they were sulfonated by immersion in concentrated H_2SO_4 (98% v/v) for different periods of time and then washed with distilled water to remove the residual acid. The different sulphonation times of polystyrene films are reported in Table 4 (page 41).
Eventually, the films were incubated for at least 2 h with the buffered solutions used for the crystallisation trials. The films released no material in solution.

2.2.2 Preparation and functionalisation of mica sheets: Mica minerals are 2:1 layer silicates formed by a sandwich of two tetrahedral layers - sheets of linked [SiO_4] tetrahedra - joined by a layer of Al^{3+} in octahedral coordination. The mica group of silicate (phyllosilicate) minerals has perfect basal cleavage and can be spited into thin laminae. Chemically, they contain complex silicate of aluminium and alkalies with hydroxyl. Muscovite (also known as Common mica, Isinglass, or Potash mica) is the most common mica.
Muscovite is a phyllosilicate mineral of aluminium and potassium with formula $KAl_2(AlSi_3O_{10})(F,OH)_2$, or $(KF)_2(Al_2O_3)_3(SiO_2)_6(H_2O)$. It has a highly-perfect basal cleavage yielding remarkably-thin laminæ (sheets) which are often highly elastic (Fig. 14).

Figure 14. Muscovite sheets.

A perfect muscovite is made by repetition of 8 monolayers (4 O monolayers, 2 Si,Al monolayers, 1 Mg, Fe, Al monolayer and one K monolayer) (Fig. 15) (Biino *et al.*, 1998).

Freshly cleaved muscovite mica surfaces have an outstanding even surface, are optically flat, clear, transparent, scratchless and free from fingerprints. They are very useful in electron microscopy for production of carbon support films, particle imaging, cell growing and thin film coating research. Muscovite mica surface are also suitable as substrates for high resolution atomic force microcopy studies such as DNA, DNA-protein and thin films.

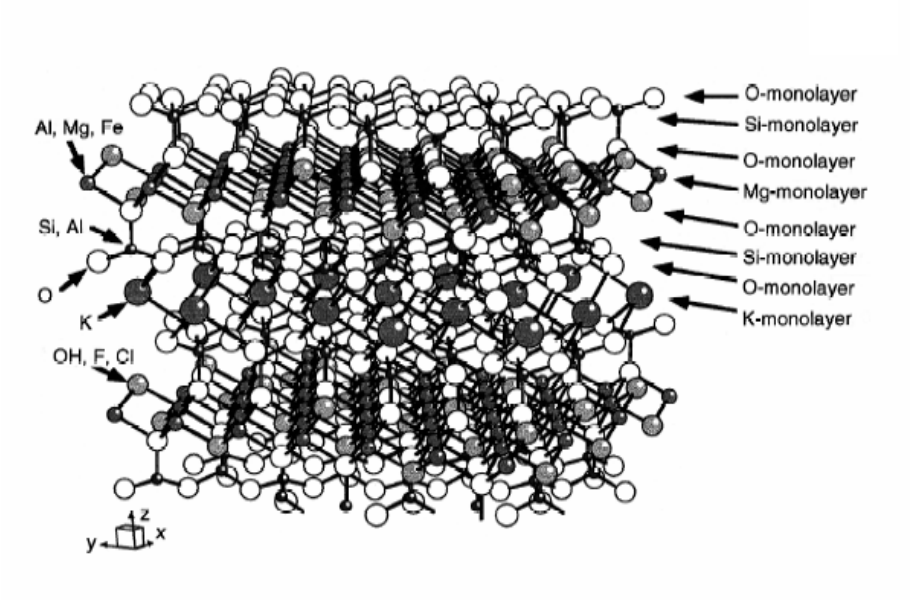

Figure 15. The ideal crystal structure of muscovite.

The hydrophilic properties of the mica samples were reduced by modifying their surfaces with a silanisation reaction (Luda *et al.*, 1999). The mica sheets were immersed in 0.5 M HCl solution for

2 h (Fang *et al.*, 1995) and then left to dry overnight in a nitrogen-gas atmosphere in a desiccator. The silanisation reaction was carried out in vapour phase for 18 hours in a desiccator containing 130 µl of a silane mixture. Before each reaction the mica was carefully cleaved in air along its basal plane. To vary the density of the ionisable groups on the mica surface mixtures of two silanes, n-propyltriethoxysilane and 3-aminopropyltriethoxysilane, in different percentages starting from 0 to 100% of aminosilane, were used in the reaction. The composition of the five mixtures used for the silanisation reaction are reported in Table 4 (page 41). These mica sheets were incubated at least 3 hours with the buffered solutions used for the crystallisation trials. No materials were released in solution as checked by atomic absorption for metal ions and chromatographic analyses.

2.2.3 Characterisation of the functionalised surfaces: Studies of contact angles and roughness demonstrated that both surfaces are substrates suitable for macromolecular crystallisation: they do not allow topographic effects during nucleation, and their hydrophilicity still allows the deposition of a spheric drop. These surfaces are transparent to light and can be checked by an optical microscope. The conventional chlorinated organopolysiloxane-coated glass cover slip was used as a reference.

Contact angles were determined using the sessile-drop method at room temperature. 5 ml of pure water was dropped onto the surface of the functionalised samples and onto the surface of the silanised glass cover slip, respectively. The drop was left undisturbed for about 1 min and its shape was then recorded with a digital camera.

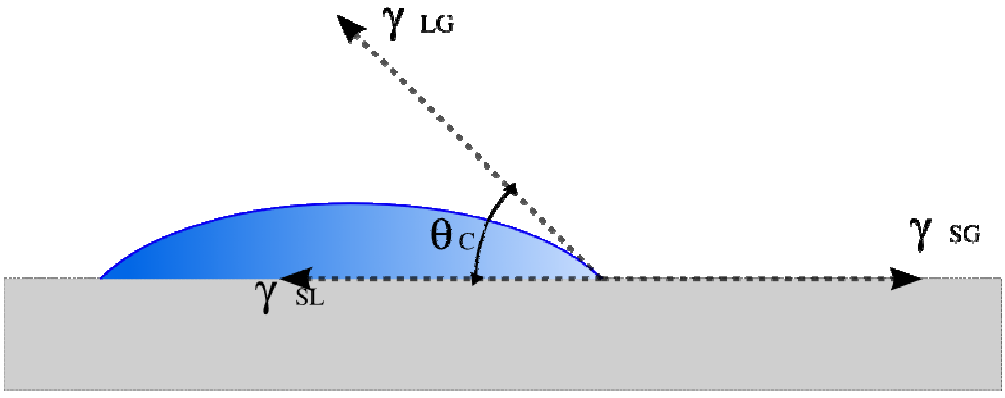

Figure 16. Diagram that shows the contact angle and interphase-energy between 3 phases: Solid-Liquid: γ_{SL}; Liquid-Gas: γ_{LG} ; Solid-Gas: γ_{SG}.

The contact-angle values reported in Table 4 (page 41) were the average of at least three measurements. The surface roughness was evaluated by means of atomic force microscopy. A Digital Instruments Nanoscope III atomic force microscope (AFM) was used to observe the topography of sulfonated polystyrene films, chemically modified mica sheets and silanised glass cover slips. All images were obtained in tapping mode using micro-fabricated silicon nitride cantilevers (Digital Instruments). The measurement of surface contact angles gives an evaluation of surface hydrophilicity (or hydrophobility). The mica silanised with neutral silane shows the same contact angle as the siliconised cover slip, used as control. An increase of the percentage of aminosilane in the reaction mixture causes a decrease of the contact angle, in agreement with the increase of the surface wettability due to a higher density of amino charged functional groups on the surface. As expected, surface hydrophilicity increases with the sulfonation time of polystyrene films.
In a heterogeneous crystallisation experiment the roughness of the surfaces is a crucial parameter to address the crystal nucleation mechanism.
The mean roughness, defined as the arithmetic average of the absolute values of the surface height deviation measured from the mean plane surface, was calculated over a square of 1 mm using the Nanoscope software. The values reported in Table 4 were the average of at least four measurements.
The data reported in Table 4 show that the silanisation process increases the roughness of the mica surfaces, however mica surfaces showed a roughness that was always lower than that of the reference surface, irrespective of the silane mixture used in the functionalisation reaction. Polystyrene surfaces showed a roughness of the same order of magnitude as the reference surface, apart from that prepared with the highest sulfonation time (polyst. 48h). The low roughness of these two types of surfaces gives confidence that topographical factors should be almost absent in the crystallisation process.
The distribution of charged functional groups on these surfaces has been studied. It has been reported that a mixture of silanes forms a monolayer on the mica surface in which silanes cluster in islands of different sizes (Lyubchenko *et al.*, 1993; Crampton *et al.*, 2005). In contrast, sulfonate groups are homogeneously distributed on polystyrene-film surfaces (Addadi *et al.*, 1987). The increase in the number of ionisable groups on the film with the sulfonation time was checked by ATR-FTIR (Addadi *et al.*, 1987) . After a period of 48 h, the peak corresponding to the sulfonate groups (1176.5) is saturated and its intensity does not increase by prolonging the treatment.

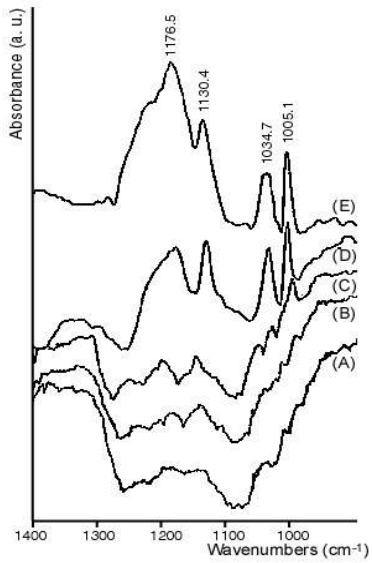

Figure 17. ATR-FTIR spectra of a) not sulphonated, b) 5min, c) 1h, d) 8h and e) 48h sulphonated polystyrene films.

Table 4. The surface-contact angles and roughness of functionalised surfaces. (Standard deviations are given in parentheses).

	Surface functionalization	**Contact angle (°)**	**Roughness (nm)**
reference[#]		104.4 (1.5)	0.50 (0.06)
Mica	-	<10	0.11 (0.05)
Mica A	0 % 3-apes*	104.4 (1.5)	0.25 (0.09)
Mica B	30 % 3-apes	86.9 (1.9)	0.38 (0.17)
Mica C	50 % 3-apes	83.0 (2.3)	0.29 (0.07)
Mica D	70 % 3-apes	81.7 (2.5)	0.30 (0.12)
Mica E	100 % 3-apes	81.3 (2.7)	0.29 (0.07)
polyst.	-	97.5 (1.5)	0.35 (0.09)
polyst. 5’	5 min [§]	81.5 (2.0)	0.40 (0.09)
polyst. 30’	30 min	78.1 (2.2)	0.42 (0.15)
polyst. 1h	1 h	76.4 (2.4)	0.38 (0.17)
polyst. 8h	8 h	53.3 (2.5)	0.68 (0.18)
polyst. 48h	48 h	35.1 (3.5)	1.5 (0.5)

† Siliconized cover slip, on which chlorinated organopolysiloxanes are the exposed groups. * 3-Aminopropyltriethoxysilane. The values indicate the percentage of 3-aminopropyltriethoxysilane in the 3-aminopropyltriethoxysilane/N-propyltriethoxysilane binary mixture. § Sulfonation time of polystyrene surfaces in sulforic acid.

2.3 CRYSTALLISATION OF MODEL PROTEINS ON FUNCTIONALISED SURFACES

The influence of the functionalised surfaces (sulfonated polystyrene films and aminosilanised mica sheets) on the crystallisation of insulin and ribonuclease A has been studied. The obtained results have been compared with previously reported work on the crystallisation of lysozyme, concanavalin A and thaumatin in the presence of the same type of surfaces (Fermani *et al.,* 2001; Falini *et al.,* 2002). The capability of the surface to affect protein crystallisation was evaluated by comparing parameters such as the median waiting time, the density of crystallisation and the average crystal sizes (Tosi *et al.,* 2008). In probability theory and statistics, a *median* is described as the number separating the higher half of a sample, a population, or a probability distribution, from the lower half.

2.3.1 Set up of the crystallisation experiments: The crystallisation trials were carried out at 293 K by the hanging drop vapour diffusion method using a well tissue culture tray. The traditional hanging-drop vapour diffusion technique was modified introducing between the glass cover slip and the drop the surface opportunely functionalised (Fig. 18).

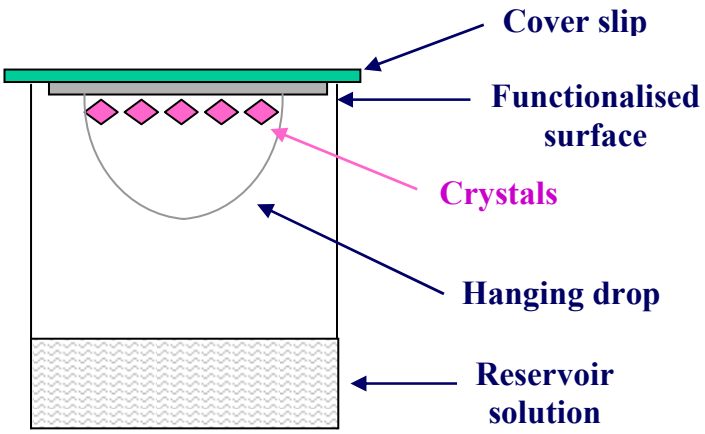

Figure 18. The modified hanging drop technique.

As reference, the conventional chlorinated organopolysiloxane-coated glass cover slips were used. Each well contained 750 µl of reservoir solution and the final volume of each drop was 5 µl, containing the protein and reservoir solutions in an equal ratio. All the experiments were repeated at least five times. In order to estimate the median waiting time (defined as the time spanning from the settling of the experiment to the observation of the first crystals using an optical microscope with

crossed polarizers), all the experiments were monitored at least twice per day using an optical microscope. In each drop, the number and average size of the crystals were noted.

The model proteins used were insulin and ribonuclease A, both from bovine pancreas. Insulin is a peptide hormone composed of 51 amino acid residues and has a molecular weight of 5808 Da. It is produced in the isles of Langerhans in the pancreas. Ribonuclease A (RNase A) is an endonuclease that cleaves single-stranded RNA. Bovine pancreatic RNase A (Mw 13.7 kDa) is one of the classic model systems of protein science. The pI (calculated using a ExPASy server tool) is of 6.2 for insulin and 9.9 for ribonuclease A.

Both proteins were crystallised using the experimental conditions reported in the literature but slightly adapted to the used experimental setup. Insulin was crystallised in the presence of 0.01 M EDTA, 0.30 M Na_2HPO_4 pH 9.5 and 0.50% (v/v) xylene (Dodson *et al.*, 1978) and ribonuclease A was crystallised in the presence of 55% (v/v) 2-methyl-2,4-pentanediol, 0.10 M sodium cacodylate pH 6.5 and 3.7 mM nickel chloride (King *et al.*, 1956). The starting concentration of both proteins, insulin (20.0 mg/ml in 5 mM EDTA, 0.15 M Na_2HPO_4 pH 9.5 and 0.25% (v/v) xylene) and ribonuclease A (25.0 mg/ml in water) was lowered until no crystal growth was observed on the reference surface.

2.3.2 Crystallisation of insulin on the functionalised surfaces: Insulin was crystallised on functionalised surfaces using a range of starting concentrations from 20.0 to 0.75 mg/ml. This protein has a high tendency to crystallise using starting concentrations above 2.0 mg/ml. Under these conditions, the influence of surfaces on crystallisation parameters can only be evaluated qualitatively. In Fig. 19a, a view of crystals grown on sulfonated polystyrene surfaces using a starting concentration of 10.0 mg/ml is shown. A large number of crystals formed on functionalised surfaces (Figs. 19a–e) with respect to the reference surface (Fig. 19f). Moreover, the crystallisation density increased proportionally to the density of sulfonate groups on the surfaces (Figs. 19a–e), with a concomitant reduction of the average crystal size. Similar behaviour was observed using silanised mica sheets. The waiting times, average sizes and crystallisation densities of insulin crystals grown on mica and polystyrene functionalised surfaces using starting protein concentrations of 2.0, 1.0 and 0.75 mg/ml are reported in Table 5.

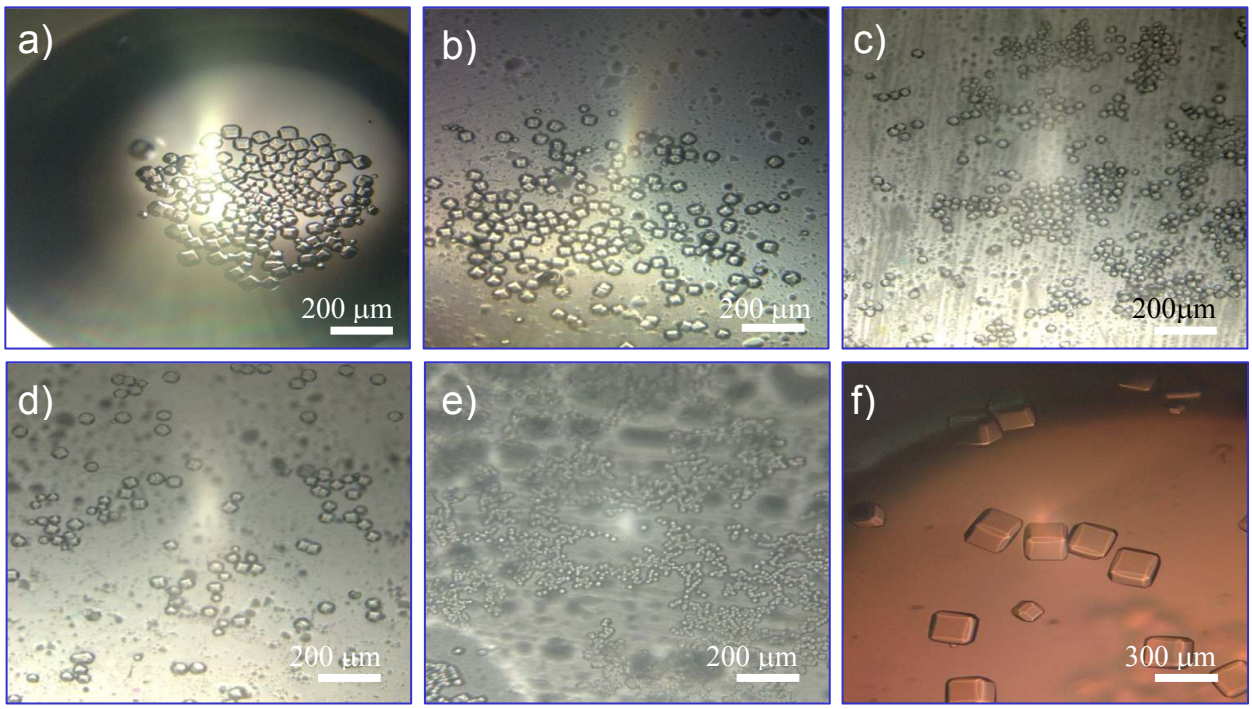

Figure 19. Optical micrographs of insulin crystals grown on sulfonated polystyrene surfaces (a–e) and the reference surface (f). (a) polyst. 5', (b) polyst. 30', (c) polyst. 1h, (d) polyst. 8h, (e) polyst. 48h. The crystals were grown using a starting protein concentration of 10.0 mg/ml.

Table 5. Waiting times (w.t.), average crystal sizes (D) and crystallisation densities (c.d.) for insulin.

	2.0 mg/mL			1.0 mg/mL			0.75 mg/mL		
	w.t. (days)	D* (mm)	c.d. (n. c./mm^2)	w.t. (days)	D* (mm)	c.d. (n. c./mm^2)	w.t. (days)	D* (mm)	c.d. (n. c./mm^2)
Control[#]	1	0.02	12	2	0.02	9	7[a]	0.03	6
Mica A	1	0.02	34	0.5	0.03	10	3	0.02	8
Mica B	1	0.03	35	1	0.02	20	2	0.03	10
Mica C	1	0.06	34	1	0.01	30	2	0.03	15
Mica D	1	0.01	46	1	0.02	35	1	0.02	35
Mica E	1	0.01	48	1	0.01	35	1	0.02	50
Polyst. 5'	1	0.01	45	1	0.01	12	6	0.02	6
Polyst. 30'	1	0.09	50	2	>0.01	20	6	0.02	9
Polyst. 1h	1	0.01	55	3	0.013	35	4	0.01	9
Polyst. 8h	1	mass[b]	mass[b]	3	>0.01	50	3	0.01	12
Polyst. 48h	1	mass[b]	mass[b]	2	mass[b]	mass[b]	2	>0.01	30

* D: the value refers to the average length of the longest axis of the crystal calculated on a set of several dozen of crystals.
[#] siliconised cover slip.
[a] only in few experiments (less than 25%).
[b] mass.: massive crystallisation.

When a starting insulin concentration of 2.0 mg/ml was used, the waiting time was about 1 day in the presence of both the functionalised surfaces and the reference. At a concentration of 1.0 mg/ml the waiting time on the reference was almost double that on all mica functionalised surfaces while the waiting time on sulfonated polystyrene surfaces was unrelated to the density of sulfonation. Using a starting protein concentration of 0.75 mg/ml, on the reference crystals formed after about one week and only in a few experiments (less than 25%), while they always appeared after a waiting time of about 1 day and not longer than 5 days using amino-silanised mica sheets and sulfonated polystyrene films, respectively. Moreover, in the presence of functionalised polystyrene surfaces the waiting time decreased with the increase of the amount of sulfonate groups from about 6 days on polyst. 30' to about 2 days using polyst. 48h. The crystallisation density on the reference decreased as the protein concentration was reduced (Table 5). In the presence of surfaces with an increasing number of ionisable functional groups, an increase in crystallisation density was observed at each protein concentration. Interestingly, the crystallisation densities observed on mica and polystyrene functionalised surfaces were always higher than those observed on the reference. This effect was also present for mica A, which has a reference-like hydrophobic surface but differs in roughness and contact angle (Table 4). At a protein starting concentration of 2.0 mg/ml the crystallisation densities of insulin using silanised mica surfaces increased to a value of about 48 crystals mm^2. This value is close to the lowest crystallisation density observed in the presence of polyst .5' (45 crystals mm^2) at the same protein concentration. Under the same conditions the crystallisation density increased to 55 crystals mm^2 in the presence of polyst.1h and appeared as a massive precipitation using polyst. 8h and polyst. 48h. When the starting protein concentration was reduced to 1.0 or 0.75 mg/ml a progressive decrease in crystallisation density was observed. This influence was more marked using sulfonated polystyrene films than with silanised mica sheets. Insulin precipitated in all the experiments, forming small crystals (around 10 mm along the main axis). As the density of charged functional groups on the surfaces increased, the average crystal size slightly decreased, while the crystallisation density increased.

2.3.3 Crystallisation of ribonuclease A on the functionalised surfaces: Ribonuclease A was crystallised using a starting concentration between 25.0 and 2.5 mg/ml on mica or polystyrene functionalised surfaces. Crystal formation was not influenced by the presence of functionalised mica surfaces until the starting concentration was reduced to values equal or below 10.0 mg/ml (Table 6).

Table 6. Waiting times (w.t.), average crystal sizes (D) and crystallisation densities (c.d.) for ribonuclease A.

	10 mg/mL			7.5 mg/mL			2.5 mg/mL		
	w.t. (days)	D* (mm)	c.d. (n. c./mm^2)	w.t. (days)	D* (mm)	c.d. (n. c./mm^2)	w.t. (days)	D* (mm)	c.d. (n. c./mm^2)
Control[#]	5	0.33	3	5	0.29	3	-	-	-
Mica A	5	0.43	3	4	0.26	2	-	-	-
Mica B	5	0.36	6	11	0.30	3	-	-	-
Mica C	5	0.39	6	11	0.27	3	11[a]	0.17	0.5
Mica D	4	0.26	5	12	0.16	2	9[a]	0.16	0.5
Mica E	2	0.43	6	6	0.21	4	35[a]	0.17	1
Polyst. 5’	5	0.40	3	4	0.26	3	-	-	-
Polyst. 30’	5	0.30	3	4	0.24	6	-	-	-
Polyst. 1h	5	0.29	4	6	0.32	5	4[a]	0.13	1
Polyst. 8h	5	0.21	6	6	0.14	6	4[a]	0.14	1
Polyst. 48h	2	0.34	9	2	0.14	10	4[a]	0.11	1.5

* D: the value refers to the average length of the longest axis of the crystal calculated on a set of several dozen of crystals.
[#] siliconised cover slip.
[a] only in few experiments (less than 25%).

At this concentration, using mica E functionalised only with hydrophilic silane, the waiting time was about 2 days, in contrast to waiting times that were at least doubled using the other silanised surfaces (Table 6). At a protein concentration of 7.5 mg/ml, the waiting time was about 4 days for crystals grown in the presence of mica A or the reference, both of which have a hydrophobic surface, about two weeks in the presence of mica surfaces functionalised with silane mixtures (micas B–D) and about 6 days in the presence of mica E. When the starting concentration was reduced to 2.5 mg/ml, crystals only grew on mica surfaces with a high content of amino (hydrophilic) groups (micas C–E). The density of crystallisation did not appear to be strongly influenced by the silanised mica surfaces.

However, at each concentration the highest value of crystallisation density was observed in the presence of mica E. The average size of the ribonuclease A crystals was mainly controlled by the starting concentration and not by the type of mica surface used (Table 6). In the presence of sulfonated surfaces, ribonuclease A crystallised as large aggregates when starting concentrations above 10.0 mg/ml were used. Figure 20 shows crystals grown at a concentration of 20.0 mg/ml using polystyrene film sulfonated for 48 h and the reference surface.

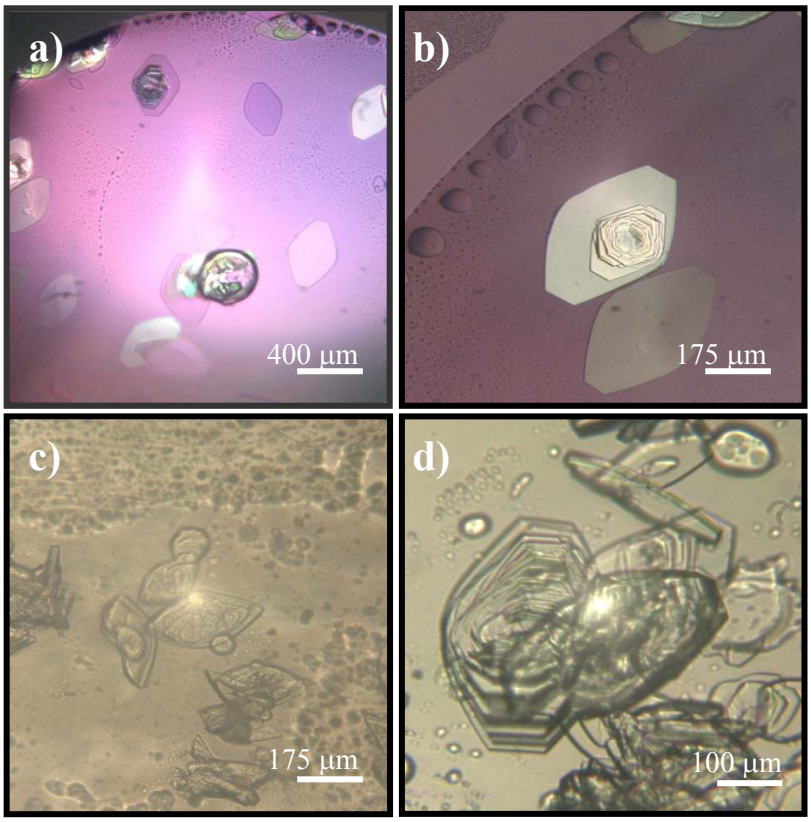

Figure 20. Optical micrographs at different magnifications of ribonuclease A crystals grown on the reference cover slip (a and b) and polystyrene surface with the highest content of sulfonated groups (c and d). The crystals were grown using a starting protein concentration of 20.0 mg/ml.

The formation of these aggregates made difficult to evaluate the average crystal size and the crystallisation density. The waiting time was affected by the presence of sulfonated surfaces only when starting protein concentrations equal or lower than 10.0 mg/ml were used. At this concentration and for polyst. 48h the waiting time was shorter (2 days) than for other polystyrene surfaces (5 days). A similar influence of the surface was observed at a protein concentration of 7.5 mg/ml. When the protein concentration was reduced to 2.5 mg/ml a waiting time of about 4 days was observed and, more importantly, crystals formed only in the presence of polystyrene films that had been sulfonated for more than 1 h. The average crystal size at the concentration of 10.0 mg/ml varied between 0.2 and 0.4 mm and was independent of the type of polystyrene film used. At a protein concentration of 7.5 mg/ml the average crystal size was around 0.25 mm using polyst. 5'–1h and about 0.14 mm for polyst. 8h and 48h. At the lowest starting protein concentration (2.5 mg/ml) an average crystal size of about 0.14 mm was observed. In the presence of these surfaces, the crystallisation density increased proportionally to the degree of sulfonation. It is important to note that at a starting ribonuclease A concentration of 2.5 mg/ml crystal formation was observed only in about 25% of trials for both surface families (more than ten on each surface). However, this

observation does undermine the nucleating role of the functionalised surfaces as crystal formation was not observed on the reference surface. The ribonuclease A waiting time using functionalised surfaces showed a significant variability and in some experiments was longer than that observed on the reference surface (silanised surface with high hydrophobicity). A possible reason for this variability could be the presence of trace amounts of impurities in solution. Moreover, minimal protein degradation cannot be excluded in lengthy crystallisation experiments.

2.3.4 Effects of both the functionalised surfaces on model proteins crystallisation: The results for the crystallisation of insulin and ribonuclease A in the presence of functionalised surfaces have been compared with findings obtained using lysozyme, thaumatin and concanavalin A on the same surfaces (Fermani *et al.*, 2001; Falini *et al.*, 2002). A summary of the variation of crystallisation parameters using functionalised surfaces with respect to the reference surface is reported in Table 7. Concerning the protein concentration the first and second values (reported in parenthesis) indicate the lowest starting protein concentration at which crystals formed in the presence of functionalised surfaces and the reference, respectively.

In the Table 7, the symbol = indicates that the functionalised surfaces did not influence the crystallization process with respect the control; + indicates an increase of the crystal density (crystal per surface unit) with respect to the control; - indicates a reduction of the average size of the crystal with respect to the control. The observations refer to the lowest starting protein concentration when crystals were observed both on the functionalised surfaces and the control. The surfaces are those that gave the most evident influences on the crystallization process, usually the ones with the highest content of ionisable functional groups.

Insulin and ribonuclease A have a net charge of about -9 and +8, respectively, at the pH values of the crystallisation conditions. Under the same pH conditions amino-silanised mica surfaces (micas B–E) are positively charged, whereas sulfonated polystyrene surfaces are negatively charged.

Thus, electrostatic attractions or repulsions may be present as a function of the relative charges of the surface and the protein. Similar considerations can be performed for the other model proteins reported. It is possible to note that with the exception of lysozyme, charged surfaces always increased the crystallisation density and reduced the nucleation time (measured here as the median waiting time) with respect to the reference surface.

Table 7. Summary of the results of the model protein crystallisation experiments using the sulfonated polystyrene films and the silanised mica sheets that gave the most evident effects with respect to the reference.

Protein				Sulphonated polystyrene films			Silanised Mica		
	Prot conc.[#] (mg/ml)	Cryst. pH	Prot. net charge*	w.t.	c.d.	D	w.t.	c.d.	D
Lysozyme	5.0 (10)	4.5	+ 2	=	=	=	-	=	=
Concanavalin A[a]	3.0 (10)	6.0	- 9	/	/	/	-	+	-
Concanavalin A[b]	10 (10)	9.0	~ 0	-	+	-	/	/	/
Thaumatin	2.0 (2.0)	6.8	+ 5	/	/	/	-	+	-
Ribonuclease A	2.5 (7.5)	6.5	+ 8	-	+	-	=	+	-
Insulin	0.75 (1.0)	9.5	- 9	=	+	-	-	+	-

Waiting times (w.t.), crystallization densities (c.d.) and average crystal size (d) are reported as relative values, equal (=), higher (+) or lower (-) in comparison to those for the reference.
[#] The value refers to the lowest starting concentration of protein at which crystals formed on functionalised surface.
* The protein net charge at the crystallization pH was calculated using the pI, MW, titration curve tool from ExPASy server.
[a] The protein was crystallized at pH 6.0; [b] The protein was crystallized at pH 9.0.
/ Crystallization trials have not been carried out.

It has been demonstrated experimentally and theoretically that the interaction between proteins and surfaces promoting nucleation requires weak forces that concentrate proteins in the proximity of the surface (Chayen *et al.*, 2006; Sear, 2007). While the physics and chemistry which govern homogeneous nucleation of proteins have been accurately investigated (Garcìa-Ruiz, 2003), research on the processes that control their heterogeneous nucleation is still in progress. Recent studies suggest that the heterogeneous nucleation of protein crystals cannot be described in the same way as the heterogeneous nucleation of ionic solids, in which an epitaxial mechanism of nucleation is commonly involved (Galkin *et al.*, 2000; Sear, 2007). Protein crystals are stabilised by weak lattice energies (McPherson, 1999). Thus, the interaction between proteins and heterogeneous surface should be weak enough to let protein molecules be free to reorganise themselves in rotation and translation to associate in stable crystal nuclei. The ionisable functional groups present on the surfaces should allow protein–surface interactions by electrostatic forces. Since the superficial charge density can be modulated, the force of the electrostatic interaction can be also varied. When attractive interactions are present, protein molecules tend to concentrate close to the surface, locally

increasing the supersaturation that favours crystal nucleation and growth. In addition to this effect, the surface can also stabilise already formed nuclei by interaction with a specific crystal face or it can favour the formation of crystal nuclei by clustering ordered motifs of protein molecules. It can be supposed (similarly to the concept used to explain the nucleation properties of glass substrates with pores of a wide range of sizes; Chayen *et al.*, 2006) that surfaces with a random distribution of functional groups offer many different potential patterns of interaction with crystal nuclei. This can be described as a controlled mechanism with the surface playing an active role in the nucleation process. In the presence of repulsive forces, the protein molecule does not settle in the thin layer close to the surface. As a consequence, it can be supposed that the protein concentrates in the upper layer and its crystallisation can be achieved using a lower starting protein concentration. As the surface does not play a direct role in affecting the crystallisation process in this case, this mechanism is described as surface-induced. A schematic representation of these two mechanisms is shown in Fig. 21.

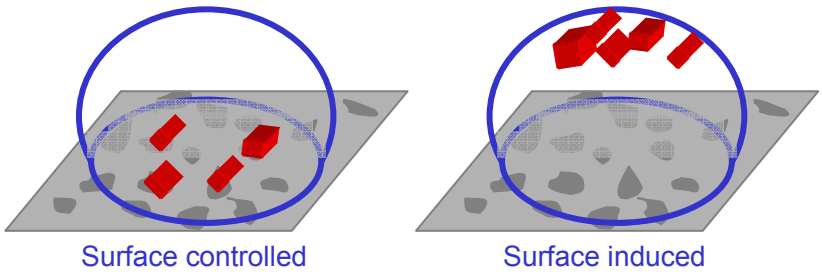

Figure 21. Schematic representation of surface effects on protein crystallization. Crystallization can be controlled (left) or induced (right). In the first case protein nucleation occurs on the surface, which stabilises the nuclei. In the second case repulsive forces are present between the surface and the protein. These move the proteins out from the surface and increase their concentration in a thin layer in its proximity (dashed circles). In the scheme, drops and crystals are not shown on the same scale.

In conclusion, it has been shown that functionalised surfaces are able to induce protein crystallisation at concentrations lower than those required by the reference surface. The random distribution of the functional groups on the surfaces results in a reduction of the waiting time occurring in some cases, which may suggest surface stabilisation of the crystal nuclei. Thus, it is conceivable to design surfaces suitable to control nucleation kinetics in order to resolve the conflict between the necessity of nucleation at low supersaturation and the need for a protein concentration sufficient to sustain crystal growth.

2.4 PROTEINS CRYSTALLISATION ON FUNCTIONALISED SURFACES IN AN INNOVATIVE DEVICE: THE CRYSTALLISATION MUSHROOM

The effect of sulfonated polystyrene films and silanised mica on crystal nucleation and growth of two model proteins, thaumatin and glucose isomerase, has been investigated together with a crystallisation device, the Crystallisation Mushroom (Triana S&T) (García-Ruiz *et al.*, 2005). It offers the advantage to perform simultaneously crystallisation experiments under identical environmental conditions. Some of the experiments have been carried out in the *Laboratorio de Estudios Cristalográficos* of Professor Garzia Ruiz in Granada (Spain) thanks to the financial support of the bilateral project 0013890 **CNR/CSIC (**2007/2008). The groups of Bologna (Italy) and Granada (Spain) have a parallel experience in the studies of new strategies for macromolecular crystallisation. The bilateral project has been finalised to join the experiences of each group to design and realise a crystallisation system that has much as possible a "universal" applicability and allows to crystallise a wide number of uncrystallised proteins. For this reason, three months during the PhD period have been spent in Spain to the development of this new technique to promote and ease the protein crystals nucleation and growth.

2.4.1 Set up of the crystallisation experiments: The crystallisation trials were carried out using the crystallisation mushroom (Fig. 22), a glass modified essicator to perform sitting drop vapour diffusion experiments under identical environmental conditions. It allows to follow the equilibration of 12 drops against a unique reservoir (5 mL). The final volume of each drop was 6 µl. Trials were set up at 293 K in an incubator.

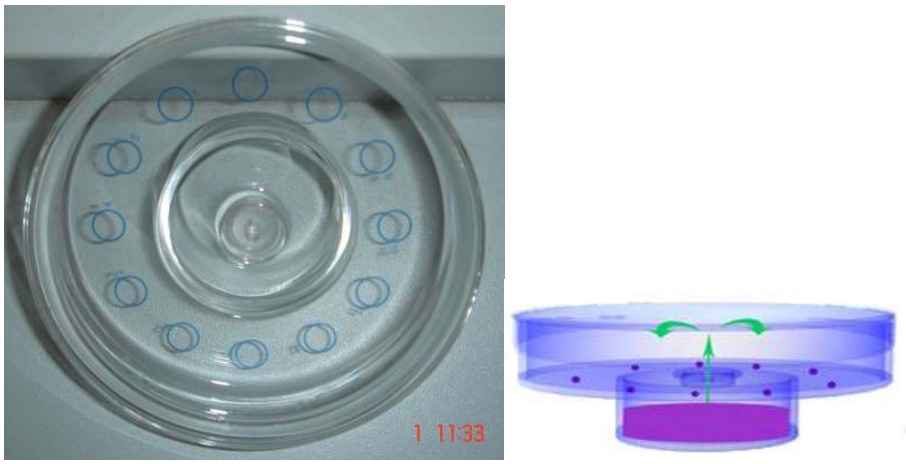

Figure 22. The crystallisation mushroom.

The model proteins used for these experiments were thaumatin from *Thaumatococcus daniellii* and glucose isomerase purified from *Streptomyces rubiginosus*. Thaumatin is a low-calorie protein sweetener and flavour modifier, glucose isomerase (D-glucose ketoisomerase) is an enzyme that converts glucose to fructose.

Firstly, several crystallisation mushrooms were set up for both model proteins in which 12 drops were made mixing the protein solution (three protein concentrations could be tested at the same time each experiment) and the reservoir solution in four different ratios: 1:1, 1:2, 1:3 and 2:1. Before to test the functionalised surfaces, it was needed to adapt the crystallisation conditions reported in literature for the used model proteins, thaumatin and glucose isomerase, to the new system, the crystallisation mushroom. A wide area of the diagram phase of each model protein could be screened in every performed experiment. The aim of this step was to identify the crystallisation conditions that gave at the same time countable number of crystals of sizes as big as possible. The screening of thaumatin diagram phase carrying out experiments in the crystallisation mushrooms showed that in this system countable number of crystals (less then 20) with big average sizes (0.40 mm) were generally obtained dissolving the protein in milliQ water at starting concentration of 40 mg/mL using 0.26 M Na/K tartrate and 0.1 M KH_2PO_4 pH 6.8 as reservoir solution. Thaumatin has theoretical pI 8.05 and at the crystallisation pH 6.8, net charge of + 4.7.

Glucose isomerase was purchased as a crystalline suspension in an ammonium sulfate-rich solution, dialysed and successively concentrated in 100 mM HEPES pH 7.0. Glucose isomerase was crystallised at high and low ionic strength: in the first case, the best crystallisation condition was determined to be a reservoir solution of 0.8 M $(NH_4)_2SO_4$ and 100 mM HEPES pH 7.0 with starting protein concentration of 35 mg/mL, while in the second case the reservoir solution was composed by 10% (w/w) PEG 1000 and 0.2 M $MgCl_2$ and the starting protein concentration was 13 mg/mL.

Glucose isomerase has theoretical pI 5.14 and at the crystallisation pH 7.0, net charge of -15.8. For both model proteins, theoretical pI and net charge at corresponding crystallisation pH were calculated using protein calculator v3.3 (www.scripps.edu).

Once reservoir solution and protein concentration giving few and big crystals were determined, experiments in the crystallisation mushroom were performed using functionalised surfaces. In each experiment, one of the twelve positions in the crystallisation mushroom was used as reference (the device is made of siliconised glass and can be considered as a common siliconised cover slide used in the hanging drop technique) while the 6 types of sulfonated polystyrene films (with respect to the experiments previously described, also sulfonated polystyrene films at 24 h were tested) the five types of silanised mica were attached each at one of the eleven remaining positions with double-steak tape. In a thirteenth position not sulfonated polystyrene film (polyst. 0') was added and tested

(Fig. 23 a,b). The starting protein concentration of each protein was lowered until to reach the concentration at which no crystals appeared on reference. For each tested protein concentration of both model proteins, the experiments were repeated at least five times and the reported data were calculated as median of obtained results. In order to estimate the median waiting time, all experiments were monitored every day by optical microscopy and in each drop number and medium size of crystals were noted.

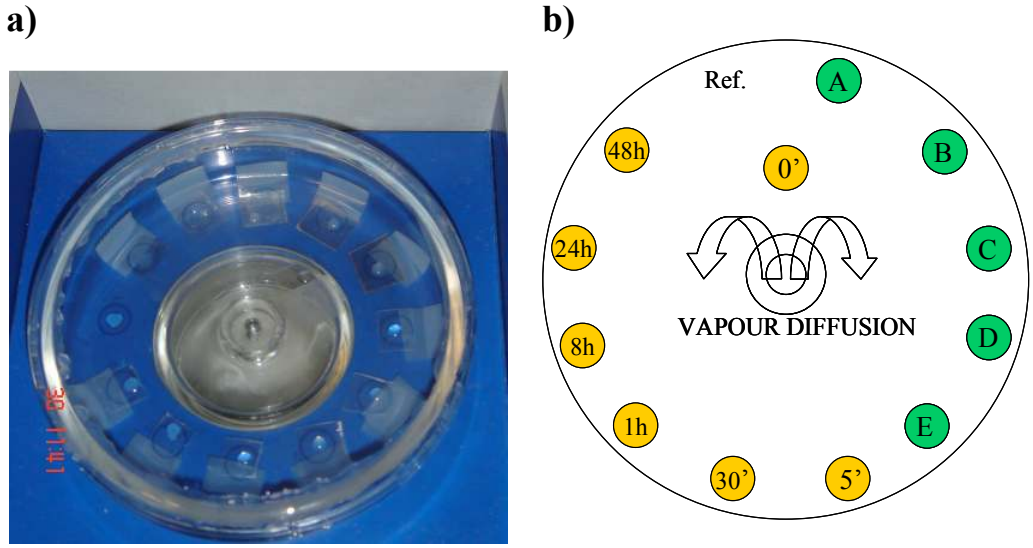

Figure 23. (a) the crystallisation mushroom with the functionalised surfaces; (b) schematic representation of crystallisation experiments with functionalised surfaces into the crystallisation mushroom. Reference, silanised micas and polystyrene films are represented in white, green and yellow, respectively. The letters A-E indicate the different mixtures used in the silanisation of mica sheets. For sulfonated polystyrene films, the different times of sulfonation are reported.

2.4.2 Crystallisation of thaumatin on the functionalised surfaces in the crystallisation mushroom: Thaumatin has been crystallised at different protein concentrations, from 40 mg/mL to 15 mg/mL. At the latter concentration crystals always appeared using surfaces but never with the reference (Table 8). At high protein concentrations (about 30 mg/mL), there was not substantial difference between the use of reference or functionalised surfaces. In fact, median waiting time, crystallisation density, and average crystal size were in the same order of magnitude (data not reported).

Table 8. Median waiting time (w.t.), crystallisation density (c.d.) and average crystal sizes (D) for thaumatin grown on functionalised surfaces in the crystallisation mushroom.

	30.0 mg/ml			25.0 mg/ml			20.0 mg/ml			15.0 mg/ml		
	w.t. (d)*	c.d.† (n.c./mm^2)	D‡ (mm)	w.t. (d)	c.d.† (n.c./mm^2)	D‡ (mm)	w.t (d)	c.d.† (n.c./mm^2)	D‡ (mm)	w.t. (d)	c.d.† (n.c./mm^2)	D‡ (mm)
refer.#	15	~10	0.38	30	~10	0.30	25	~10	0.23	-----	----	----
mica A	13	< 5	0.30	14	~10	0.38	11	< 30	0.26	24	~15	0.11
mica B	13	mass.§	0.23	14	< 5	0.38	9	~30	0.15	21	~15	0.20
mica C	9	mass.§	0.38	14	< 5	0.38	9	~30	0.30	21	~25	0.30
mica D	9	mass.§	0.38	15	< 5	0.31	19	< 30	0.23	17	~20	0.30
mica E	9	mass.§	0.38	22	< 5	0.56	7	< 40	0.19	17	~20	0.30
polyst. 0’	7	~20	0.23	15	mass.§	0.15	-	-	-	-	-	-
polyst. 5’	14	~15	0.38	19	< 5	0.60	18	~10	0.30	17	~20	0.34
polyst. 30’	13	~10	0.22	19	~10	0.23	18	mass.§	0.15	21	~15	0.26
polyst. 1h	14	~20	0.30	26	< 5	0.38	18	~10	0.23	21	~10	0.23
polyst. 8h	13	~10	0.23	14	< 10	0.38	18	~10	0.38	21	mass.§	0.15
polyst. 24h	14	~20	0.38	14	~10	0.23	24	~15	0.30	24	< 40	0.23
polyst. 48h	9	~15	0.38	20	~10	0.23	14	mass.§	0.15	24	~15	0.26

siliconised glass of the crystallisation mushroom.
† Number of crystals observed per surface unit (mm^2).
‡ The value refers to the average length of the longest axis of the crystal calculated from a set of several dozen crystals.
§ Massive crystallization
* days

From starting protein concentration equal or lower than 30 mg/mL, the surfaces influence the crystallisation process differently from the reference. At 30 mg/mL, micas C, D, E, which have the highest contents of exposed hydrophilic ionisable groups, decreased the median waiting time of about 1 week with respect to the reference. Also polystyrene films at the highest degree of sulfonation (polyst. 48h) affected this parameter in the same way. Interestingly, not sulfonated polystyrene films halved the median waiting time. All micas exposing amino groups (mica B-E) drastically increased the crystallisation density compared with the reference, although the average crystal sizes did not significantly change for any mica excepted for mica B. At the lowest and highest times of sulfonation (polyst. 5’ and 48h), the crystallisation density was 33% higher than that one of reference, although crystals had same sizes.

For the remaining kind of polystyrene films, the crystal density was double using polyst. 1h and 24h with crystal sizes slightly smaller (0.30 mm) or identical to reference (0.38 mm), respectively. On the contrary, on polyst. 30’ and 8h an amount of crystals identical to the reference grew but in this case the average dimensions of the crystals were strongly reduced to 0.23 mm. An influence on

the two parameters was present also using not sulfonated polystyrene films (about 20 crystals/mm^3 with size of 0.23 mm).

At 25 mg/mL, the reduction of the median waiting time became much more evident for both functionalised surfaces, all micas and sulfonated polystyrene films, with respect to the reference. Micas A-D halved this parameter while for mica E the reduction, even if present, was less marked than that caused by micas A-D. At this concentration, the median waiting time using sulfonated polystyrene films was always lower than that of reference, but without a clear trend using from polyst. 5'-48h. On the contrary, polyst. 0' halved the median waiting time compared with the reference, although it does not expose any chemical ionisable groups. At this concentration, high increase of the crystal density wasn't observed for any functionalised surface, but it became substantial using not sulfonated polystyrene films, unique case in which also the average crystal sizes (0.15 mm) were strongly reduced with respect to the reference (0.30 mm).

At 20 mg/mL the effect of the two functionalised surfaces was marked (Fig. 24) aswell the presence of exposed ionisable groups on the t surfaces became an important requirement to favour the nucleation event. This was confirmed by the fact that no crystals appeared on not sulfonated polystyrene films at concentration equal or below 20 mg/mL.

With respect to the reference, the median waiting time was more than halved using mica A, the less charged mica, and reduced of three times and half using mica E, the most hydrophilic mica. Going from mica A to mica E, the crystal density increased showing values three times equal or greater than the reference. Only using mica B and E the average crystal sizes were slightly lower than those of reference.

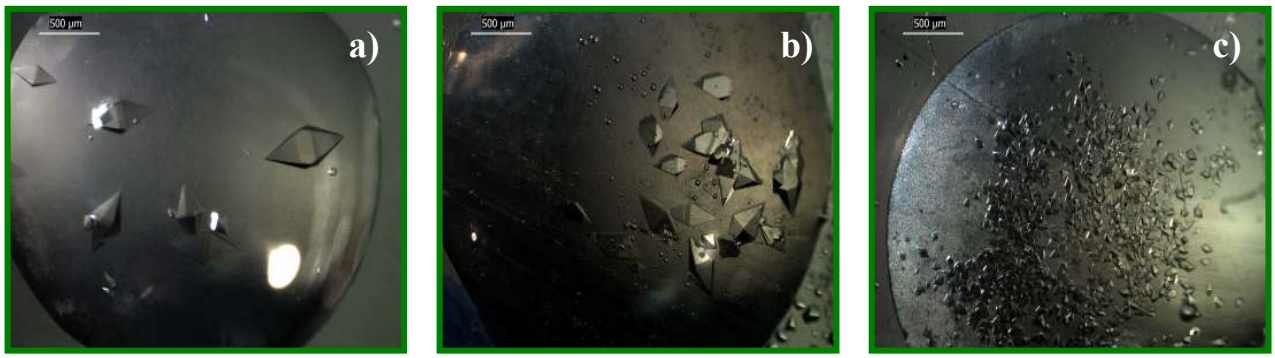

Figure 24. Optical micrographs of thaumatin crystals grown on (a) the reference, (b) mica E, (c) polyst. 48h. The crystals were grown using starting protein concentration of 20 mg/ml.

The median waiting time of reference (25 days) was reduced to 14 days on polyst. 48h, which also showed a strong effect on thaumatin crystallisation density compared with the reference. On it, a massive crystallisation occurred while on reference few crystals grew. Moreover, crystals grown on polyst. 48h were smaller (0.15 mm) than those grown on reference (0.23 mm).
At 15 mg/mL, crystals did not growon reference, while they always appeared when functionalised surfaced were used. The median waiting time decreased going from mica A to mica E, but increased going from polyst. 5' to polyst. 48h. All micas and sulfonated polystyrene films seemed to influence the crystallisation density at the same manner, excepted for polyst. 8h and 24h that resulted more efficient. The crystals with the smallest average crystal sizes grew on mica A and polyst. 8h.

2.4.3 Crystallisation of glucose isomerase on the functionalised surfaces in the crystallisation mushroom: Glucose isomerase was crystallised using as precipitant salts or polymers in order to investigate the behaviour of the protein at high or low ionic strength. The presence of the salt in solution influences the nature of protein-surface electrostatic interactions and consequentially the entire crystallisation process.
At high ionic strength it was possible only to determine the optimal crystallisation conditions for this protein in the crystallisation mushroom and at the moment experiments of crystallisation on functionalised surfaces are being carried out but no clear results have been obtained yet.
On the contrary, at low ionic strength after identifying the optimal crystallisation condition of ribonuclease A in the crystallisation mushroom, experiments with functionalised surfaces-mushroom were carried out. Glucose isomerase was crystallised in a protein concentration range going from 13 mg/mL to 7 mg/mL (Table 9).
At the highest protein concentration, crystals always appeared earlier on micas and polystyrene sulfonated films than on reference. In fact, all functionalised surfaces were able to decrease the median waiting time from 120 minutes (reference) to 30 minutes, except mica C, for which the median waiting time was of 1 h. With respect to the reference, not sulfonated polystyrene films also decreased of four times the median waiting time. The influence of functionalised surfaces on median waiting time was lost at concentration lower than 13 mg/mL.
At 13 mg/mL, crystallisation density of all micas was always higher than that one of reference (Fig. 25). Amongst the five tested micas, the two most hydrophobic (mica A-B) showed massive crystals growth. When the amount of amminosilane used to functionalised mica was higher than 30% (v/v) (micas C-E), the effect was reduced. The crystallisation density of mica C-E still remained much more higher compared with reference, increasing going from mica C to E. Also sulfonated

polystyrene films increased the crystallisation density with respect to reference, but no clear effect was observed. At the lowest (polyst. 0') and highest (polyst. 48h) sulfonation times, the less marked influence on number of grown crystals was detected.

At a concentration of 8 mg/mL, only few crystals grew on reference and not sulfonated polystyrene films (less than 5). While sulfonated polystyrene films seemed not to affect strongly the crystallisation density with respect to reference, completely hydrophobic (mica A) and hydrophilic (mica E) micas were able to induce the highest increase of the crystallisation density, especially marked for mica E. Moreover, for mica E the reduction of crystals sizes (0.08 mm) was well evident with respect to reference (0.14 mm). The sizes of crystals were also of 0.08 mm when polyst 30',1h, 8h and 48h were used as nucleant substrates. Lowering the concentration from 8 to 7 mg/mL, crystals did not appear anymore on reference.

Table 9. Median waiting time (w.t.), crystallisation density (c.d.) and average crystal sizes (d) for glucose isomerase grown in the presence of PEG 1000 on functionalised surfaces in the crystallisation mushroom.

	13 mg/mL			8.0 mg/mL			7.0 mg/mL		
	w.t. (min)	c.d.† (n.c./mm^2)	D‡ (mm)	w.t. (min)	c.d.† (n.c./mm^2)	D‡ (mm)	w.t. (days)	c.d.† (n.c./mm^2)	D‡ (mm)
refer.#	120	<10	0.20	240	<5	0.14	---	---	---
mica A	30	mass.§	0.20	240	~30	0.14	1	~10	0.11
mica B	30	mass.§	0.20	12h	~20	0.10	1	mass.§	0.11
mica C	60	>50	0.20	24h	~10	0.14	1	> 20	0.15
mica D	30	>100	0.18	240	~10	0.14	1	mass.§	0.15
mica E	30	>200	0.20	240	mass.§	0.08	1	~10	0.18
polyst. 0'	30	15	0.20	24h	<5	0.15	1	~10	0.15
polyst. 5'	30	mass.§	0.20	240	~10	0.17	1	~10	0.76
polyst. 30'	30	>50	0.18	240	~10	0.08	1	~10	0.38
polyst. 1h	30	>100	0.18	240	~10	0.08	1	~10	0.38
polyst. 8h	30	mass.§	0.20	240	~10	0.08	1	>50	0.38
polyst. 24h	30	mass.§	0.18	240	~15	0.17	1	~10	0.15
polyst. 48h	30	15	0.20	240	~10	0.08	2	~10	0.15

siliconised glass of the crystallisation mushroom.
† Number of crystals observed per surface unit (mm^2).
‡ The value refers to the average length of the longest axis of the crystal calculated from a set of several dozen crystals.
§ Massive crystallization.

At the most 10 crystals grew on micas A and E and all polystyrene films (except polyst. 8h), more than 20 on mica C and massive crystallisation occurred on mica B and D. The crystals sizes did not show a well defined trend and it was not possible to establish a correlation between the presence of chemical ionisable groups exposed on the surfaces and this parameter.

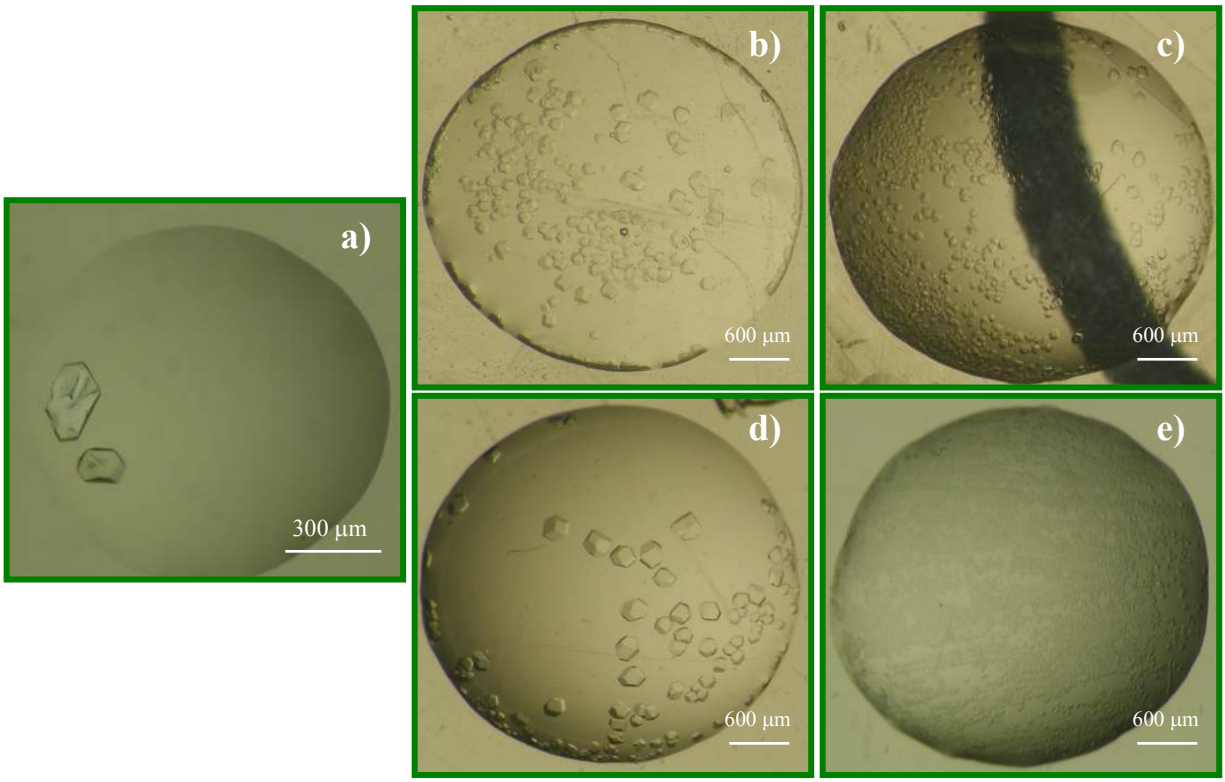

Figure 25. Optical micrographs of glucose isomerase crystals grown on (**a**) the reference, (b) mica D, (**c**) mica E, (**d**), polyst. 30' and (**e**) polyst. 8h. The crystals were grown using a starting protein concentration of 13 mg/ml.

2.4.4 The behaviour of functionalised surfaces on model proteins crystallisation in the crystallisation mushroom: For the first time, a modified essicator has been used as alternative tool for the crystallisation of proteins. It offers the advantage to perform in the same physical-chemical environment different crystallization trials. Since the crystallisation process is influenced by uncountable variables and it is difficult to establish which of them will play the crucial role for the obtainment of crystals, performing experiments in identical conditions makes easier to compare the parameters affecting the process. That could be useful to completely understand the mechanism driving the crystallisation event. The crystallisation mushroom is a tool with promising and excellent potentialities in the field of crystallisation. The first step of the previously described work, that was the research of the crystallisation conditions for model proteins that it is well know to easy crystallise, has upfront highlighted the complexity of using this tool.

Both functionalised surfaces always decreased the waiting time of thaumatin and moreover, at the highest tested protein concentration (30-25 mg/mL), polyst. 0', the surface not exposing ionisable chemical but only hydrophobic groups, showed the best capacity in affecting this parameter. At high protein concentration, it seems that the only presence of a foreign substrate can help the process regardless of the kind and amount of exposed chemical ionisable groups. As the protein concentration is decreased, the presence of ionisable groups linked to the surface becomes necessary to induce crystal growth and no crystal grew on not sulfonated polystyrene. Reached the limit concentration of 15 mg/mL, crystals stopped to grow also on the reference and between the functionalised surfaces no substantial differences in term of crystallisation density were detected. At this concentration mica E, the most hydrophilic and positively charged mica, and polyst. 5', the polystyrene film with the lowest amount of hydrophilic exposed groups, were the most efficient surfaces in decreasing the waiting time, while the less efficient surfaces were mica A that is completely hydrophobic, and polyst. 48h with the highest content of exposed negative groups. The waiting time decreased together with an increment of exposed positive groups (going from mica A to mica E) and a decrease of exposed negative groups (going from polyst. 48h to polyst. 5'). In order to understand how the presence of ionisable groups on the nucleanting substrate influences and induces the nucleation event and the nature of relationships becoming established between protein and surface, it is necessary to study the behaviour of others model proteins in the system functionalised surfaces-mushroom. For this reason, the lysozyme will be used to carry out experiments that could elucidate the possible roles of ionisable chemical groups in the process of macromolecular crystallization. A deeper analysis of the system and of the interaction protein-surface will be done by means of a comparison between the data obtained with thaumatin and those that will be obtained with lysozyme. The crystallisation pH of Lysozyme is 4.5 and at this pH the net charge is +2, very close to the neutrality (Table 7, page 50).

Regarding glucose isomerase, only at high ionic strength, some results, even if difficult to interpret, have been obtained. These results highlight that functionalised surfaces can influence nucleation starting from the highest tested protein concentration at which decreased the waiting time and increased the crystallisation density with respect to the reference. At the low concentration of 7 mg/mL, crystals did not grow on the reference but always on all the functionalised surfaces. The difficulty in interpreting and rationalising the obtained results, could be due to the presence of PEG in solution.

PEG competes with protein for water and exert excluded volume effects (which vary according to the length of the polymer). However, unlike salts, PEG decreases the effective dielectric constant of

the solution and increases the effective distance over which protein electrostatic effects occur. These effects need to be explored carrying out further crystallisation trials.

2.5 REFERENCES

- Addadi, L., Moradian, J., Shay, E., Maroudas, N.G., Weiner, S. A chemical model for the cooperation of sulfates and carboxylates in calcite crystal nucleation: Relevance to biomineralization. (1987) *Proc. Natl. Acad. Sci. USA* **84**, 2732-2736.
- Bergfors, T. Seeds to crystals. (2003) *J. Struct. Biol.* **142**, 66-76.
- Biino, G.G., Gröning. P. Cleavage mechanism and surface chemical characterization of phengitic Muscovite and Muscovite as constrained by X-Ray Photoelectron Spectroscopy. (1998) *Phys. Chem. Minerals* **25**, 168-181.
- Cacciuto, A., Auer, S., Frenkel, D. Onset of heterogeneous crystal nucleation in colloidal suspensions. (2004) *Nature* **428**, 404-406.
- Chayen, N.E., Saridakis, E. Is lysozyme really the ideal model protein? (2001) *J. Cryst. Growth* **232(1-4)**, 262-264.
- Chayen, N.E., Saridakis, E., El-Bahar, R., Nemirovsky, Y. Porous silicon: an effective nucleation-inducing material for protein crystallisation. (2001) *J. Mol. Biol.* **312(4)**, 591-595.
- Chayen, N.E., Saridakis, E., Sear, R.P. Experiment and theory for heterogeneous nucleation of protein crystals in a porous medium. (2006) *PNAS* **103(3),** 597-601.
- Chayen, N.E., Saridakis, E. Protein crystallisation: from purified protein to diffraction-quality crystal. (2008) *Nature Methods* **5**, 147-153.
- Chen, C., Li, H., Davis, M.E. Studies on mesoporous materials : Synthesis and characterization of MCM-41. (1993) *Microporous Mater.* **2,** 17-26.
- Crampton, N., Bonass, W.A., Kirkham, J., Thomson, N.H. Formation of aminosilane-functionalised mica for atomic force microscopy imaging of DNA. (2005) *Langmuir* **21**, 7884-7891.
- D'Arcy, A., Mac Sweeney, A., Haber, A. Using natural seeding material to generate nucleation in protein crystallisation experiments. (2003) *Acta Crystallogr* **D59**, 1343-1346.
- Davis, M.E., Montes, C., Hathaway, P.E., Arhancet, J.P., Hasha, D.L., Garces, J.M. Physicochemical properties of VPI-5. (1989) *J. Am. Chem. Soc.* **111(11)**, 3919-3924.
- Dodson, E.J., Dodson, G.G., Lewitova, A., Sabesan, M. Zinc-free cubic pig insulin: crystallisation and structure determination. (1978) *J. Mol. Biol.* **125(3)**, 387-396.
- Edwards, A.M., Darst, S.A., Hemming, S.A., Li, Y., Kornberg, R.D. Epitaxial growth of protein crystals on lipid layers. (1994) *Nature Struct. Biol.* **1**, 195-197.
- Falini, G., Fermani, S., Conforti, G., Ripamonti, A. Protein crystallisation on chemically modified mica surfaces. (2002) *Acta Crystallogr.* **D58,** 1649-1652.
- Fang, J., Knobler, C.M. Control of density in self-assembled organosilane monolayers by Langmuir-Blodgett deposition. (1995) *J. Phys. Chem.* **99**, 10425-10429.

- Fermani, S., Falini, G., Minnucci, M., Ripamonti, A. Protein crystallisation on polymeric film surfaces. (2001) *J. Cryst. Growth* **224**, 327-334.
- Galkin, O., Vekilov, P.G. Control of protein crystal nucleation around the metastable liquid–liquid phase boundary. (2000) *J. Am. Chem. Soc.* **122**, 156-163.
- García -Ruiz, J.M. Nucleation of protein crystals. (2003) *J. Struct. Biol.* **142**, 22-31.
- García-Ruiz, J.M., Hernández-Hernández, M.A., Gómez-Morales, J. Crystallisation Mushroom: a new crystallisation tool by vapour diffusion technique. *Industrial Crystallisation* **2005**, VDI-Berichte Nr.1901, 963-968.
- Georgieva, D.G., Kuil, M.E., Oosterkamp, T.H., Zandbergen, H.W., Abrahams, J.P. Heterogeneous nucleation of three-dimensional protein nanocrystals. (2007) *Acta Crystallogr.* **D63**, 564-570.
- Grzesiak, A.L., Matzger, A.J. Selection of protein crystal forms facilitated by polymer-induced heteronucleation. (2008) *Cryst. Growth Des.* **8 (1)**, 347-350.
- Hemming, S.A., Bochkarev, A., Darst, S.A., Kornberg, R.D., Ala, P., Yang, D.S.C., Edwards, A.M. The mechanism of protein crystal growth from lipid layers. (1995) *J. Mol. Biol.* **246**, 308-316.
- Kallio, J.M., Hakulinen, N., Kallio, J.P., Niemi, M.H., Kärkkäinen, S., Rouvinen, J. The contribution of polystyrene nanospheres towards the crystallization of proteins. (2009) *PLoS ONE* **4(1)**, e4198.
- King, M.V., Magdoff, B.S., Adelman, M.B., Harker, D. Crystalline forms of bovine pancreatic ribonuclease: techniques of preparation, unit cells, and space groups. (1956) *Acta Crystallogr* . **9**, 460-465.
- Liu, Y.X., Wang, X.J., Lu, J., Ching, C.B. Influence of the roughness, topography, andphysicochemical properties of chemically modified surfaces on the heterogeneous nucleation of protein crystals. (2007) *J. Phys. Chem. B* **111**, 13971-13978.
- Luda, S., Shlyaktenko, A., Gall, J., Jeffrey, W., David, D., Hawn, D., Lyubchenko, Y. Atomic force microscopy imaging of dna covalently immobilized on a functionalised mica substrate. (1999) *Biophys. J.* **77**, 568-574.
- Lyubchenko, Y., Shlyakhtenko, L., Harrington, R., Oden, P., Lindsay, S. Atomic force microscopy of long DNA: imaging in air and under water. (1993) *Proc. Natl Acad. Sci. USA* **90**, 2137-2140.
- McPherson, A., Shlichta, P.J. Facilitation of the growth of protein crystals by heterogeneous/epitaxial nucleation. (1987) *J. Cryst. Growth* **85**, 206-214.
- McPherson, A., Shlichta, P. Heterogeneous and epitaxial nucleation of protein crystals on mineral surfaces. (1988) *Science* **239(4838)**, 385-387.
- McPherson, A. Crystallisation of biological macromolecules (edn 1), Cold Spring Harbor Laboratory Press, Woodbury, NY (1999).
- Nanev, C.N. Protein crystal nucleation: Recent notions. (2007) *Cryst. Res. Technol.* **42**, 4-12.
- Nanev, C.N. On the slow kinetics of protein crystallisation. (2007) *Cryst. Growth Des*. **7**, 1533-1540.
- Nicolini, C., Pechkova, E. Nanocrystallography: an emerging technology for structural proteomics. (2004) *Expert Rev. Proteomics* **1**, 253-256.

- Pechkova, E., Nicolini, C. Atomic structure of a CK2α human kinase by microfocus diffraction of extra-small microcrystals grown with nanobiofilm template. (2004) *J. Cell. Biochem.* **91**, 1010-1020.
- Saridakis, E., Chayen, N.E. Towards a 'universal' nucleant for protein crystallisation. In press, available on line since December 2008.
- Sanjoh, A., Tsukihara, T.J. Spatiotemporal protein crystal growth studies using microfluidic silicon devices. (1999) *J. Cryst. Growth* **196**, 691-702.
- Sanjoh, A., Tsukihara, T., Gorti, S. Surface-potential controlled Si-microarray devices for heterogeneous protein crystallisation screening. (2001) *J. Cryst. Growth* **232**, 618-628.
- Sear, R.P. Nucleation: theory and applications to protein solutions and colloidal suspensions. (2007) *J. Phys. Condens. Matter* **19**, 033101.
- Sugahara, M., Asada, Y., Morikawa, Y., Kageyama, Y., Kunishima, N. Nucleant-mediated protein crystallisation with the application of microporous synthetic zeolites. (2008) *Acta Cryst.* **D64**, 686-695.
- Takehara, M., Ino, K., Takakusagi, Y., Oshikane, H., Nureki, O., Ebina, T., Mizukami, F., Sakaguchi, K. Use of layer silicate for protein crystallisation: Effects of Micromica and chlorite powders in hanging drops. (2008) *Anal. Biochem.* **373**, 322-329.
- Thakur, A.S., Robin, G., Guncar, G., Saunders, N.F.W., Newman, J., Martin, J.L., Kobe, B. Improved success of sparse matrix protein crystallisation screening with heterogeneous nucleating agents. (2007) *PLoS ONE* **2(10)**, e1091.
- Tosi, G., Fermani, F., Falini, G., Gavira Gallardo, J.A., Garcìa Ruiz, J.M. Crystallisation of proteins on functionalised surfaces. (2008) *Acta Cryst.* **D64**, 1054-106.
- Tsekova, D., Popova, S., Nanev, C. Nucleation rate determination by a concentration pulse technique: application on ferritin crystals to show the effect of surface treatment of a substrate. (2002) *Acta Crystallogr.* **D58**, 1588-1592.
- Utracki, L.A., Sepehr, M., Boccaleri, E. Synthetic, layered nanoparticles for polymeric nanocomposites (PNCs). (2007) *Polym. Adv. Technol.* **18**, 1-37.
- Zhanga, X., Zhanga, P., Wei, K., Wanga, Y., Ma., R. The study of continuous membrane crystallisation on lysozyme. (2008) *Desalination* **219**, 101-117.

CHAPTER 3: THREE-DIMENSIONAL STRUCTURE OF RIBOSOME INACTIVATING PROTEINS (RIPs)

3.1 INTRODUCTION: classification, enzymatic activity, toxicity of RIPs

At the end of 19th century, the toxic principle of castor bean was identified to be a protein, called ricin by Stillmark (Stillmark, 1888; 1889). The identification of ricin, from the seeds of *Ricinus communis*, was an important milestone in biochemistry because for the first time a well-defined biological activity was ascribed to a plant protein. Moreover, ricin and also abrin, a similar toxic protein from the seeds of *Abrus precatorius*, played an important role in the early development of immunology. In fact, they were used by Paul Ehrlich to immunise mice raising the first antibodies (Ehrlich, 1881a; 1881b). Seventy years later, the three-dimensional structure of ricin and abrin were resolved by Montfort and Tahirov, respectively (Montfort *et al.*, 1987; Tahirov *et al.*, 1995). They were found to be composed of two polypeptide chains, an enzymatic A chain that damaged ribosomes, and a lectinic B chain, galactose specific, capable of binding to cell walls (Olsnes *et al.*, 1973(a,b); Olsnes 2004). Other and more numerous proteins were found that resemble the A chains of these toxins, in that they have a similar structure and the same activity on ribosomes. For these proteins were introduced the denomination of RIPs (Ribosome Inactivating Proteins) (Stirpe, 1982) and since then several reviews have provided lists of RIPs (Van Damme *et al.*, 2001; Girbés *et al.* 2004; Stirpe, 2004; Stirpe *et al.*, 2006) (Table 10).

The mechanism of the ribosomal damage was discovered by Endo *et al.* (1987), who found that ricin cleaved the glycosidic bond of a single adenine residue (A_{4324} in rat liver rRNA) (Fig. 26). This residue is adjacent to the site of cleavage of rRNA by α-sarcin, in a tetranucleotide $GA_{4324}GA$ in a highly conserved loop at the top of a stem, for this called α-sarcin/ricin loop (Endo *et al.*, 1987; Wool *et al*., 1992; Barbieri *et al.*,1993). This observation was extended to other RIPs (Stirpe *et al.*, 1988), which were officially classified as rRNA *N*-glycosidases (EC 3.2.2.22). RIPs catalytically inactivate eukaryotic as well as prokaryotic ribosomes (Barbieri *et al.*, 1993) by removing single adenine residues from the large rRNA (A_{4324} from rat liver 28S rRNA, A_{2660} of E. coli rRNA) and thus interrupting the interaction of elongation factors I and II with the ribosomes and ultimately arresting protein synthesis at the translocation step (Stirpe *et al.*, 1992; Mehta *et al.*, 1998; Tumer *et al.*, 1999; Nielsen *et al.*, 2001; Van Damme *et al.*, 2001). At the cellular level, RIPs (Griffiths *et al.*, 1987; Bergamaschi *et al.*, 1996; Bolognesi *et al.*, 1996; Büssing, 1996; Narayanan *et al.*, 2004) cause apoptosis and subsequently, or at higher doses, severe necrosis both in the organs of poisoned

animals and in cultured cells (Hughes *et al.*, 1996). Some RIPs remove more than one adenine residue per ribosome (Barbieri *et al.*, 1994). In addition to the *N*-glycosidase activity, some RIPs have DNAse, DNA glycosylase, and apurinic pyrimidinic lyase activities (Li *et al.*, 1991; Roncuzzi *et al.*, 1996; Nicolas *et al*., 1997; Nicolas *et al*., 1998; Nicolas *et al*., 2000; Hudak *et al.*, 2000). However, it has been suggested that the sporadically observed nuclease activities are due to contamination by other enzymes (Day *et al.*, 1998; Barbieri *et al.*, 2000; Van Damme *et al.*, 2001), whereas all RIPs tested remove adenine from DNA and some of them also from poly(A) (Barbieri *et al.*, 1997). Their enzymatic activity though may be better described as adenine polynucleotide glycosylase in agreement with the nomenclature utilised for other depurinating enzymes involved in purine removal from DNA. RIPs depurinate also non-mammalian ribosomes, from insects (Zhou *et al.*, 2000), plants (Iglesias *et al.*, 1993), yeast (Roberts *et al.*, 1986), and bacteria (Girbés et al., 1993).

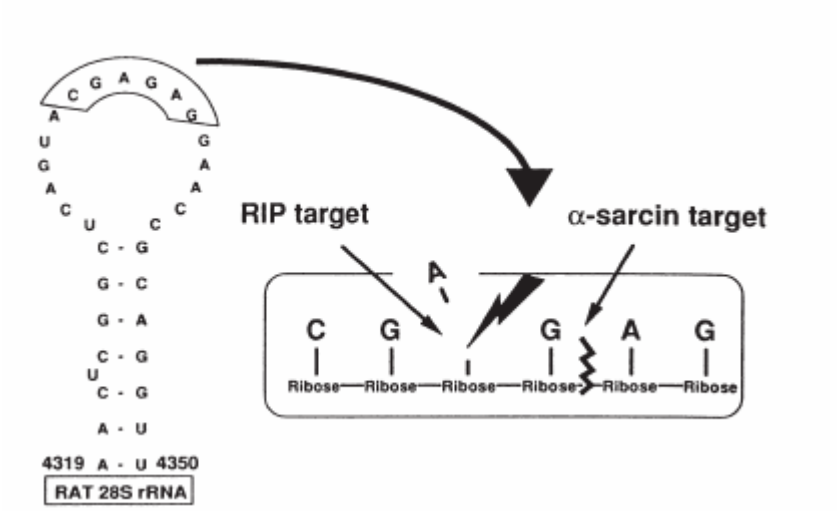

Figure 26. 28S rRNA loop and the site of depurination by RIPs and α-sarcin.

RIPs are classified type 1, type 2, and type 3 (Fig. 27) (Mehta *et al.*, 1998;). Type 1 RIPs, such as pokeweed antiviral protein (PAP), trichosantin and gelonin (Table 10), possess a single enzimatic polypeptide chain with an approximate molecular mass of 30 KDa. They are strongly basic proteins. PAP, (pokeweed antiviral protein) extracted from pokeweed leaves, was the first known identified type 1 RIP and it was found to inhibit protein synthesis by the same mechanism as the A chain of ricin (Irvin, 1983).

Type 2 RIPs, such as ricin, abrin, modeccin and ebulin (Table 10) consist of two disulfide-bonded subunits, one of approximately 30 kDa with enzymic activity (A chain, functional homologue of

type 1) and one of approximately 35 kDa with lectin properties (B chain, a galactose-binding lectin).

Type 3 RIPs have an N-terminal domain closely related to the A chain of RIPs and linked to an unrelated C-terminal domain with unknown function (Reinbothe *et al.*, 1994). Type 3 RIPs, like type 1 RIPs, are single chain proteins that do not contain lectin-binding moiety, but differ from type 1 because they are synthesised as inactive forms that require proteolytic processing of internal regions to form active proteins. A type 3 RIP, a 60-kDa protein (JIP60), has been identified in barley (*Hordeum vulgaris*) (Reinbothe *et al.*, 1994).

Generally, type 1 RIPs, being devoid of a B chain, enter with difficulty into cells and consequently are much less toxic than type 2 RIPs, but become highly toxic if they are introduced into cells by linkage to an appropriate carrier capable of binding to cells. The first demonstration of this was obtained with gelonin conjugated with concanavalin A, which resulted more toxic to cells than the free RIP (Stirpe *et al.*, 1980). Type 1 RIPs can still be internalized by fluid-phase endocytosis. In the case of saporin obtained from *Saponaria officinalis*, it was reported that saporin first binds to the alpha2-macroglobulin receptor on human cells and is then internalised to cytosol.

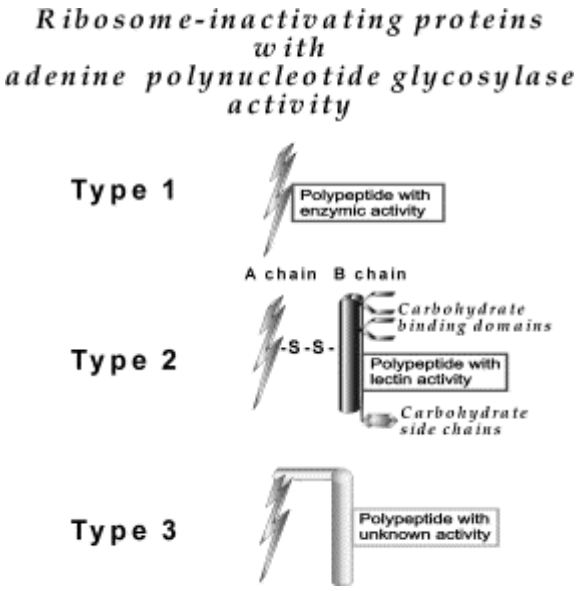

Figure 27. Schematic representation of the structure of ribosome-inactivating proteins. (Courtesy of Professor L. Barbieri).

Some type 2 RIPs are potent toxins and they are regarded to be highly toxic by virtue of their carbohydrate-binding lectin chain, which interacts with cell membranes and facilitates the uptake of RIP into the cytosol space (Barbieri *et al.,* 1993). This occurs through binding of the lectin site to galactosyl-terminated residues on most cells.

Table 10. Ribosome-inactivating proteins isolated from plant tissues.

TYPE 1 RIPs	TYPE 2 RIPs
Agrostins from *Agrostemma githago* seeds Amaranthin from*Amaranthus viridis* leaves Asparins from *Asparagus officinalis* seeds Hispin from *Benincasa hispida* seeds Beetin27 from *Beta vulgaris* leaves Betavulgin from *Beta vulgaris* seedling cDNA Bouganin from *Bougainvillea spectabilis* leaves Bryodins from *Bryonia dioica* leaves roots CCP 25 from *Celosia cristata* CAP30B from *Chenopodium album* plant CAP from *Chenopodium amaranticolor* leaves Camphorin from *Cinnamomum camphora* seeds Colocins from *Citrullus colocynthis* seeds CA-SRI protein from *Clerodendron aculeatum* leaves cDNA CIP-29, CIP-34 from *Clerodendron inerme* leaves Cucurmosin from *Cucurbita moschata* sarcocarp Pepocin from *Cucurbita pepo* sarcocarp Dianthin 29 from *Dianthus barbatus* leaves Dianthins from *Dianthus caryophyllus* leaves Gelonin from *Gelonium multiflorum* seeds Gypsophilin from *Gypsophila elegans* leaves Barley RIP and JIP 60 from *Hordeum vulgare* seeds H. crepitans RIP from *Hura crepitans* latex IRIPs from *Iris hollandica* bulbs Luffaculin from *Luffa acutangola* seeds Luffins from *Luffa cylindrica* seeds Lychnin from *Lychnis chalcedonica* seeds Mapalmin from *Manihot palmate* seeds Manutins from *Manihot utilissima* seeds MOR from *Marah oreganus* seeds ME 1,2 from *Mirabilis expansa* roots, cell cultures Mirabilis antiviral protein, MAP from *Mirabilis jalapa* seeds, roots, tissue culture Momordin II from *Momordica balsamina* seeds Momordins from *Momordica charantia* seeds Momorcochin from *Momordica cochinchinensis* seeds Momorsgrovin from *Momordica grosvenori* seeds Musarmins from *Muscari armeniacum* bulbs Petroglaucin from *Petrocoptis glaucifolia* whole plant Petroglandin from *Petrocoptis grandiflora* whole plant Pokeweed antiviral proteins, PAP from *Phytolacca americana* leaves, seeds, tissue culture, roots P. dioica RIPs *Phytolacca dioica* from seeds, leaves Dodecandrins from *Phytolacca dodecandra* leaves, tissue culture Insularin, PIP from *Phytolacca insularis* leaves, cDNA a- and b-sativin from *Pisum sativum* seeds Ebulin 1, ebulin f from *Sambucus ebulus* leaves and fruits Nigritins from *Sambucus nigra* fruits Sieboldin b from *Sambucus sieboldiana* bark Mexin *Sambucus mexicana* bark Ocymoidin from *S aponaria ocymoides* seeds Saporins from *Saponaria officinalis* leaves, roots, seeds S. cereale RIP from *Secale cereale* seeds Sechiumin from *Sechium edule* seeds SOP from *Spinacia oleracea* root, callus and leaves Stellarin from *Stellaria aquatica* leaves Trichobakin from Trichosanthes sp.Bac Kan 8-98 Trichoanguin from *Trichosanthes anguina* seeds b-trichosanthin from *Trichosanthes cucumeroides* tubers Trichosanthins, trichokirin, TAP 29 from *Trichosanthes kirilowii* roots, seeds Trichomaglin from *Trichosanthes lepiniate* tubers Tritins from *Triticum aestivum* germ, seeds (pyramidatin)*Vaccaria pyramidata* seeds (YLP)*Yucca recurvifolia* leaves Maize RIP from *Zea mays* seeds	Toxic ribosome-inactivating proteins Abrins from *Abrus precatorius* seeds Pulchellin from *Abrus pulchellus* seeds Modeccins from *Adenia digitata* roots Volkensin from *Adenia volkensii* roots P. californicum lectin from *Phoradendron californicum* leaves Ricins from *Ricinus communis* seeds Mistletoe lectin I, viscumin from *Viscum album* leaves VCA from *Viscum album coloratum* plant Non-toxic ribosome-inactivating proteins Cinnamomin from *Cinnamomum camphora* seeds Porrectin from *Cinnamomum porrectum* seeds Foetidissimin from *Cucurbita foetidissima* root EHL from *Eranthis hyemalis* bulbs IRA from *Iris hollandica* bulbs M. charantia lectin from *Momordica charantia* seeds PM RIP from *Polygonatum multiflorum* leaves R. communis agglutinin, RCA from *Ricinus communis* seeds Ebulin1 and ebulin f from *Sambucus ebulus* leaves and fruits Nigrin b, nigrin f and nigrin s from *Sambucus nigra* bark, fruits and seeds Sieboldin b from Sambucus sieboldiana bark

Ricin enters macrophages and liver sinusoidal cells by an alternative mechanism, through the mannose receptors of these cells, which bind the mannose residues present in the ricin molecule (Skilleter *et al.*, 1981; Simmons *et al.*, 1986; Magnusson *et al.*, 1991).

Some type 2 RIPs have low toxicity (Ferreras *et al.*, 2000; Van Damme *et al.*, 2001). Non-toxic type 2 RIPs and ricin-related proteins have been isolated from the bark, leaf and rhizome of elderberry trees belonging to the genus *Sambucus* (Girbés *et al.*, 1993a, 1993b; Rojo *et al.*, 1997). These enzymes, such as nigrin-b, sieboldin-b, ebulin-f and ebulin-r, have structure and RNA N-glycosidase activity similar to those of ricin and showed the same binding specificity towards Gal/GalNAc residues, a potent inhibitory activity against the in vitro protein synthesis of rabbit reticulocyte lysate but little toxicity to cells and mice. Once inside cells, RIPs follow an intracellular pathway through which the RIP molecules in part go to the Golgi apparatus and from there to the cytoplasm, in part go to the lysosomes, where they are largely degraded, and in part are expelled from the cell (Sandvig *et al.*, 2002). Differences in each of these destinations and processes could result in different cytotoxicity.

RIPs are phylogenetically related. In general RIPs from close families share high amino acid homologies. The sequence homology varies from 17 to 75 % identical primary structure. Type 1 RIPs and the A chains of type 2 RIPs from Magnoliopsida (dicotyledons) are closely related. RIPs from Liliopsida (monocotyledons) are at the same time closely related and distant from Magnoliopsida. In evolution, it has been proposed that type 2 RIPs were generated by the fusion of ancestral genes encoding a type 1 RIP and a Gal/GalNAc-binding lectin. The three-dimensional structure of several RIPs has shown that those proteins have a highly conserved "RIP-fold" and a structure composed of two domains, the N-terminal mainly formed by β-strands while the C-terminal by α-helix regions. In a cleft between the N- and the C-terminal domain there is the active site with four highly conserved residues involved in N-glycosidase activity: two tyrosines, responsible for the substrate binding, a glutamate and an arginine directly involved in the catalytic reaction. The majority of RIPs are glycoproteins. The carbohydrate component does not seem to play any major role in the enzymatic activity of RIPs since: (i) some of either type do not contain carbohydrates (e.g. trichosanthin and abrin A chain), (ii) the sugar composition varies; (iii) gelonin and ricin could be partially deglycosylated without affecting their capability of inhibiting protein synthesis in a rabbit reticulocytes lysate; (iv) recombinant ricin chain A produced in *E. coli* is not glycosylated and is yet fully functional (Barbieri *et al.*, 1993).

3.1.1 Distribution of RIPs: Ribosome-inactivating proteins (RIPs) are widely distributed throughout the plant kingdom as stable, highly basic proteins ranging in pI from 9 to 11 and occur in certain bacteria strains, like *Shigella* dysenteriae and pathogenic strains of *Escherichia coli*. They were initially detected mostly in Angiospermae, both mono and dicotyledonae, and also in mushrooms (Yao *et al.*, 1998; Lam *et al.* 2001a,b) and in an alga, the *Laminaria japonica* (Liu *et al.*, 2002). The highest number of RIPs has been found in Caryophyllaceae, Sambucaceae, Cucurbitaceae, Euphorbiaceae, Phytolaccaceae and Poaceae. However, there are no systematic screening studies to allow generalisations about occurrence (Girbés *et al.*, 2004). Type 1 RIPs, in particular, have been found at various concentrations in many plants, including some that are eaten raw (e.g. spinach, tomato). The level of RIPs in plant is highly variable, ranging from trace to hundreds of milligrams per 100 g (Stirpe, 2004). In some plants, they are present in many or even in all tissues examined (roots, leaves, stems, bark, flowers, fruits, seeds, latex, cultured cells), whilst in others plants they are confined to a single tissue. Often different forms were found, sometimes even in the same tissue (Girbes *et al*., 2003).

A toxic type 2 RIP, aralin, was found in the shoots of *Aralia elata* (Tomatsu *et al.*, 2004), which are described as edible and presumably can be eaten safely because the RIP is destroyed by cooking and its concentrations are probably too low (0.32 mg/100 g) to be harmful when taken by oral route. The latter observation is of general interest, because it suggests that other unknown toxic type 2 RIPs may be present in other, possibly many, plants, which have not been examined because they are non-toxic.

3.1.2 Biological activities and possible uses of RIPs: RIPs are studied primarily because of their unique biological activities toward human and animal cells and the perspectives they offer for antiviral and antitumor activities in therapeutical applications. It is evident, however, that plants do not produce RIPs just to fulfill the requirements of modern humankind for antitumor and antiviral drugs. Despite detailed knowledge on the structure, activity, and action mechanism of RIPs, there is no unequivocal answer to the question of why plants synthesise and accumulate RIPs. Concerning the biological roles played by RIPs there are several hypotheses, but the current belief is that they could play significant roles in the antipathogenic (viruses and fungi), stress and senescence responses. In addition, roles as antifeedant and storage proteins have been also proposed (Girbés *et al.*, 2004). Understanding the role of RIPs in nature must be important to justify the conservation through evolution of proteins which are energetically expensive to synthesise.

They have antiviral, antifungal and insecticidal activity. The effect of RIPs on plant viruses led to transfection of plants with RIP genes, to improve their resistance to viral infections. Some

protection from some viruses was conferred to transfected plants by several type 1 RIPs and, although with less efficiency, by type 2 RIPs (Stirpe *et al.*, 2006). They have shown broad spectrum antiviral activity against plant and animal viruses, RNA, DNA (Battelli *et al.*, 1995; Wang *et al.*, 2000). For instance, the RIP from *Mirabilis jalapa* has antiviral activity against the tobacco (*Nicotiana tabacum*) mosaic virus, potato (*Solanum tuberosum*) virus X, potato virus Y, and viroids such as the potato spindle tuber viroid (Kubo *et al.*, 1990; Kataoka *et al*., 1991; Kataoka *et al*. 1992; Vivanco, 1997). PAP protects tobacco and potato plants from viral infection, but high-level expression of PAP is toxic to tobacco (Lodge *et al.*, 1993) and bentgrass plants (Dai *et al.*, 2003). Some RIPs have specific DNA nuclease activity against supercoiled, covalently closed, circular plasmid DNA and single-stranded phage DNA (Roncuzzi *et al.*, 1996). The mechanism of the antiviral activity is still not completely clear. Normally, in their own plants RIPs are segregated from the cytoplasm, being located in protein bodies (e.g. ricin), in the cell wall matrix or in vacuoles (e.g. PAP), in the intracellular space (e.g. saporins). It was thought that the segregation could be broken by the damage caused by viral infections, so that RIPs could come into contact with plant ribosomes, which would be inactivated, with consequent death of the infected cells and arrest of viral multiplication (Stirpe, 2004).

The antiviral activity against animal viruses has led to numerous studies on the effect of RIPs, especially PAP and trichosanthin, in HIV-infected cells, after it was found that PAP inhibits HIV replication (Zarling *et al*., 1990). Other RIPs were studied as well, especially trichosanthin (McGrath *et al.*, 1989) was given to HIV-infected patients, with very modest improvement of their conditions. The replication of HIV in cells was inhibited by several RIPs (Parikh *et al.*, 2004), and investigations were started with the hope that RIPs could be used in the therapy of AIDS (Shaw *et al.*, 2005). Unfortunately, besides the obstacle of the immune response against these foreign proteins, the few clinical trials made with trichosanthin gave disappointing results, and sometimes the administered protein aggravated the neurological (Garcia *et al.,* 1993; Kahn *et al*., 1994) or mental symptoms and caused allergic reactions (Byers *et al*., 1994).

Few type 1 RIPs have been shown to inhibit fungal growth (Roberts *et al.*, 1986; Vivanco *et al.*, 1999; Park *et al.*, 2002a, 2002b). Antifungal activity of the asparagus (*Asparagus officinalis*) RIP has been reported against *Botrytis cinerea* (Wang *et al.*, 2001). Furthermore, two proteins, reportedly RIPs, from mushrooms *Hypsizygus marmoreus* and *Lyophyllum shimeji*, have been shown to be active against an array of fungi (Lam *et al.*, 2001a, 2001b). Antibacterial and antifungal activity of type 1 RIPs have also been reported from *Mirabilis expansa* RIPs (ME; Vivanco *et al.*, 1999). Transgenic tobacco plants expressing an activated form of the maize RIP showed an enhanced resistance to the insect *Helicoverpa zea* (Dowd *et al.*, 2003).

Biological effects ascribed to these proteins go back to ancient times. In the traditional Chinese medicine preparations of the root tubers of the Cucurbitacea *Trichosanthes kirilowii* containing trichosanthin had been used to induce abortion. Also other RIPs also were found to have abortifacient activity (Stirpe , 2004). Actually, RIPs are not abortifacient in the classical sense, in that they do not induce abortion by causing contractions of the uterus or a hormonal imbalance: rather, they cause the death of the fetus by killing syncytiotrophoblasts. These cells are highly sensitive to RIPs, presumably because, like macrophages, they have a high capacity of protein uptake, thus taking up a large amount of RIPs.

RIPs cause immunological effects such as immunogenicity, allergenicity, and immunosuppression (Stirpe, 2004). RIPs are strongly immunogenic and their administration to animals gives rise to formation of antibodies, with cross-reaction only among RIPs from plants belonging to the same family (Strocchi *et al.*, 1992). RIPs are also allergenic. Formation of IgE has been observed in mice after administration of several type 1 RIPs, in laboratory personnel working with RIPs, in HIV-infected patients treated with trichosanthin and in patients treated with immunotoxins containing ricin or other RIPs. Since RIPs are present in plants that are eaten raw (Girbés *et al.*, 2004; Barbieri *et al.*, 2006), their allergenic properties may have a role in the pathogenesis of the allergies caused by some vegetables.

RIPs have immunosuppressive effects and their administration prevents formation of antibodies and retards graft rejection.

RIPs have been used to prepare immunotoxins or other conjugates, either by chemical linkage or as recombinant fusion proteins mostly with monoclonal antibodies but also with other suitable carriers, e.g. hormones (hormonotoxins), cytokines, neuropeptides. Most immunotoxins have been prepared for the experimental therapy of malignancies, treatment of cancer, especially haematological (Frankel *et al.*, 2000), for immunosuppression and also for the therapy of viral diseases. For these purposes RIPs have been linked to antibodies against antigens expressed prevalently on cancer cells.

Ricin has been considered as a possible weapon for warfare and terrorist attacks being a potent poison easy to obtain, utilisable for suicidal and homicidal purposes. Although less potent than other biological toxic or infectious agents, it can be prepared more safely from easily available material with relatively simple equipment and procedures, thus without the support of a strong organisation, and could be used for limited terrorist actions. Sources of other toxic RIPs are not as easily available as castor beans, but their toxins could be obtained by biotechnological techniques. Ricin and related toxins would be lethal in small amounts only if injected or inhaled but have a much lower toxicity by the oral route, and therefore could not be used to contaminate water supplies

or large amounts of food. Aggressions to single persons could be performed by injecting a toxin as occurred in London, when an expatriate Bulgarian journalist was killed with a microbullet containing ricin, as ascertained by the autopsy (Knight, 1979).

Ricin was used in the famous "umbrella tip" assassination of Georgi Markov by the KGB and as a biological warfare agent by Iraq. Documents captured by British commandos in Afghanistan in 2001 releaved that ricin had been adopted as a terrorist weapon by the al-Qaeda group (Robertus *et al.*, 2004). For this, there is a considerable and increasing interest in developing antidotes to ricin and related toxins. Moreover, because of their possible and different applications in agriculture and in medicine RIPs have been receiving more and more attention by the scientific community.

3.2 STUDIED RIBOSOME INACTIVATING PROTEINS

Three type 1 RIPs, momorcochin S, bouganin and lychnin and one type 2 RIP, stenodactylin, have been subjects of crystallographic studies in this thesis.

3.2.1 Momorcochin S: It is extracted from seeds of *Momordica cochinchinensis* (Spiny bitter cucumber), a Cucurbitacea growing in India (Fig. 28). It is a glycoprotein with MW of approx. 30 KDa, an alkaline isoelectric point (9.4) and can be considered as an iso-form of the previously purified momorcochin from the roots of *Momordica cochinchinensis* (Bolognesi *et al.,* 1989). It is known only the N-terminal sequence of 30 amino acids: DVTFSLLGANTKSYAAFITNFRKDVASEKK. Momorcochin S was linked to a monoclonal antibody against human plasma cells and the resulting immunotoxin was selectively toxic to target cells and had remarkably low toxicity to mice (Bolognesi *et al.*, 1989). This makes this protein worthy of consideration for the preparation of immunotoxins for experimental therapeutic purposes.

Figure 28. I *Momordica cochinchinensis* fruits.

3.2.2 Bouganin: It is a type 1 RIP isolated from leaves of *Bougainvillea spectabilis* Willd (Fig. 29) (Bolognesi *et al.,* 1997). It is synthesised as a pro-peptide consisting of 305 amino acids: MGWWAIIVEP MLVMPSIVNK ETTSLGYNTV SFNLGEAYEY PTFIQDLRNE LAKGTPVCQL PVTLQTIADD KRFVLVDITT TSKKTVKVAI DVTDVYVVGY QDKWDGKDRA VFLDKVPTVA TSKLFPGVTN RVTLTFDGSY QKLVNAAKVD RKDLELGVYK LEFSIEAIHG KTINGQEIAK FFLIVIQMVS EAARFKYIET EVVDRGLYGS FKPNFKVLNL ENNWGDISDA IHKSSPQCTT INPALQLISP SNDPWVVNKV SQISPDMGIL KFKSSKLTQF ATMIRSAIVE DLDGDELEIL EPNIA.

Figure 29. Image of flowers and leaves of *Bougainvillea spectabilis* Willd.

The first 26 (in yellow) amino acids act as a leader signal while the 29 C-terminal amino acids (in red) are cleaved during processing of the molecule (Den Hartog *et al.,* 2002). The mature protein consists of 250 amino acids (the last residue is a Lys) with MW of 26.2 KDa and pI ~ 9.0.

Bouganin has a very low *in vivo* toxicity as compared to its intrinsic enzymatic activity. Immunotoxins containing bouganin inhibit cell protein synthesis, induce apoptosis, and block the

clonogenic growth of target cells, although with a different kinetics, suggesting the presence of different mechanisms of cell killing (Bolognesi *et al.*, 2000).

3.2.3 Lychnin: It is a type 1 RIP isolated from *Lychnis chalcedonica* seeds (Bolognesi *et al.*, 1990) (Fig. 30). It had been previously studied in the Biomineralisation and Biocrystallography group of Bologna and in 2003 it was crystallised by the vapour-diffusion method. Although the crystals diffracted at 1.7 Å, it was not possible to resolve the three-dimensional structure being the primary sequence not yet available at that time (Fermani *et al.*, 2003). In fact, only in 2006 Chambery *et al.* determined the complete amino acid sequence of lychnin which consists of 234 amino acid residues with an atypical primary structure and has a molecular mass of about 26 KDa (Chambery *et al.*, 2006).

Figure 30. Image of *Lychnis chalcedonica*.

3.2.4 Stenodactylin: It is a recently characterised type 2 ribosome-inactivating protein (Stirpe *et al*, 2007), purified from the caudices of *Adenia stenodactyla*, Passifloraceae (Fig. 31) (Pelosi *et al.*, 2004). It is found in eastern Africa, growing in a well drained soil with some water and some to lots of sun.

Stenodactylin showed a high enzymatic activity both on ribosomes and hsDNA used as substrates and was extremely toxic to all cell lines tested, its cytotoxicity being higher than other toxins of this type (Stirpe *et al.*, 2007). Stenodactylin was highly toxic to mice and it caused 100% death at a very low dose. The exceedingly high biological activity of stenodactylin makes it a good candidate for studies on structure/function relationship. The A chain of stenodactylin inhibited protein synthesis, as expected, whereas the B chain did not agglutinate erythrocytes, a surprising result since the B chain of modeccin and volkensin had hemagglutinating properties (Barbieri *et al.*, 1980; Stirpe *et al.*, 1985). The lack of agglutinating capacity can be due either to conformational changes or to aggregation of the B chain after separation from the A chain. Alternatively, it is possible that the B chain is monovalent, and that the whole toxin can agglutinate cells only after formation of aggregates, as other type 2 RIPs do (e.g. viscumin, Olsnes *et al.*, 1982).

Figure 31. Image of *Adenia stenodactyla* showing a big caudex characteristic of this specie. The caudex, a perennial swollen base, can grow up to 30 m in diameter, and the vines up to 1,5 m in length.

3.3 CRYSTALLISATION EXPERIMENTS

The aim of the work was to crystallise momorcochin S, bouganin and stenodactylin and to obtain crystals of high quality that could allow to resolve the three-dimensional structures and successively to correlate molecular structures to biological activities. With regard to lychnin, being already known its crystallisation conditions, its three-dimensional structure was studied. All the RIPs used were extracted and purified by the group of Professor Bolognesi (Experimental Pathology Department, University of Bologna).

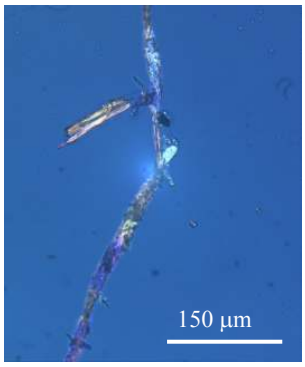

Figure 32. Optical micrographs of momorcochin S fibres.

3.3.1 Momorcochin S: The protein was dissolved in PBS buffer (5mM KH_2PO_4 pH 7.5 and 0.14 M NaCl) at a concentration of 11,3/11,6 mg/mL. All experiments were carried out in vapour diffusion (hanging and/or sitting drop) at 293 K and the drops (5 µl) contained the protein and the reservoir solution (750 µL in each well) in equal volume. Hundreds of crystallisation conditions were tested and initially only fibres were obtained (Fig. 32). The crystallisation conditions tested were those reported by commercial screens sold by companies, such as Hampton research or Jena BioScience. After 18 months, crystals appeared in a drop in which the protein had been mixed with a reservoir solution containing 8% (w/v) PEG 4K(Fig. 33).

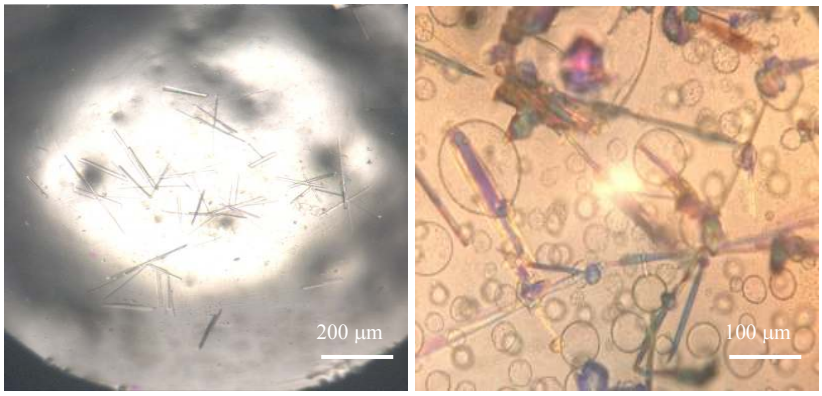

Figure 33. Optical micrographs of momorcochin S crystals.

3.3.2 Bouganin: The crystallisation trials were carried out at 293 K using the vapour diffusion method with the sitting drop technique. Drops contained 2 µl of protein, at a concentration of 12 mg/mL in PBS (5 mM NaH_2PO_4 pH 7.5 and 0.14 M NaCl), mixed to an equal volume of reservoir solution. Single crystals of bouganin were obtained with a reservoir solution composed of 20% (w/v) 20 kDa PEG, in about two or three months. The crystals have a needle-like shape with maximum length of 0.5 mm (Fig. 34).

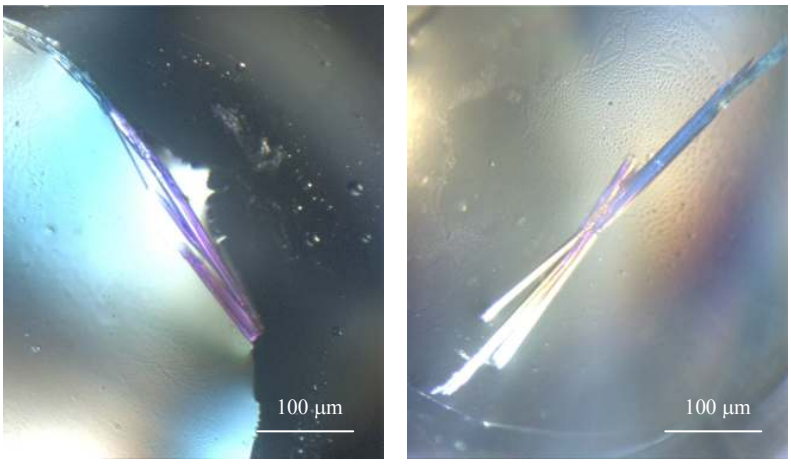

Figure 34. Optical micrographs of bouganin crystals.

3.3.3 Lychnin: Lychnin was dissolved in a solution containing PBS buffer (5 mM NaH_2PO_4 pH 7.5 and 0.14 M NaCl) at a concentration of 10 mg/ml. Each drop was prepared mixing equal volumes (2.5 µl) of protein solution and reservoir and was equilibrated against 700 µl of the reservoir at 293 K. It was crystallised as previously described (Fermani *et al.*, 2003). The best crystals (Fig. 35) grew in few days using a reservoir solution containing 30% (w/v) PEG 8K and 0.1 M NaH_2PO_4 pH 6.5-7.2.

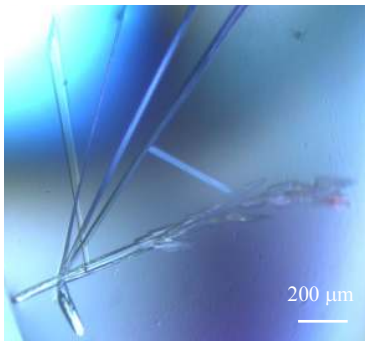

Figure 35. Optical micrographs of lychnin crystals.

3.3.4 Stenodactylin: The conventional sitting drop vapour diffusion technique was used to crystallise stenodactylin and all the experiments were carried out at 293 K. The droplets (4 µl) contained the protein and the reservoir solution (750 µL in each well) in equal ratio. The best condition to grow single crystals was obtained using 1.4-1.5 M sodium malonate pH 6.8-7.5 as precipitant and a protein concentration of 5.76 mg/mL in PBS buffer (5 mM NaH_2PO_4 pH 7.0 and

0.14 M NaCl) and 4 mM galactose. The crystals grew in about one month with maximum dimensions approximately of 0.3×0.2×0.1 mm (Fig. 36).

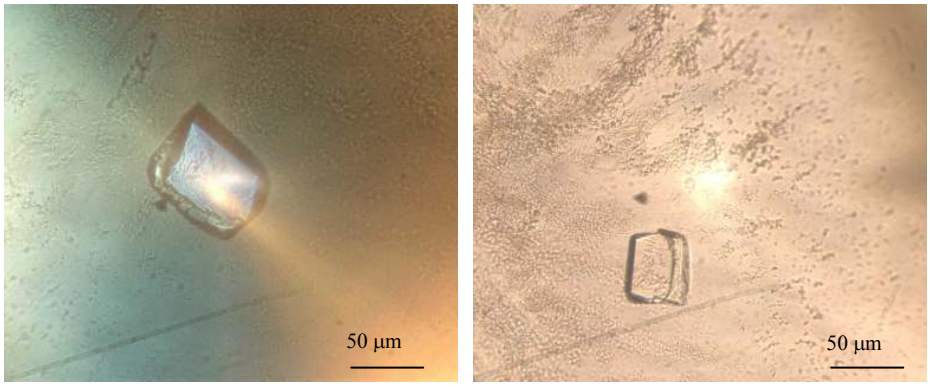

Figure 36. Optical micrographs of stenodactylin crystals.

3.4 CRYSTALLOGRAPHIC STUDIES

3.4.1 Momorcochin S: The obtained crystals were tested at the ESRF (European Synchrotron Radiation Facility) of Grenoble (France) but they did not diffract. Optimisation crystallisation trials are in progress in order to obtain crystals of quality suitable for X-ray studies.

3.4.2 Bouganin: Diffraction data were collected at ESRF (microfocusing beamline ID13), from one crystal, irradiated in three different regions (beam size 5 μm × 5 μm). Crystal was soaked for few seconds in a cryogenic solution composed of 30% (w/v) PEG 8K and 20% (v/v) PEG 400 and positioned in the nitrogen stream at 100 K. Data were recorded at a wavelength of 0.976 Å, using an oscillation range of 1° and a crystal-to-detector distance of 100 mm. Data were processed and scaled using DENZO/SCALEPACK package (Otwinowski *et al.*, 1997) and statistics are reported in Table 11.

Table 11. Cell parameters and data collection statistics for bouganin.

Space group	$P2_12_12_1$
Unit cell *a*,*b*,*c*, β (Å, °)	40.84, 78.50, 79.38
N° molecules in a.u.	1
Resolution range*	35-1.8 (1.86-1.8)
Measured reflections	79398
Unique reflections	23985
Completeness (%)*	98.9 (99.7)
Redundancy	3.3
R_{sym}*	0.104 (0.331)
$I/\sigma(I)$*	15.9 (4.4)

*Value in parenthesis refers to the last resolution shell

Structure of bouganin was solved by molecular replacement (Navaza, 1994), using the structure of α-PAP-R (Ago *et al.*, 1994; PDB ID code 1apa) as probe. The two proteins show 29% of sequence identity. Rotational and translational searches clearly indicate the presence of one molecule in the asymmetric unit as expected from Mattews coefficient calculation (Matthews, 1968). The correctness of the solution was verified by building the whole crystal packing. The model was refined with alternate cycles of simulated-annealing, energy minimisation, temperature factor refinement using the program CNS (Brünger, 1998), and manual rebuilding using O (Jones *et al.*,

1991). Refinement was carried out in a resolution range of 8.0-1.8 Å, applying a sigma cut-off on amplitudes of 2.0, only in the initial stages of refinement, and selecting 5% of reflections for R_{free} calculations. Water molecules were automatically added, and after a visual inspection they were conserved in the model only if contoured at 0.8σ on the ($2F_o$ - F_c) map and if they fell into an appropriate hydrogen bonding environment. Refinement statistics for bouganin are given in Table 12. Final model of bouganin has tight stereochemical restraints (Table 12). The Ramachandran plot, obtained using PROCHECK (Laskowski, 1993), shows that 88.0% of bouganin residues lie in the most favored regions, and the remaining ones in the additional allowed regions. In bouganin structure only Lys247, belonging to the C-terminal coil, is found in a generously allowed region, but the well defined electron density map confirmed its conformation. The root-mean-square error in the atomic positions, evaluated with the Luzzati method (Luzzati, 1952), is 0.17.

Table 12. Refinement statistics for bouganin.

No. protein atoms	1974
No. water molecules	378
R (%)	17.6
R_{free} (%)	20.2
B mean (Å^2)	12.8
B (Wilson Plot, Å^2)	8.1
B protein atoms (Å^2)	9.9
B solvent atoms (Å^2)	27.4
rmsd bond length (Å)	0.005
rmsd bond angles (°)	1.2

3.4.3 Lychnin: Lychnin crystals were measured using synchrotron radiation (Eletttra X-ray diffraction beam line in Trieste, Italy) at 100 K. The crystals were soaked for few seconds into a cryogenic solution containing 30% (w/v) PEG 8 KDa and 30% (v/v) PEG 400 and rapidly exposed to a cold nitrogen stream (Oxford Cryosystem Cryostream). The diffraction data were collected to a resolution of 1.7 Å, on a MAR Research CCD using a radiation wavelength of 1.0 Å, an oscillation angle of 2.00° and a crystal-detector distance of 120mm. The diffraction data were processed and scaled for both proteins with the DENZO-SCALEPACK package (Otwinowski *et al.*, 1997). The data reduction, including a search for systematic absences, clearly indicates that lychnin crystals

belong to the $P2_1$ space group. The unit cell parameters and the data collection statistics are listed in Table 13.

Table 13. Cell parameters and data collection statistics for lychnin.

Space group	$P2_1$
Unit cell *a*,*b*,*c*, β (Å, °)	35.25, 57.33, 52.23, 106.2
N° molecules in a.u.	1
Resolution range*	29-1.7 (1.76-1.7)
Measured reflections	151602
Unique reflections	21895
Completeness (%)*	99.4 (98.3)
Redundancy	6.9
R_{sym}*	0.048 (0.084)
$I/\sigma(I)$*	39.7 (14.2)

*Value in parenthesis refers to the last resolution shell

Matthews coefficient (Matthwes, 1968) calculations show the presence of one chain for asymmetric unit. The V_m value is 1.95 for lychnin with a solvent content of 36.4%.

Several attempts to solve the structure of lychnin were made by molecular replacement, using the coordinates of different type 1 RIPs (saporin-S6, dianthin 30, PAP-R and α-PAP-R, ricin A chain), but no correct solution was found. Structure solution was achieved by the program AmoRe (Navaza, 1994) using bouganin, which shares the 29% of sequence identity with lychnin, as template. The ($2F_o$ - F_c) map calculated after a rigid body refinement showed several regions with very poor electron density. These regions were deleted from model and rebuilt during the subsequent cycles as the electron density became clearer. The refinement was performed with CNS (Brünger *et al.*, 1998) in a resolution range of 8.0-1.7 Å with a starting σ cut-off on amplitudes of 2.0, which was later decreased to 0. A total of 10% of the data was randomly selected for R_{free} calculations. The model was rebuilt with the graphic program XtalView (McRee, 1999). In the final stage of the refinement the solvent network was built: water molecules were added following the criteria used for bouganin structure. Refinement statistics are listed in Table 14.

Final model of lychnin has tight stereochemical restraints (Table 14). The Ramachandran plot, obtained using PROCHECK (Laskowski *et al.*, 1993), shows that 91.2% of lychnin residues lie in the most favored regions, and the remaining ones in the additional allowed regions. The root-mean-

square error in the atomic positions, evaluated with the Luzzati method (Luzzati, 1952), is 0.15 for lychnin.

Table 14. Refinement statistics for lychnin.

No. protein atoms	1879
No. water molecules	364
R (%)	16.2
R_{free} (%)	19.6
B mean (Å^2)	13.6
B (Wilson Plot, Å^2)	13.8
B protein atoms (Å^2)	11.2
B solvent atoms (Å^2)	26.5
rmsd bond length (Å)	0.005
rmsd bond angles (°)	1.2

3.4.4 Stenodactylin: Several crystals of stenodactylin were tested in X-ray diffraction experiments. Each crystal was briefly soaked in a cryo-protectant solution containing 2.0 M sodium malonate at the same pH of the reservoir solution and 20% (v/v) glycerol and transferred into a cold N_2 gas stream (100 K) for data collection. Data were collected using an ADCD Quantum CCD detector on beam lines ID29 and ID14-1 at ESRF (Grenoble, France) using a wavelength of 0.976 Å and 0.934 Å, a crystal-to-detector distance of 283.88mm and 265.31mm, respectively, and in both cases an oscillation range of 1°. The best crystal diffracted to a resolution of 1.9 Å, but the data were trimmed to 2.15 Å to achieve good values of completeness and I over $\sigma(I)$ in the last resolution shell. The data were processed and scaled using DENZO and SCALEPACK programs (Otwinosky *et al.*, 1997). All tested crystals showed a centred monoclinic space group with similar unit cell dimensions. The unit cell parameters and the data collection statistics obtained merging two data sets collected from different crystals are reported in Table 15.

Matthwes coefficient calculations (Matthews, 1968) indicate the presence of two heterodimers in the asymmetric unit, corresponding to a V_M of 2.61 Da^{-1} and a solvent content of 52.5%. Molecular replacement procedures to solve the structure of stenodactylin are in progress, the structure of ricin is used as probe.

Table 15. Data collection statistics of stenodactylin.

Space group	C2
Unit cell (Å, °)	a = 220.54, b = 64.26, c = 91.75, β = 105.68
Resolution (Å)	50.0-2.15 (2.23-2.15)
Observed reflections	612.719
Unique reflections	64.284
Mosaicity (°)	0.885
Completness (%)	94.0 (72.9)
$I/\sigma(I)$	18.7 (2.5)
Redundancy	9.5 (7.0)
Rmerge	0.183 (0.574)

3.5 RESULTS

The three dimensional structures of two type RIPs, bouganin and lychnin, have been solved and compared with structures of other RIPs.

3.5.1 Overall structures of bouganin and lychnin: The final model of bouganin lacks the last thirty-one residues of the sequence previously reported (Den Hartog *et al.*, 2002). 29 C-terminal amino acids are proteolytically cleaved during the processing of the molecule from a precursor to a smaller mature protein, while Ser249 and Lys250 are disordered. All residues of lychnin sequence (Chambery *et al.*, 2006) have been built in the high quality electron density maps. No glycosilation sites were found in either structure.

Both bouganin and lychnin structures show the common 'RIP fold'. The N-terminal domain (in red and magenta in Fig. 37a,b) is composed of a mixed β-sheet of seven strands (β1, β4, β5, β6, β7, β8 and β9 in bouganin and β1, β3, β4, β5, β6, β7 and β8 in lychnin). Five strands in the centre are antiparallel and those at the edge are parallel to the near one. In both proteins an helix, α2 in bouganin and α1 in lychnin, followed by a short structural motif of two strands in bouganin (β2 and β3) or a strand plus a helix in lychnin (β2 and α2), connects the first two strands of the sheet, while a second helix, α3 in bouganin and α4 in lychnin, the last two.

The C-terminal domain (in gold and green in Fig. 37a,b) is predominantly α-helical: eight helices are observed both in bouganin and lychnin. The C-terminal region of bouganin shows a loop, flanking helix α9, composed of two anti-parallel β-strands (β10, β11) connected by a short helix (Fig. 37a). In lychnin helix α11 is connected to the last helix α12 by a random coil (Fig. 37b).

RIP family has five highly conserved residues, which have been identified by site-directed mutagenesis experiments to be the residues involved in N-glycosidase activity (Ready *et al*., 1991; Day *et al.*, 1996; Poyet *et al.*, 1998; Li *et al.*, 1999a; Li *et al.*, 1999b). These residues correspond to Tyr70, Tyr114, Glu165 Arg168 and Trp198 in bouganin, and Tyr69, Tyr119, Glu170 Arg173 and Trp203 in lychnin (Fig. 38). Only recently, a type 1 RIP, charybdin, with a natural substitution of a catalytic residue has been identified: a valine replaces the first (in numbering) tyrosine (Touloupakis *et al.*, 2006). Moreover, it has been proposed that in PD-L4 a type 1 RIP isolated from leaves of *Phytolacca dioica*, a conserved serine, the fourth residue after the catalytic tryptophan (Fig.38), could be also involved into the catalytic mechanism (Chambery *et al.*, 2007; Ruggiero *et al.*, 2008).

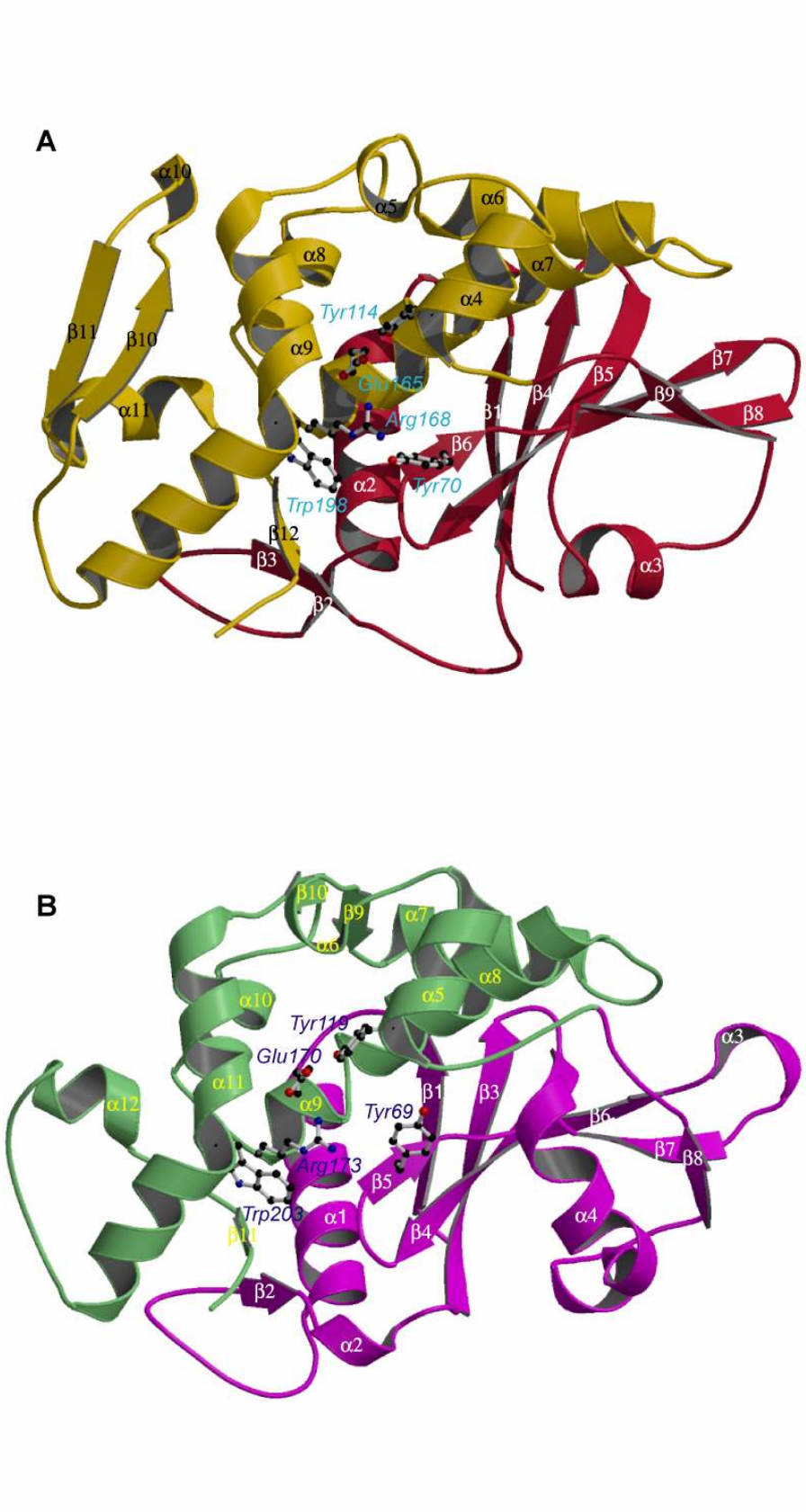

Figure 37. Ribbon model of the crystal structure of (A) bouganin and (B) lychnin. The N-terminal and the C-terminal domains are differently colored. The secondary structure elements and the conserved residues of the catalytic site are indicated. The figure was produced by MOLSCRIPT (Kraulis, 1991) and rendered by RASTER3D (Merritt *et al.*, 1997).

```
MOMORDIN        -------DVSFRLSGADPRSYGMFIKDLRNALPFREKVYNIPLLLPSVSG---AGRYLLM 50
RICIN chain A   IFPKQYPIINFTTAGATVQSYTNFIRAVRGRLTTGADVRHEIPVLPNRVGLPINQRFILV 60
DIANTHIN 30     -----ATAYTLNLANPSASQYSSFLDQIRNNVRDTSLIYGGTDVA--VIGAPSTTDKFLR 53
SAPORIN S6      ----AVTSITLDLVNPTAGQYSSFVDKIRNNVKDPNLKYGGTDIA--VIGPPSK-EKFLR 53
PAP             -----VNTIIYNVGSTTISKYATFLNDLRNEAKDPSLKCYGIPMLP---NTNTNPKYVLV 52
LYCHNIN         --------RPSWTVDSDSAKYSSFLDSLREEFGRGTPKVCNIPVTK---KANNDKFVLVN 49
BOUGANIN        -------YNTVSFNLGEAYEYPTFIQDLRNELAKGTPVCQLPVTLQ---TIADDKRFVLV 50
                                .*  *:  :*                              .:

MOMORDIN        HLFNYDGKTITVAVDVTNVYIMGYLADT-----TSYFFN-----EPAAELASQYVFRDAR 100
RICIN chain A   ELSNHAELSVTLALDVTNAYVVGYRAGN-----SAYFFHPD---NQEDAEAITHLFTDVQ 112
DIANTHIN 30     LNFQGPRGTVSLGLRRENLYVVAYLAMDNANVNRAYYFKNQ---ITSAELTALFPEVVVA 110
SAPORIN S6      INFQSSRGTVSLGLKRDNLYVVAYLAMDNTNVNRAYYFRSE---ITSAESTALFPEATTA 110
PAP             ELQGSNKKTITLMLRRNNLYVMGYSDPFETNKCRYHIFNDISGTERQDVETTLCPNANSR 112
LYCHNIN         LVLPFNRNTITLAFRASDAYLVGFQDRDSKTNKLRANFFSDEYRALSGKYKSIFTDAEVL 109
BOUGANIN        DITTTSKKTVKVAIDVTDVYVVGYQDKWDGKDRAVFLDKVP-------TVATSKLFPGVT 103
                        ::.: .   : *::.:

MOMORDIN        RKITLPYSGNYERLQIAAGKP-----REKIPIGLPALDSAISTLLHYDS-----TAAAGA 150
RICIN chain A   NRYTFAFGGNYDRLEQLAGNL-----RENIELGNGPLEEAISALYYYSTGGTQLPTLARS 167
DIANTHIN 30     NQKQLEYGEDYQAIEKNAKITTGDQSRKELGLGINLLITMIDGVNKKVR---VVKDEARF 167
SAPORIN S6      NQKALEYTEDYQSIEKNAQITQGDQSRKELGLGIDLLSTSMEAVNKKAR---VVKDEARF 167
PAP             VSKNINFDSRYPTLESKAGVK----SRSQVQLGIQILDSNIGKISGVMS--FTEKTEAEF 166
LYCHNIN         AP-ALPCASTYTDLQNKAGVS-----REKLSLGVSSLQTAFTAVYGKVFTG---KNVAKF 160
BOUGANIN        NRVTLTFDGSYQKLVNAAKVD-----RKDLELGVYKLEFSIEAIHGKTING---QEIAKF 155
                    :     *  :   *        *..: :*   *   :  :             *

MOMORDIN        LLVLIQTTAEAARFKYIEQQIQERA--YRDEVPSLATISLENSWSGLSKQIQLAQGNNGI 208
RICIN chain A   FIICIQMISEAARFQYIEGEMRTRIRYNRRSAPDPSVITLENSWGRLSTAIQES--NQGA 225
DIANTHIN 30     LLIAIQMTAEAARFRYIQNLVTKNFP--NKFDSENKVIQFQVSWSKISTAIFGD-CKNGV 224
SAPORIN S6      LLIAIQMTAEAARFRYIQNLVIKNFP--NKFNSENKVIQFEVNWKKISTAIYGD-AKNGV 224
PAP             LLVAIQMVSEAARFKYIENQVKTNFN--RAFNPNPKVLNLQETWGKISTAIHDA--KNGV 222
LYCHNIN         ALISIQMVAEAARFKYIEDQVINRGMY-SSFEAGARITLLENNWSKISEQYHKS------ 213
BOUGANIN        FLIVIQMVSEAARFKYIETEVVDRGLY-GSFKPNFKVLNLENNWGDISDAIHKSSPQCTT 214
                 :: **  :*****:**:  :  .       .      :: .*  :*

MOMORDIN        FRTPIVLVDNKGNRVQITNVTSKVVTSNIQLLLNTRNIAEGDNGDVSTTHGFSSY----- 263
RICIN chain A   FASPIQLQRRNGSKFSVYDVS--ILIPIIALMVYRCAPPPSSQF---------------- 267
DIANTHIN 30     FNKDYDFGFGKVRQAKDLQMGLLKYLGRPKSSSIEANSTDDTADVL------------- 270
SAPORIN S6      FNKDYDFGFGKVRQVKDLQMGLLMYLGKPKSS-NEANSTVRHYGPLKPTLLIT------- 276
PAP             LPKPLELVDASGAKWIVLRVDEIKPDVALLNYVGGSCQTTYNQNAMFPQLIMSTYYNYMV 282
LICHNIN         -------CKLGGGQFTEEEMKLGLLLYN------------------------------- 234
BOUGANIN        INPALQLISPSNDPWVVNKVSQISPDMGILKFKSSKLTQFATMIRSAIVEDLDGDELEIL 274
                :     :           :                                :      ::

MOMORDIN        ---------
RICIN chain A   ---------
DIANTHIN 30     ---------
SAPORIN S6      ---------
PAP             NLGDLFEGF 291
LYCHNIN         ---------
BOUGANIN        EPNIA---- 279
```

Figure 38. Sequence alignment of different type 1 RIPs and ricin A chain. Residues highlighted in yellow correspond to conserved catalytic residues, positive and negative residues cited in the text are highlighted in light blue and red, respectively, and the C-terminal portion of the sequence proteolitically cleaved to obtain the mature form of the protein is highlighted in dark green. Disordered bouganin residues (Ser249 and Lys250) are indicated in green. Sequence homologies: bouganin-lychnin 29%, bouganin- or lychnin-momordin I 25% or 24%, bouganin- or lychnin-ricin A chain 27% or 23%, bouganin- or lychnin-dianthin 30 22% or 26%, bouganin- or lychnin-saporin-S6 23% or 25%, bouganin- or lychnin-PAP-R 30% or 27%. The sequence alignments have been performed with CLUSTALW (Combet *et al.*, 2000).

Several mechanisms have been proposed to explain the RIP enzymatic activity (Mozingo *et al.*, 1992; Ren *et al.*, 1994; Huang *et al.*, 1995): in all of them the two tyrosines are responsible for substrate adenine binding through a stacking interaction, whereas the arginine protonates the N3 atom of adenine and the glutamate stabilises the transition state. Alternatively, Huang *et al*. (1995) proposed that the N7 atom of adenine is protonated by an acidic residue not conserved in RIP family, corresponding to Asp96 in ricin A chain and Glu85 in α-momorcharin. In the same region of the three-dimensional structure, bouganin shows an aspartate (Asp113), while lychnin has a glutamate (Glu91) or an aspartate (Asp90) which could play the same role. Similarly to the other RIP structures the residues forming the active site are located in a cleft in the central part of the molecule, between the N- and the C-terminal domains. The cleft is formed by strand β6 and helices α4, the C-terminal portion of α7 and α9 in bouganin (Fig. 37a), and by strand β5 and helices α5, the C-terminal portion of α8, α9 and α11 in lychnin (Fig. 37b). In both structures the active pocket contains several ordered water molecules. Active site residues are involved in a hydrogen bond network including residues forming the cavity and water molecules.

The electrostatic surface potential calculated for bouganin shows that the active site is a wide cavity, predominantly negative, except for a small positive zone determined by the catalytic residue Arg168 (Fig. 39a). Negative and positive well defined regions are observed around the cavity corresponding to Asp200, Asp203, Lys245 and Lys247 on the left, Lys116 on the right and Arg46 on the bottom (Fig. 39a). The C-terminal region, corresponding to the structure motif β10-loop-β11, is mainly hydrophobic.

The active site of lychnin structure is characterised by a deeper cavity with an electrostatic surface potential less negative than that one of bouganin (Fig. 39c). Two well-defined charged regions on the side part of the cavity are determined by the catalytic residues Arg173 and Glu170 and by Glu200 which strengthens the negative zone. The side chain of Tyr69 partially obstructs the access to the cavity. Several arginines and lysines come out from the surface of the protein, in regions far from the active site (N- and C-terminal regions) and around the catalytic pocket: on the left Lys205, on the bottom Lys39 and Lys98, on the top Lys132 and Arg195, and on the right Lys123 and Arg93 (Fig. 39c). The electrostatic surface potential of saporin-S6 is also reported for comparison (Fig. 39e).

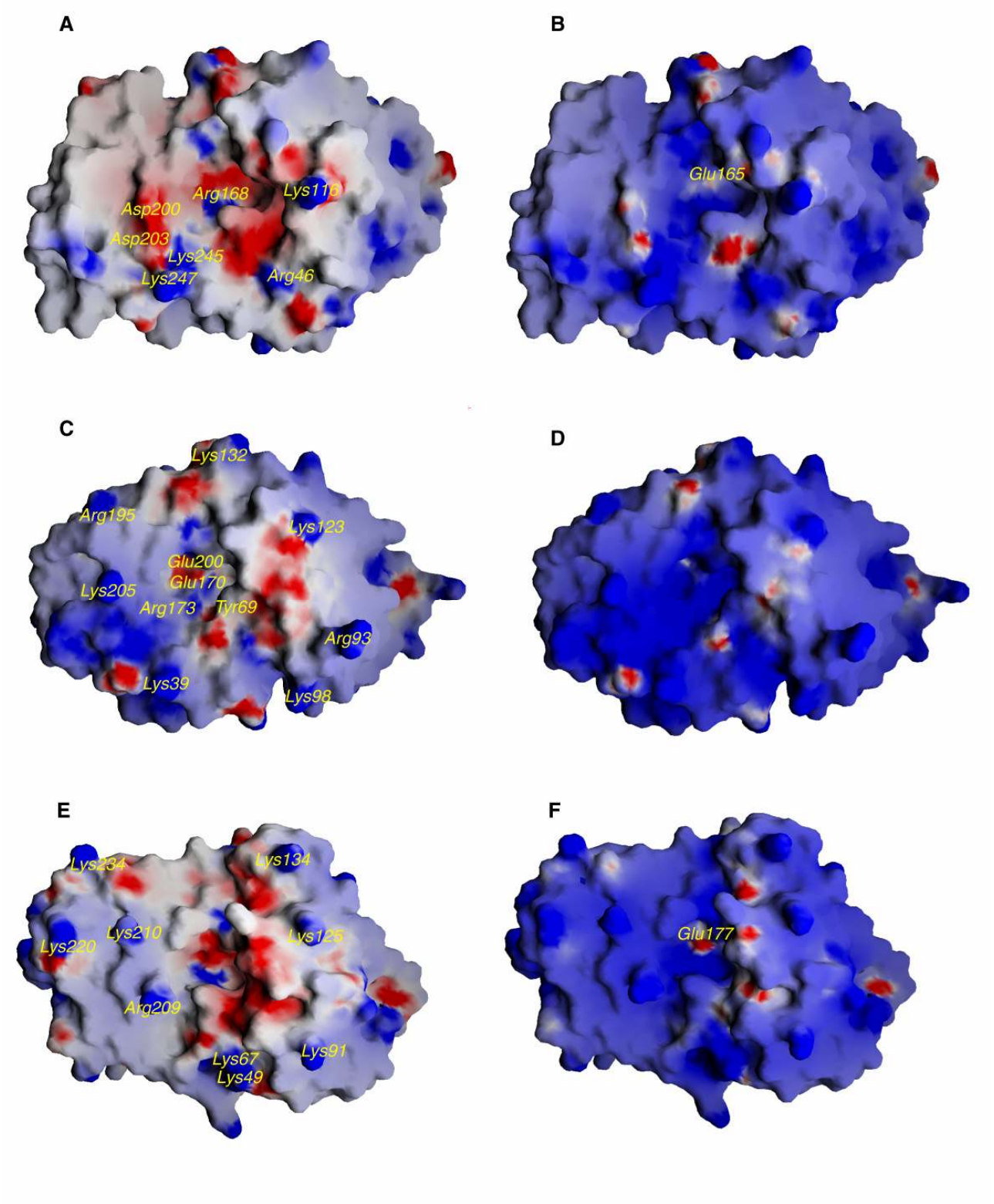

Figure 39. Electrostatic surface potential of bouganin (A) at pH 7 and (B) at pH 4; lychnin (C) at pH 7 and (D) at pH 4; saporin-S6 (E) at pH 7 and (F) at pH 4. The position of the residues cited in the text is indicated. The electrostatic surface potential at the two pHs has been calculated assigning to the side chain group of ionisable residues the charge present at the considered pH. This charge was evaluated from ExPASy server on the basis of the pKa of the residue. The values of electrostatic surface potential are expressed as a spectrum ranging from +10 *kT/e* (deep blue) through 0 *kT/e* (white) to -10 *kT/e* (deep red). At a temperature of 298.15 K, *kT/e* = 25.7 mV. The figure was produced by GRASP (Nicholls *et al.*, 1991).

3.5.2 Comparison between structures: The backbone superimpositioning of bouganin and lychnin, which gave a root main square deviation (rmsd) of 1.306 Å for 192 superimposed C_α atoms (fitting was performed using McLachlan algorithm (McLachlan, 1982) as implemented in Profit V2.5.3), shows that the central portion of the molecules is well superimposable, while major differences are observed in the external regions (Fig. 40a).

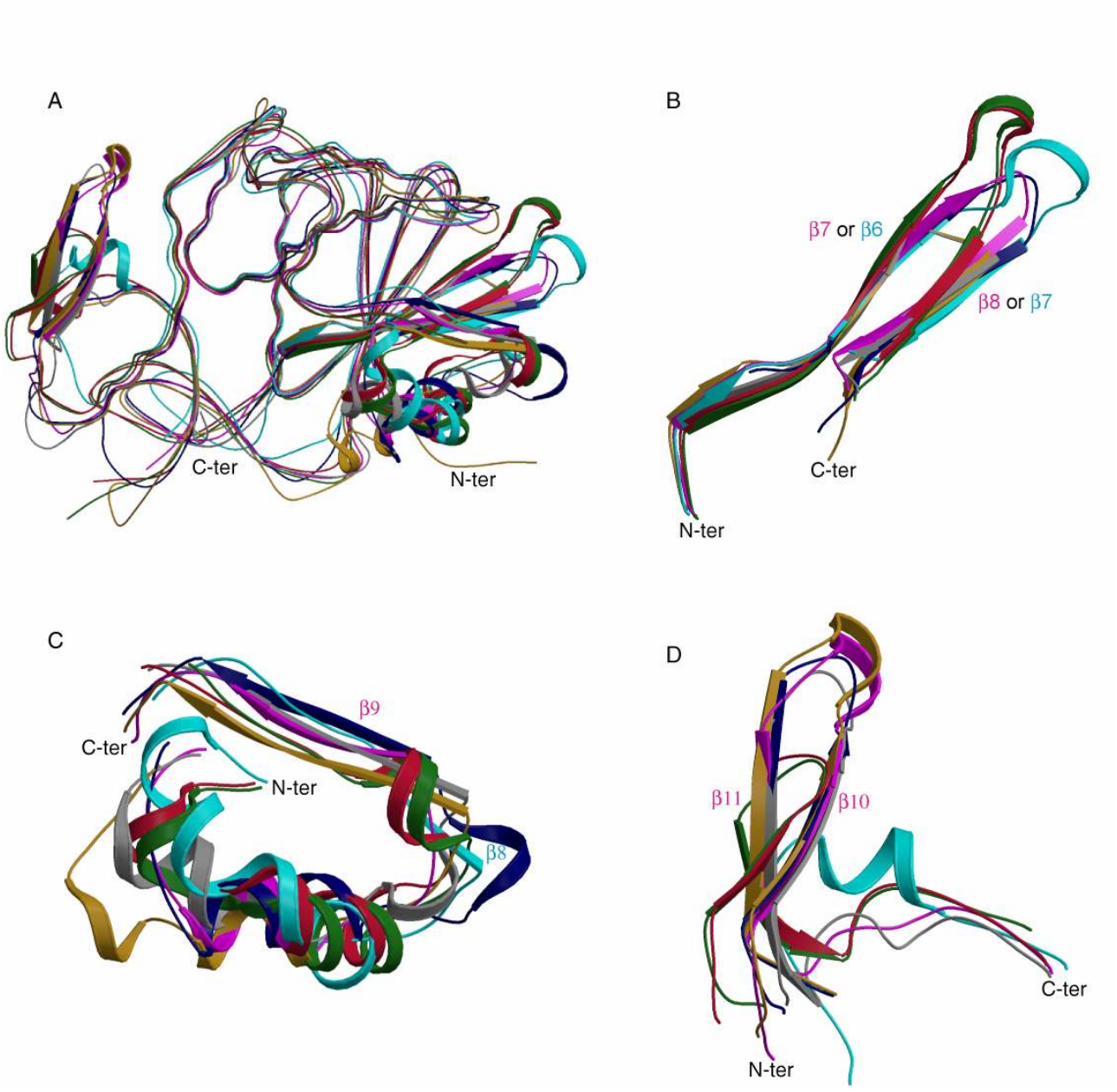

Figure 40. Structural comparison between different type 1 RIPs and ricin A chain. (A) Superimposition of the C_α atoms of bouganin (magenta), lychnin (cyan), dianthin 30 (green), saporin-S6 (red), PAP-R (dark blue), momordin I (grey) and ricin A chain (gold). The regions showing the major differences are indicated with their secondary structure elements and zoomed (B), (C) and (D). The indicated secondary structure elements correspond to bouganin (magenta) or lychnin (cyan). The figure was produced by MOLSCRIPT (Kraulis, 1991) and rendered by RASTER3D (Merritt *et al.*, 1997).

In the N-terminal domain strand β1 is longer in bouganin, while helix α3 is shorter than the corresponding α4 in lychnin and the subsequent strand is differently oriented in the two structures (Fig. 37a,b). The fold of the C-terminal region is absolutely different from bouganin to lychnin: the structural motif, composed of two antiparallel β-strands (β10 and β11), which connects helices α9 and α11 in bouganin is completely absent in lychnin where the last two helices α11 and α12 are joined by a less bulky coil (Fig. 37a,b).

Lychnin differs more than bouganin from the other examined RIPs: dianthin 30 (Fermani *et al.*, 2005), PAP-R (Mozingo *et al.*,1993), momordin I (Husain *et al.*, 1994), saporin-S6 (Savino *et al.*, 2000) and ricin A chain (Mlsna *et al.*, 1993). In the case of lychnin the rms deviations exceed 1.3 Å for all considered RIPs. The rms deviation for bouganin superimposition on PAP-R, ricin A chain and momordin I is around 1.1 Å (1.090 Å for 234 C_α, 1.147 for 233 C_α and 1.156 on 229 C_α, respectively) while it is higher for the superimposition on dianthin 30 and saporin-S6 (1.399 Å and 1.340 Å on 210 C_α, respectively). Aside from the rmsd values, lychnin and bouganin are well superimposed to the considered RIPs in the central part of the molecule, which includes the active site (Fig. 40a).

At the N-terminal region, the length and orientation of the loop connecting the fourth (β7 in bouganin and β6 in lychnin) and the fifth (β8 in bouganin and β7 in lychnin) strands of the mixed β-sheet, substantially differ among the considered RIP structures (Fig. 40b): it is longer in dianthin 30 (green), saporin-S6 (red) and lychnin (cyan), but in the latter differently oriented; it is intermediate in bouganin (magenta) and PAP-R (dark blue); while in ricin A chain (gold) and momordin I (grey) the loop is much shorter with respect to the others. Variations in folding are also observed in the subsequent region composed by (i) an α-helix, common to all considered RIPs, with significant variability in length, and by (ii) a β-strand, found in bouganin, PAP-R, momordin I, ricin A chain and lychnin, in this last structure smaller in size and not superimposable to the others (Fig. 40c). Dianthin 30 and saporin-S6 lack this last strand of the N-terminal mixed β-sheet.

In all known RIP structures, the C-terminal region is characterised by a structural motif composed of two antiparallel β-strands connected by a loop or a small helix. These two strands are almost parallel to a long helix forming a wall of the catalytic cleft. In bouganin structure this motif is similar to those found in PAP-R, momordin I and ricin A chain (Fig. 40d). In dianthin 30 and saporin-S6 it is also observed, but it is much shorter than in the previous RIPs. Lychnin structure lacks this motif (Fig. 37b).

3.5.3 Differences at the active site: The positions of the residues involved in the catalysis are well conserved except for the orientation of one tyrosine (the first in sequence numbering, Fig. 38): the two aromatic rings are almost parallel, as required to form a stack interaction with the adenine of the substrate, in bouganin, dianthin 30, PAP-R, momordin I and saporin-S6, while in lychnin the aromatic ring of Tyr69 is perpendicular to that one of Tyr119, and oriented to form a double hydrogen bond with Ser117 (Fig. 41). Similarly, in ricin A chain structure the hydroxyl group of Tyr80 forms an hydrogen bond with the Gly121 carbonyl group (Mlsna *et al.*, 1993). In bouganin and the other considered RIP structures, including ricin, the first catalytic tyrosine has a higher thermal factor (B) than the second one, indicating a greater mobility. In lychnin structure Tyr69 and Tyr119 are similarly ordered (mean B calculated on side chain atoms 15.4 $Å^2$ and 17.8 $Å^2$, respectively).

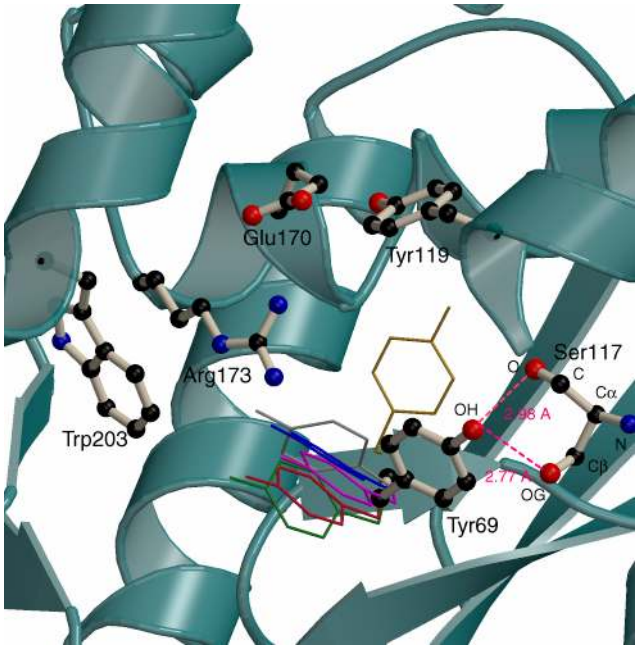

Figure 41. Catalytic site of lychnin. The conserved important residues and Ser117, are showed in ball-and-sticks and the orientation of the side chain of the catalytic tyrosine, in other RIPs is also shown: bouganin (magenta), lychnin (cyan), dianthin 30 (green), saporin-S6 (red), PAP-R (dark blue), momordin I (grey) and ricin A chain (gold). Tyr69 interacts with Ser117 through two hydrogen bonds between the OH group of Tyr69 and O and OG atoms of Ser117. The figure was produced by MOLSCRIPT (Kraulis, 1991) and rendered by RASTER3D (Merritt *et al.*, 1997).

3.6 DISCUSSION AND CONCLUSION

Two novel structures have been added to the bank of RIP structures. Lychnin and bouganin have been chosen because of some peculiarities in their properties in experimental assays. In particular, bouganin has a very low *in vivo* toxicity as compared to its intrinsic enzymatic activity (data not shown) whereas lychnin has an atypical primary structure. The other representative RIPs chosen for comparison were dianthin 30, PAP-R, momordin I, saporin-S6 and ricin A chain, for which crystal and activity data were either available in literature or obtainable in our laboratory.

Bouganin, lychnin, the different type 1 RIPs and ricin A chain structures share the typical "RIP fold", conserved despite the sequence homology is around or less than 30%, except for dianthin 30 and saporin-S6 (87%) (Fermani *et al.*, 2005).

Important structural differences are observed at the end of the mixed β-sheet of the N-terminal domain and at the C-terminal region (Fig. 40a), which are highly exposed regions. Segments connecting the final strands at the N-terminal domain show various arrangements between RIPs (Fig. 40b,c). It has been proposed that (i) this region, ranging from Tyr91 to Thr116 in ricin A chain, binds to monoclonal antibodies that neutralise the toxicity of these proteins (Lebeda *et al.*, 1999) and (ii) it forms the top of a putative recognition site for ribosomes (Mishra *et al.*, 2004). At the C-terminal region, the structural motif composed of two antiparallel β-strands is absent in lychnin while it is shorter in dianthin 30 and saporin-S6 compared to the other considered RIPs (Fig. 40d). The core of the molecule, containing the active site, is highly conserved among RIPs (Fig. 41a). The side chains of catalytic residues are superimposable, except for the first tyrosine, which assumes different orientations in the considered RIPs (Fig. 41). Moreover, the high thermal parameters of this residue indicate that it is quite mobile and could work as a moving door for the adenine entering in the catalytic site. On the contrary, in lychnin structure Tyr69 shows a B value comparable to that one of Tyr119, and it is oriented to interact with Ser117 through two hydrogen bonds formed between the OH group of Tyr69 and atoms O and OG of Ser117 (Fig. 41). Similarly, in ricin structure Tyr80 forms an hydrogen bond with Gly121, but it keeps an higher B value with respect to Tyr123 (Mlsna *et al.*, 1993).

The observed structural differences between these proteins do not fully explain the differences in the amount of adenine released from various polynucleotides and the inhibitory activity in a cell-free system (Table 15) (Fermani *et al.*, submitted). The experiments on various substrates (hsDNA, poly(A) and rat ribosomes) were carried out by the group of Professor Bolognesi (Experimental Pathology Department of Bologna University).

Table 16. Adenine polynucleotide glycosylase activity (PNAG) and protein synthesis inhibitory activity of different type 1 RIPs and ricin A chain.

		PNAG activity (pmol A released)[$]			Protein synthesis inhibitory activity (10^3 U x mg^{-1})*
		hsDNA	Poly(A)	Rat Ribosomes	
Group 1	**Lychnin**	29.5 (±6.3)	n.d.[#]	7.2 (±1.2)	176
	Momordin I	27.1 (±3.8)	n.d.[#]	3.9 (±0.2)	526
	Ricin A chain	48.5 (±1.4)	n.d.[#]	6.2 (±1.4)	300
Group 2	**Bouganin**	377.7 (±3.7)	n.d.[#]	4.8 (±0.9)	75
	PAP	503.2 (±33.4)	n.d.[#]	5.1 (±0.5)	125
Group 3	**Dianthin 30**	239.9 (±10.4)	5.4 (±1.7)	5.7 (±1.2)	96
	Saporin-S6	376.1 (±15.8)	>300	19.1 (±2.7)	813

[$] Glycosylase activity was determined with reaction mixtures containing 10 pmol of RIP, 10 µg of hsDNA and poly(A) and 10 pmol of rat ribosomes. Data are expressed as mean ± S.D.
* One unit of inhibitory activity (U) is defined as the amount of protein causing 50% inhibition in 1 ml of reaction mixture.
[#] Not determinable (less than the threshold of sensitivity of the analysis apparatus).

There was no correlation between the inhibition of translation by mammalian ribosomes and the activity on simpler substrates. Depurination activity was measured at different pHs, including pH 4.0, to maximise the amount of adenine released, choosing for each assay the optimal pH for RIP activity on any given substrate. In particular acidic pH allows for the detection of much lower amounts of adenine released from DNA. On the other hand (i) we can suppose on the basis of the high structure similarity between crystallised RIPs, that the global protein folding is not much altered by the ionisation of the surface groups at pH 4.0, and (ii) some intracellular plant cell compartments actually present acidic environments.

The activity of assayed RIPs indicates that saporin-S6 is the most efficient both in the protein synthesis inhibition and deadenilation of ribosomes (Table 15).

Analysis of RIP activities on DNA and poly(A) allow to identify three possible groups: group 1, without measurable activity on poly(A) and with low activity on DNA (tens of adenines released), group 2, without activity on poly(A) and with high activity on DNA (hundreds of adenines released) and group 3, active on poly(A) and with high activity on DNA. Group 1 applies to lychnin, momordin-I, ricin A chain, group 2 to bouganin and PAP-R and group 3 to saporin-S6 and dianthin-30, respectively.

The efficiency of saporin-S6 on ribosomes corresponds to a lower specificity: the molar ratio of adenine released indicates that this enzyme removes more than one base (almost two, in the given reaction time) for each ribosome, the Endo's adenine and an additional one (Table 15). All other considered RIPs specifically release the Endo's adenine from ribosome molecules (Barbieri *et al.*, 1993). It has been already proposed that beside their structural similarity, the higher efficiency of saporin-S6 on protein synthesis inhibition, with respect to dianthin 30, could be ascribed to a more negative electrostatic surface potential in the active cleft (Fermani *et al.*, 2005) which may efficiently stabilise the oxacarbenium-like transition state.

We can suppose that the previous observation may justify the lower specificity on rat ribosomes and the higher activity on poly(A) of saporin-S6 compared to dianthin 30. It is not clear why dianthin 30 has a detectable activity on poly(A) respect to others considered RIPs. Evidently the stabilisation of the oxacarbenium-like transition state is not the unique factor determining the activity on this substrate.

Bouganin shows a wide active site characterised by a negative potential with a small positive zone determined by Arg168 (Fig. 39a). However, its inhibitory activity on ribosomes is the lowest one and its deadenilation efficiency is almost negligible on poly(A) (Table 15). Similarly, lychnin is inefficient on poly(A), but shows a light increased inhibitory activity with respect to bouganin (Table 15). Various simulation models of ricin A chain X-ray structure bound to a modelled hexanucleotide CGAGAG loop or to a 29mer oligonucleotide hairpin (Olson,1997; Olson *et al.*, 1999), indicated that Arg134 and Arg213 formed a ion-pair with the phosphodiester backbone of the first cytidine and the subsequent guanosine, respectively. Arg134 (numbering correspond to ricin) is conserved in all RIP family, while Arg213 is replaced by lysine in lychnin, dianthin 30, saporin-S6 and PAP-R, by a non-polar residue (Gly194) in momordin I and by a residue with an opposite charge (Asp200) in bouganin (Fig. 39). Mutations R213A and R213D lowered the enzymatic activity respect to wild-type ricin, by 10-fold and over 100-fold, respectively (Marsden *et al.*, 2004). It was also proposed that Asn78 in ricin (Olson *et al.*, 1999) or the corresponding Asn70 in PAP-R (Rajamohan *et al.*, 2001) is involved in the interactions with the substrate, probably with the phosphodiester group between the target adenosine and the subsequent guanosine. This residue is conserved in all considered RIPs, except for bouganin and lychnin, which have an aspartate in the corresponding position (Fig. 38). The previous reported sequence substitutions could cause for bouganin and lychnin unfavourable interactions with the substrate, justifying the low efficiency in protein synthesis inhibition and deadenilation of poly(A) or the stricter specificity for the Endo's adenine on rat ribosomes with respect to saporin-S6. Moreover, saporin-S6 structure shows in the region surrounding the active cleft, several lysines (46, 67, 91, 125, 134, 210, 220, 234) and an

arginine (209) pointing out from the protein surface (Fig. 39e). They could be accessible coupler for the substrate backbone phosphate groups. Lychnin structure shows six hypothetic anchoring points (Lys39, Arg93, Lys98, Lys123, Arg195, and Lys205) (Fig. 39c), but the catalytic reaction could be hampered by the electrostatic surface potential at the active site, not highly negative as in saporin-S6. No other of considered RIPs shows a comparable number of positive exposed residues. Moreover, in lychnin the orientation of Tyr69 aromatic ring almost perpendicular to Tyr119 (Fig. 41), is not suitable to form a stack interaction stabilising the target adenine. The correct positioning of Tyr69, which partially hinders on the right side the access to the active cavity, would require the break of a double hydrogen bond with Ser117 followed by a rotation of the aromatic ring.

The above considerations can not be addressed to explain the activity of RIPs on hsDNA. The experimental conditions (pH 4) affect the electrostatic potential on the protein surface. All type 1 RIPs have an highly basic isoelectric point (equal or higher than 9) and at pH 4 the surface becomes almost all positively charged (Fig. 39b,d,e). Only bouganin, saporin-S6 (Fig. 40b,f) dianthin 30 and PAP-R (not shown), corresponding to the toxins showing a high activity on DNA (Table 15), still maintain in these acidic conditions a negatively charged zone in the active cleft corresponding to the catalytic glutamate. Supposing that the deadenilation of DNA occurs with the same mechanism proposed for ribosomes (Mozingo *et al.*, 1992; Ren *et al.*, 1994; Huang *et al.*, 1995), the reaction can proceed only if the catalytic glutamate, responsible for the nucleofilic attack on the positive transition state or the polarization of a water molecule, has a negative charge.

In conclusion, the higher protein synthesis inhibitory activity and efficiency of saporin-S6 in the deadenilation of various polynucleotides, as rat ribosomes, poly(A) and hsDNA, compared to other RIPs can be ascribed to an efficient interaction between the enzyme and the substrate, guaranteed by several exposed arginines or lysines surrounding the active site cleft, and to the negative electrostatic surface potential into the active cavity, which stabilise the positively charged transition state. These two conditions are not present at the same time in any other of the considered RIPs: bouganin shows a negative potential at the active site, but the interaction with the substrate could be prevented by the negative charge of some surrounding residues, while in lychnin the interaction could be as efficient as in saporin-S6, but the position and the interactions of Tyr69 and the electrostatic surface potential at the active site probably do not favour the adenine removal. Moreover, the structural differences observed in the exposed regions of the N- and C-terminal domains may influence the enzyme-substrate interaction and probably the RIP enzymatic activity.

The gained information from this research show that although the structures give some useful indications to explain RIPs' action on polynucleotides and protein synthesis, the high complexity of the enzyme/substrate system still prevents the complete evaluation and final understanding of all the

parameters that could influence RIP activity. Moreover, the wide range of heterogenous substrates on which they acts with different activity enhances the interest on their biological function. Knowledge of structural differences between type 1 RIPs is of great importance for their pharmacological and medical applications. Our results also encourage the extension of crystallographic investigations on other RIPs from diverse sources to elucidate important differences that can be linked to their biological activities on various substrates.

3.7 REFERENCES

- Ago, H., Kataoka, J., Tsuge, H., Habuka, N., Inagaki, E., Noma, M., Miyano, M. X-ray structure of a pokeweed antiviral protein, coded by a new genomic clone, at 0.23 nm resolution. (1994) *Eur. J. Biochem.* **225**, 369-374.
- Barbieri, L., Zamboni, M., Montanaro, L., Sperti, S., Stirpe, F. Purification and properties of different forms of modeccin, the toxin of *Adenia digitata*. Separation of subunits with inhibitory and lectin activity. (1980) *J. Biochem.* **185**, 203-210.
- Barbieri, L., Battelli, M.G., Stirpe, F. Ribosome-inactivating proteins from plants. (1993) *Biochim. Biophys. Acta* **1154**, 237-282.
- Barbieri, L., Gorini, P., Valbonesi, P., Castiglioni, P., Stirpe, F. Unexpected activity of saporins. (1994) *Nature* **372**, 624.
- Barbieri, L., Valbonesi, P., Bonora, E., Gorini, P., Bolognesi, A., Stirpe, F. Polynucleotide:adenosine glycosidase activity of ribosome-inactivating proteins: effect on DNA, RNA and poly(A). (1997) *Nucleic Acids Res* **25**, 518-522.
- Barbieri, L., Valbonesi, P., Righi, F., Zuccheri, G., Monti, F., Gorini, P., Saporì, B., Stirpe, F. Polynucleotide:adenosine glycosidase is the sole activity of ribosome-inactivating proteins on DNA. (2000) *J. Biochem.* **128,** 883-889.
- Barbieri, L., Polito, L., Bolognesi, A., Ciani, M., Pelosi, E., Farini, V., Jha, A., Sharma, N., Vivanco, J. M., Chambery, A., Parente, A., Stirpe, F. Ribosome-inactivating proteins in edible plants and purification and characterization of a new ribosome-inactivating protein from *Cucurbita moschata*. (2006) *Biochim. Biophys. Acta* **1760**, 783-792.
- Battelli, M.G., Stirpe, F. Ribosome-inactivating proteins from plants. (1995) *In* Chessin, M., Deborde, D. Zipf, A. eds, Antiviral proteins in higher plants. CRC Press, Boca Raton, FL, 39-64.
- Bergamaschi, G., Perfetti, V., Tonon, L., Novella, A., Lucotti, C., Danova, M., Glennie, M.J., Merlini, G., Cazzola, M. Saporin, a ribosome-inactivating protein used to prepare immunotoxins, induces cell death via apoptosis. (1996) *Br. J. Haematol.* **93**, 789-794.
- Bolognesi, A., Barbieri, A., Carnicelli, D., Abbondanza, A., Cenini, P., Falasca, A.I., Dinota, A., Stirpe, F. Purification and properties of a new ribosome-inactivating protein with RNA N-glycosidase activity suitable for immunotoxin preparation from the seeds of Momordica cochinchinensis. (1989) *Biochim. Biofis. Acta* **993**, 287-292.
- Bolognesi, A., Barbieri, L., Abbondanza, A., Falasco, A.I., Carnicelli, D., Battelli, M.G., Stirpe, F. Purification and properties of new ribosome-inactivating proteins with RNA N-glycosidase activity. (1990) *Biochim. Biophys. Acta* **1087**, 293-302.
- Bolognesi, A., Tazzari, P.L., Olivieri, F., Polito, L., Falini, B., Stirpe, F. Induction of apoptosis by ribosome-inactivating proteins and related immunotoxins. (1996) *Int. J. Cancer* **68**, 349-355.

- Bolognesi, A., Polito, L., Oliveri, F., Valbonesi, P., Barbieri, L., M., Battelli, G., Carusi, M.V., Benvenuto, E., Del Vecchio Blanco, F., Di Maro, A., Parente, A., Di Loreto, M., Stirpe, F. New ribosome-inactivating proteins with polynucleotide:adenosine glycosidase and antiviral activities from Basella rubra L. and Bougainvillea spectabilis Willd. (1997) *Planta* **203**, 422-429.
- Bolognesi, A., Polito, L., Tazzari, P. L., Lemoli, R. M., Lubelli, C., Fogli, M., Boon, L., De Boer, M., Stirpe, F. *In vitro* anti-tumour activity of anti-CD80 and anti-CD86 immunotoxins containing type 1 ribosome-inactivating proteins. (2000) *Brit. J. Haematol*. **110**, 351-361.
- Brünger, A.T., Adams, P.D., Clore, G.M., DeLano, W.L., Gros, P., Grosse-Kunstleve, R.W., Jiang, J.S., Kuszewski, J., Nilges, N., Pannu, N.S., Read, R.J., Rice, L.M., Simonson, T., Warren, G.L. Crystallography and NMR system: a new software suite for macromolecular structure determination. (1998) *Acta Crystallogr. Sect. D: Biol. Crystallogr.* **54**, 905-921.
- Büssing, A. Induction of apoptosis by the mistletoe lectins: a review on the mechanisms of cytotoxicity mediated by *Viscum album* L. (1996) *Apoptosis* **1**, 25-32.
- Byers, V.S., Levin, A.S., Malvino, A., Waites, L.A., Robins, R. A., Baldwin, R.W. A phase II study of effect of addition of trichosanthin to zidovudine in patients with HIV disease and failing antiretroviral agents. (1994) *AIDS Res. Human Retroviruses* **10**, 413-420.
- Chambery, A., De Donato, A., Bolognesi, A., Polito, L., Stirpe, F., Parente, A. Sequence determination of lychnin, a type 1 ribosome-inactivating protein from *Lychnis chalcedonica* seeds. (2006) *Biol. Chem.* **387**, 1261-1266.
- Chambery, A., Pisante, M., Di Maro, A., Di Zazzo, E., Menotti, R., Costantini, S., Colonna, G., Parente, A. Invariant Ser211 is involved in the catalysis of PD-L4, type 1 RIP from *Phytolacca dioica* leaves. (2007) *Proteins: Struct. Func. Bioinf.* **67(1)**, 209-218.
- Combet, C., Blanchet, C., Geourjon, C., Deléage, G. NPS@: Network Protein Sequence Analysis. (2000) *TIBS* **25(291)**, 147-150.
- Dai, W.D., Bonos, S., Guo, Z., Meyer, W.A., Day, P.R., Belanger, F.C. Expression of pokeweed antiviral proteins in creeping bentgrass. (2003) *Plant Cell Rep.* **21**, 497-502.
- Day, J.D., Ernst, S.R., Frankel, A.E., Mozingo, A.F., Pascal, J.M., Molina-Svinth, M.C., Robertus J.D. Structure and activity of an active site substitution of ricin A chain. (1996) *Biochemistry* **35**, 11098-11103.
- Day, P.J., Lord, J.M., Roberts, L.M. The deoxyribonuclease activity attributed to ribosome-inactivating proteins is due to contamination. (1998) *Eur. J. Biochem.* **258,** 540-545.
- Den Hartog, M., Lubelli, C., Boon, L., Heerkens, S., Ortiz Buijsse, A.P., De Boer, M., Stirpe, F. Cloning and expression of cDNA coding for bouganin A type-I ribosome-inactivating protein from *Bougainvillea spectabilis* Willd. (2002) *Eur. J. Biochem.* **269**, 1772-1779.
- Ehrlich, P. Experimentelle Untersuchungen über Immunität I. (1891a) *Ueber Ricin. Dtsch. Med. Wochenschr.* **17**, 976-979.

- Ehrlich, P. Experimentelle Untersuchungen über Immunität II. Ueber Abrin. (1891b) *Dtsch. Med. Wochenschr*. **17**, 1218-1219.
- Endo, Y., Tsurugi, K. RNA N-glycosidase activity of ricin A-chain. Mechanism of action of the toxic lectin ricin on eukaryotic ribosomes. (1987) *J. Biol. Chem.* **262**, 8128-8130.
- Fermani, S., Falini, G., Ripamonti, A., Bolognesi, A., Polito, L., Stirpe, F. Crystallisation and preliminary X-ray diffraction analysis of two ribosome-inactivating proteins: lychnin and dianthin 30. (2003) *Acta Cryst.* **D59**, 1227-1229.
- Fermani, S., Falini, G., Ripamonti, A., Polito, L., Stirpe, F., Bolognesi, A. The 1.4.Å structure of dianthin 30 indicates a role of surface potential at the active site of type 1 ribosome inactivating proteins. (2005) *J. Struct. Biol.* **149**, 204-212.
- Fermani, F., Tosi, G., Farini, V., Polito, L., Falini, G., Ripamonti, A., Barbieri, L., Chambery, A., Bolognesi, A. Structure/function studies on two type 1 ribosome inactivating proteins: bouganin and lychnin. (2009) *J. Struct. Biol.* Submitted.
- Ferreras, J.M., Citores, L., De Benito, F.M., Arias, F.J., Rojo, M.A., Muñoz, R., Iglesias, R., Girbés, T. Ribosome-inactivating proteins and lectins from *Sambucus*. (2000) *Curr. Topics Phytochem.* **3**, 113-128.
- Frankel, A.E., Kreitman, R.J., Sausville, E.A. Targeted toxins. (2000) *Clin. Cancer Res.* **6**, 326-334.
- Garcia, P.A., Bredesen, D.E., Vinters, H.V., Von Einsiedel, R.G., Williams, R.L., Kahn, J.O. Byers, V.S., Levin, A.S., Waltes, L.A., Messing, R.O. Neurological reactions in HIV-infected patients treated with trichosanthin. (1993) *Neuropathol. Appl. Neurobiol.* **19**, 402-405.
- Girbés, T., Barbieri, L., Ferreras, J.M., Arias, F.J., Rojo, M.A., Iglesias, R., Alegre, C., Escarmis, C., Stirpe, F. Effects of ribosome-inactivating proteins on *Escherichia coli* and *Agrobacterium tumefaciens* translation systems. (1993) *J. Bacteriol.* **175**, 6721-6724.
- Girbés, T., Citores, L., Ferreras, J.M., Rojo, M.A., Iglesias, R., Muñoz, R., Arias, J., Calonge, M., Garcia, J.R., Mendez, E. Isolation and partial characterization of nigrin b, a non-toxic novel type 2 ribosome-inactivating protein from the bark of *Sambucus nigra* L. (1993a) *Plant Mol. Biol.* **22**, 1181-1186.
- Girbés, T., Citores, L., Iglesias, R ., Ferreras, J.M., Munoz, R., Rojo, M.A., Arias, F.J., Garcia, J.R., Mendez, E., Calonge, M. Ebulin 1, a nontoxic novel type 2 ribosome-inactivating protein from *Sambucus ebulus* L. leaves. (1993b) *J. Biol. Chem.* **268(24)**, 18195-18199.
- Girbés, T., Ferreras, J.M., Arias, F.J., Stirpe, F. Description, distribution, activity and phylogenetic relationship of ribosome-inactivating proteins in plants, fungi and bacteria. (2004) *Mini Rev. Med. Chem.* **4**, 461-476.
- Griffiths, G.D., Leek, M.D., Gee, D.J. The toxic plant proteins ricin and abrin induce apoptotic changes in mammalian lymphoid tissues and intestine. (1987) *J. Pathol.* **151**, 221-229.
- Huang, Q., Liu, S., Tang, Y., Jin, S., Wang, Y. Studies on crystal structures, active-centre geometry and depurinating mechanism of two ribosome-inactivating proteins. (1995) *Biochem. J.* **309**, 285-298.

- Hudak, K.A., Wang, P., Tumer, N.E. A novel mechanism for inhibition of translation by pokeweed antiviral protein: depurination of the capped RNA template. (2000) *RNA* **6,** 369-380.
- Hughes, J.N., Lindsay, C.D., Griffiths, G.D. Morphology of ricin and abrin exposed endothelial cells is consistent with apoptotic cell death. (1996) *Hum. Exp. Toxicol.* **15**, 443-451.
- Husain, J., Tickle, I.J., Wood, S.P. Crystal structure of momordin, a type I ribosome inactivating protein from the seeds of *Momordica charantia*. (1994) *FEBS Lett.* **342**, 154-158.
- Iglesias, R., Arias, F.J., Rojo, M.A., Escarmis, C., Ferreras, J.M., Girbés, T. Molecular action of the type 1 ribosome-inactivating protein saporin 5 on *Vicia sativa* ribosomes. (1993) *FEBS Lett.* **325**, 291-294.
- Irvin, J.D. Pokeweed antiviral protein. (1983) *Pharmacol. Ther.* **21**, 371-387.
- Jones, T.A., Zou, J.Y., Cowan, S.W., Kjeldgaard, M. Improved methods for building protein models in electron density maps and the location of errors in these models. (1991) *Acta Crystallogr. Sect. A: Fund. Crystallogr.* **47**, 110-119.
- Kahn, J.O., Gorelick, K.J., Arri, C.J., Lifson, J.D, Gambertoglio, J.G., Bostrom, A., Williams, R.L. Safety and pharmacokinetics of GLQ223 in subjects with AIDS an AIDS-related complex. (1994) *Antimicrob. Agents Chemother.* **38**, 260-267.
- Kataoka, J., Habuka, N., Miyano, M., Takanami, Y., Koiwai, A. DNA sequence and of *Mirabilis* antiviral protein (MAP), a ribosomeinactivating protein with antiviral property, from *Mirabilis jalapa* L. and its expression in *E. coli*. (1991) *J. Biol. Chem*. **266**, 8426-8430.
- Kataoka, J., Habuka, N., Miyano, M., Masuta, C., Koiwai, A. Adenine depurination and inactivation of plant ribosomes by an antiviral protein of *Mirabilis jalapa* (MAP). (1992) *Plant Mol. Biol.* **20**, 1111-1119.
- Knight, B. Ricin – a potent homicidal poison. (1979) *BMJ* **i**, 350-351.
- Kraulis, P.J. MOLSCRIPT: A program to produce both detailed and schematic plots of protein structures. (1991) *J. Appl. Crystallogr*. **24**, 946-950.
- Kubo, S., Ikeda, T., Imaizumi, S., Takanami, Y., Mikami, Y. A potent plant virus inhibitor found in *Mirabilis jalapa* L. (1990) *Ann. Phytopathol. Soc. Jpn* **56**, 481-487.
- Lam, S.K., Ng, T.B. First simultaneous isolation of a ribosome inactivating protein and an antifungal protein from a mushroom (Lyophyllum shimeji) together with evidence for synergism of their antifungal effects. (2001a) *Arch. Biochem. Biophys.* **393(2)**, 271-80.
- Lam, S.K., Ng, T.B. Hypsin, a novel thermostable ribosome-inactivating protein with antifungal and antiproliferative activities from fruiting bodies of the edible mushroom *Hypsizigus marmoreus*. (2001b) *Biochem. Biophys. Res Commun*. **285,** 1071-1075.
- Laskowski, R.A., MacArthur, M.W., Moss, D.S., Thornton, J.M. PROCHECK: A program to check the stereo chemical quality of protein structure. (1993) *J. Appl. Crystallogr.* **26**, 283-291.
- Lebeda, F.J., Olson, M.A. Prediction of a conserved, neutralising epitope in ribosome-inactivating proteins. (1999) *Int. J. Biol. Macromol.* **24**, 19-26.

- Li, M.X., Yeung, H.W., Pan, L.P., Chan, S.I. Trichosanthin, a potent HIV-1 inhibitor, can cleave supercoiled DNA in vitro. (1991) *Nucleic Acid Res* **19**, 6309-6312.
- Li, Y., Shen, W., Li, H.G., Li, J.H., Wong, R.N.–S., Shi, Q.L., Dong, Y.C. Role of TYR70 in the N-glycosidase activity of neotrichosanthin. (1999a) *Toxicon* **37**, 961-972.
- Li, H.G., Xu, S.Z., Wu, S., Yan, L., Li, J.H., Wong, R.N.-S., Shi, Q.L., Dong, Y.C. Role of Arg163 in the N-glycosidase activity of neo-trichosanthin. (1999b) *Protein Eng.* **12(11)**, 999-1004.
- Liu, R.S., Yang, J.H., Liu, W.Y. Isolation and enzymatic characterization of lamjapin, the first ribosome-inactivating protein from cryptogamic algal plant (*Laminaria japonica* A). (2002) *Eur. J. Phycol.* **37**, 163-172.
- Lodge, J.K., Kaniewski, W.K., Tumer, N.E. Broad-spectrum virus resistance in transgenic plants expressing pokeweed antiviral protein. (1993) *Proc. Natl Acad. Sci. USA* **90**, 7089-7093.
- Luzzati, V. Traitement statistique des erreurs dans la determination des structures cristallines. (1952) *Acta Crystallogr.* **5**, 802-810.
- Magnusson, S., Berg, T., Turpin, E., Frénoy, J.P. Interactions of ricin with sinusoidal endothelial rat liver cells. Different involvement of two distinct carbohydrate-specific mechanisms in surface binding and internalization. (1991) *J. Biochem.* **277**, 855-861.
- Marsden, C.J., Fülöp, V., Day, P.J., Lord, J.M. The effect of mutations surrounding and within the active site on the catalytic activity of ricin A chain. (2004) *Eur. J. Biochem.* **271**, 153-162.
- Matthews, B.W. Solvent content of protein crystals. (1968) *J. Mol. Biol*. **33**, 491-497.
- McGrath, M.S., Hwang, K.M., Caldwell, S.E., Gaston, I., Luk, K.-C., Wu, P., Mg, V.L., Crowe, S., Daniels, J., Marsh, J., Deinhart, T., Lekas, P.V., Vennari, J.C., Yeung, H.-W., Lifson, J.D. GLQ223: an inhibitor of human immunodeficiency virus replication in acutely and chronically infected cells of lymphocyte and mononuclear phagocyte lineage. (1989) *Proc. Natl Acad. Sci., USA* **86**, 2844-2848.
- McLachlan, A.D. Rapid comparison of protein structures. (1982) *Acta Crystallogr. Sect. A: Found. Crystallog*. **38**, 871-873.
- McRee, D.E. XtalView/Xfit-A versatile program for manipulating atomic coordinates and electron density. (1999) *J. Struct. Biol.* **125**, 156-165.
- Merritt, E.A., Bacon, D.J. Raster3D photorealistic molecular graphics. (1997) *Methods Enzymol*. **277**, 505-524.
- Mehta, A.D., Boston, R.S. Ribosome-inactivating protein. (1998) *In* J Bailey-Serres, DR Gallie, eds, A Look beyond transcription: mechanisms determining mRNA stability and translation in plants. American Society of plant physiologists, Rockville MD, 145-152.
- Mishra, V., Ethayathulla, A.S., Sharma, R.S., Yadav, S., Krauspenhaar, R., Betzel, C., Babu, C.R., Singh, T.P. Structure of a novel ribosome-inactivating protein from a hemi-parasitic plant inhabiting the northwestern Himalayas. (2004) *Acta Crystallogr. Sect. D: Biol. Crystallogr.* **60**, 2295-2304.
- Mlsna, D., Monzingo, A.F., Katzin, B.J., Ernst, S., Robertus, J.D. Structure of recombinant ricin A chain at 2.3 Å. (1993) *Protein Sci.* **2**, 429-435.

- Montfort, W., Villafranca, J.E., Monzingo, A.F., Ernst, S.R., Katzin, B., Rutenber, E., Xuong, N.H., Hamlin, R., Robertus, J.D. The three-dimensional structure of ricin at 2.8 Å. (1987) *J. Biol. Chem*. **262(11)**, 5398-5403.
- Mozingo, A.F., Robertus, J. D. X-ray analysis of substrate analogs in the ricin A-chain active site. (1992) *J. Mol. Biol.* **227**, 1136-1145.
- Mozingo, A.F, Collins, E.J., Ernst, S.R., Irvin, J.D., Robertus, J.D. The 2.5 Å structure of pokeweed antiviral protein. (1993) *J. Mol. Biol.* **233**, 705-715.
- Narayanan, S., Surolia, A., Karande, A.A. Ribosome inactivating protein and apoptosis: abrin causes cell death via mitochondrial pathway in Jurkat cells. (2004) *J. Biochem.* **377**, 233-240.
- Navaza, J. *AMoRe*: an automated package for molecular replacement. (1994) *Acta Crystallogr. Sect. A: Fund. Crystallogr*. **50**, 157-163.
- Nicholls, A., Sharp, K.A., Honig, B. Protein folding and association: Insights from the interfacial and thermodynamic properties of hydrocarbons. (1991) *Proteins: Struct. Func. Genet.* **11**, 281-296.
- Nicolas, E., Beggs, J.M., Haltiwanger, B.M., Taraschi, T.F. Direct evidence for the deoxyribonuclease activity of the plant ribosome inactivating protein gelonin. (1997) *FEBS Lett*. **406**, 162-164.
- Nicolas, E., Beggs, J.M., Haltiwanger, B.M., Taraschi, T.F. A new class of glycosylase/apurinic/apyrimidinic lyase that act on specific adenines in single stranded DNA. (1998) *J. Biol. Chem.* **273**, 17216-17220.
- Nicolas, E., Beggs, J.M., Taraschi, T.F. Gelonin is an unusual DNA glycosylase that removes adenine from single-stranded DNA, normal base pairs and mismatches. (2000) *J. Biol. Chem.* **275**, 31399-31406.
- Nielsen, K., Boston, R.S. Ribosome-inactivating proteins: a plant perspective. (2001) *Annu. Rev. Plant Physiol. Plant. Mol. Biol.* **52,** 785-816.
- Olsnes, S., Pihl, A. Different biological properties of the two constituent peptide chains of ricin, a toxic protein inhibiting protein synthesis. (1973a) *Biochem.* **12**, 3121-3126.
- Olsnes, S., Pihl, A. Isolation and properties of abrin: a toxic protein inhibiting protein synthesis: evidence for different biological functions of its constituents – peptide chains. (1973b) *Eur. J. Biochem.* **35**, 179-185.
- Olsnes, S., Stirpe, F., Sandvig K., Pihl, A. Isolation and characterization of viscumin, a toxic lectin from *Viscum album* L. (mistletoe). (1982) *J. Biol. Chem.* **257**, 13263-13270.
- Olsnes, S. The history of ricin, abrin and related toxins. (2004) *Toxicon* **44**, 361-370.
- Olson, M.A. Ricin A-chain structural determinant for binding substrate analogues: a molecular dynamics simulation analysis. (1997) *Proteins: Struct. Funct. Genet.* **27**, 80-95.
- Olson, M.A., Cuff L. Free energy determinants of binding the rRNA substrate and small ligands to ricin A-chain. (1999) *Biophys. J.* **76**, 28-39.
- Otwinowski, Z., Minor, W. Processing of X-ray diffraction data collected in oscillation mode. (1997) *Methods Enzymol.* **276**, 307-326.

- Park, S.W., Lawrence, C.B., Linden, J.C., Vivanco, J.M. Isolation and characterization of a novel ribosome-inactivating protein from root cultures of pokeweed and its mechanism of secretion from roots. (2002a) *Plant Physiol.* **130**, 164-178.
- Park, S.W., Stevens, N.A., Vivanco, J.M. Enzymatic specificity of three ribosome-inactivating proteins against fungal ribosomes, and correlation with antifungal activity. (2002b) *Planta* **216,** 227-234.
- Parikh, B.A., Tumer, N.E. Antiviral activity of ribosome inactivating proteins in medicine. (2004) *Mini Rev. Med. Chem.* **4**, 523-543.
- Pelosi, E., Lubelli, C., Polito, L., Barbieri, L., Bolognesi, A., Stirpe, F. Ribosome-inactivating proteins and other lectins from Adenia (Passifloraceae). (2005) *Toxicon* **46(6)**, 658-663.
- Poyet, J.L., Hoeveler, A., Jongeneel, C.V. Analysis of active site residues of the antiviral protein from summer leaves from *Phytolacca Americana* by site-directed mutagenesis. (1998) *Biochem. Biophys. Res. Commun.* **253**, 582-587.
- Rajamohan, F., Mao, C., Uckun, F.M. Binding interactions between the active center cleft of recombinant pokeweed antiviral protein and the α-Sarcin/Ricin stem loop of ribosomal RNA. (2001) *J. Biol. Chem.* **276(26)**, 24075-24081.
- Ready, M.P., Kim, Y., Robertus, J.D. Directed alterations of active site residues in ricin A chain and implications for the mechanism of action. (1991) *Proteins: Struct. Funct. Genet.* **10(3)**, 270-278.
- Reinbothe, S., Reinbothe, C., Lehmann, J., Becker, W., Apel, K., Parthier, B. JIP60, a methyl jasmonate-induced ribosome-inactivating protein involved in plant stress reactions. (1994) *Proc. Natl. Acad. Sci. USA* **91**, 7012-7016.
- Ren, J., Wang, Y., Dong, Y., Stuart, D.I. The N-glycosidase mechanism of ribosome-inactivating proteins implied by crystal structures of alpha-momorcharin. (1994) *Structure* **2**, 7-16.
- Roberts, W.K., Selitrennikof, C.P. Isolation and characterization of two antifungal proteins from barley. (1986) *Biochim. Biophys. Acta* **880**, 161-170.
- Robertus, J.D., Monzingo, A.F. The structure of Ribosome Inactivating Proteins. (2004) *Mini-Rev. Med. Chem.* **4(5)**, 477-486.
- Rojo, M.A., Yato, M., Ishii-Minami, N., Minami, E., Kaku, H., Citores, L., Girbés, T., Shibuya, N. Isolation, cDNA cloning, biological properties and carbohydrate binding specificity of sieboldin-b, a type II ribosome-inactivating protein from the bark of Japanese elderberry (*Sambucus sieboldiana*). (1997) *Arch. Biochem. Biophys.* **340**, 185-194.
- Roncuzzi, L., Gasperi-Gampani, A. DNA-nuclease activity of the single-chain ribosome-inactivating proteins dianthin 30, saporin 6 and gelonin. (1996) *FEBS Lett*. **392,** 16-20.
- Ruggiero, A., Chambery, A., Di Maro, A., Parente, A., Berisio, R. Atomic resolution (1.1 Å) structure of the ribosome-inactivating protein PD-L4 from *Phytolacca dioica L.* leaves. (2008) *Proteins: Struct. Func. Bioinf.* **71(1)**, 8-15.
- Sandvig, K., Van Deurs, B. Transport of protein toxins into cells: pathways used by ricin, cholera toxin and Shiga toxin. (2002) *FEBS Lett.* **529**, 49-53.

- Savino, C., Federici, L., Ippoliti, R., Lendaro, E., Tsernoglou, D. The crystal structure of saporin SO6 from *Saponaria officinalis* and its interaction with the ribosome. (2000) *FEBS Lett.* **470**, 239-243.
- Shaw, P.C., Lee, K.M., Wong, K.B. Recent advances in trichosanthin, a ribosome-inactivating protein with multiple pharmacological properties. (2005) *Toxicon* **45**, 683-689.
- Simmons, B.M., Stahl, P.D., Russell, J.H. Mannose receptor-mediated uptake of ricin toxin and ricin A chain by macrophages. Multiple intracellular pathways for A chain translocation. (1986) *J. Biol. Chem.* **261**, 7912-7920.
- Skilleter, D.N., Paine, A.J., Stirpe, F. A comparison of the accumulation of ricin by hepatic parenchymal and non-parenchymal cells and its inhibition of protein synthesis. (1981) *Biochim. Biophys. Acta* **677**, 495-500.
- Stillmark, H. Ueber Ricin, ein giftiges Ferment aus den Samen von *Ricinus comm.* L und einigen anderen Euphorbiaceen. (1888) Thesis, Dorpat.
- Stillmark, R. Ueber Ricen. Arbeiten des Pharmacologischen Institutes zu Dorpat, iii, 1889. Cited in: Flexner, J. The histological changes produced by ricin and abrin intoxications. (1897) *J Exp Med.* **(2),** 197-216.
- Stirpe, F., Olsnes, S., Pihl, A. Gelonin, a new inhibitor of protein synthesis, nontoxic to intact cells. Isolation, characterization, and preparation of cytotoxic complexes with concanavalin A. (1980) *J. Biol. Chem.* **255**, 6947-6953.
- Stirpe, F. On the action of ribosome-inactivating proteins are plant ribosomes species-specific? (1982) *J. Biochem.* **202,** 279-280.
- Stirpe, F., Barbieri, L., Abbondanza, A., Falasca, A.I., Brown, A.N.F., Sandvig, K., Olsnes, S., Pihl, A. Properties of volkensin, a toxic lectin from *Adenia volkensii*. (1985) *J. Biol. Chem.* **260**,. 14589-14595.
- Stirpe, F., Bailey, S., Miller, S.P., Bodley, J.W. Modification of ribosomal RNA by ribosome-inactivating proteins from plants. (1988) *Nucleic Acids Res.* **16**, 1349-1357.
- Stirpe, F, Barbieri, L., Battelli, M.G., Soria, M., Lappi, D.A. Ribosome inactivating proteins from plants: present status and future prospects. (1992) *Bio/Technol.* **10,** 405-412.
- Stirpe, F. Ribosome-inactivating proteins. (2004) *Toxicon* **44**, 371-383.
- Stirpe, F., Battelli, M.G. Ribosome-inactivating proteins: progress and problems. (2006) *Cell. Mol. Life Sci.* **63**, 1850-1866.
- Stirpe, F., Bolognesi, A., Bortolotti, M., Farini, V., Lubelli, C., Pelosi, E., Polito, L., Dozza, B., Strocchi, P., Chambery, A., Parente, A., Barbieri L. Characterization of highly toxic type 2 ribosome-inactivating proteins from *Adenia lanceolata* and *Adenia stenodactyla* (Passifloraceae). (2007) *Toxicon* **50(1)**, 94-105.
- Strocchi, P., Barbieri, L., Stirpe, F. Immunological properties of ribosome-inactivating proteins and of a saporin-IgG conjugate. (1992) *J. Immunol. Methods* **155**, 57-63.
- Tahirov, T.H., Lu, T.H., Liaw, Y.C., Chen, Y.L., Lin, J.Y. Crystal structure of abrin-a at 2.14 Å. (1995) *J. Mol. Biol.* **250(3)**, 354-67.

- Tomatsu, M., Kondo, T., Yoshikawa, T., Komeno, T., Adachi, N., Kawasaki, Y., Ikuta, A., Tashiro, F. An apoptotic inducer, aralin, is a novel type II ribosome-inactivating protein from Aralia elata. (2004) *Biol.Chem.* **385**, 819-827.
- Touloupakis, E., Gessmann, R., Kavelaki, K., Christofakis, E., Petratos, K., Ghanotakis, D.F. Isolation, characterization, sequencing and crystal structure of charybdin, a type 1 ribosome-inactivating protein from *Charybdis maritime* Willd. (2006) *FEBS J.* **273**, 2684-2692.
- Tumer, N.E., Hudak, K., Di, R., Coetzer, C., Wang, P., Zoubenko, O. Pokeweed antiviral protein and its applications. (1999) *Curr. Top Microbiol. Immunol.* **240,** 139-158.
- Van Damme, E.J.M., Hao, Q., Barre, A., Vandenbussche, F., Desmyter, S., Rougé, P., Peumans, W.J. Ribosome-inactivating proteins: a family of plant proteins that do more than inactivate ribosomes. (2001) *Crit. Rev. Plant Sci* **20**, 395-465.
- Vivanco, J.M., Savary, B.J., Flores, H.E. Characterization of two novel type I ribosome-inactivating proteins from the storage roots of the Andean crop *Mirabilis expansa*. (1999) *Plant Physiol.* **119,** 1447-1456.
- Yao, Q.Z., Yu, M.M., Ooi, L.S.M., Ng, T.B., Chang, S.T., Sun, S.S.M., Ooi, V.E.C. Isolation and characterization of a type 1 Ribosome-Inactivating Protein from fruiting bodies of the edible mushroom (*Volvariella volvacea*). (1998) *J. Agric. Food Chem.* **46(2)**, 788-792.
- Wang, P., Tumer, N.E**.** Virus resistance mediated by ribosome inactivating proteins. (2000) *Adv. Virus Res.* **55,** 325-355.
- Wang, H.X., Ng, T.B. Isolation of a novel deoxyribonuclease with antifungal activity from *Asparagus officinalis* seeds. (2001) *Biochem. Biophys. Res Commun.* **289,** 120-124.
- Wool, I.G., Gluck, A., Endo, Y. Ribotoxin recognition of ribosomal RNA and a proposal for the mechanism of translocation. (1992) *Trends Biochem. Sci.* **17,** 266-269.
- Zarling, J.M., Moran, P.A., Haffar, O., Sias, J., Richman, D., Spina, C.A., Myers, D.E., Kubelbeck, V., Ledbetter, J.A., Uckun, F.M. Inhibition of HIV replication by pokeweed antiviral protein targeted to CD4+ cells by monoclonal antibodies. (1990) *Nature* **347**, 92-95.
- Zhou, X., Li, X.D., Yuan, J.Z., Tang, Z.H., Liu, W.Y. Toxicity of cinnamomin—a new type II ribosome-inactivating protein to bollworm and mosquito. (2000) *Insect Biochem. Mol. Biol.* **30**, 259-264.

CHAPTER 4: LOOKING AT THE INTERACTIONS BETWEEN CISPLATIN AND METAL IONS WITH PROTEINS

4.1 INTRODUCTION

This research aimed at the structural characterisation, through X-ray technique, of platinum drugs, copper and other biologically relevant ions complexed to proteins involved in copper trafficking.
The ability of anticancer drugs to enter cells and to reach an adequate concentration within the appropriate intracellular compartments is an important determinant for the efficacy of a chemotherapy. Platinum coordination compounds have been successfully applied in cancer chemotherapy for more than 25 years since the introduction of the parent compound for this class of antitumor agents, namely, *cis*-[diamminedichloroplatinum(II)], known as cisplatin (DDT) (Rosenberg, 1999). They are the most effective antineoplastic agents for a number of malignancies (e.g., testicular, ovarian, head and neck, and bladder cancer) (Samimi *et al.*, 2003).
Over decades, a great deal of effort has been devoted to synthesis and testing of the tumor-inhibiting profiles for new metal complexes, with the major impetus toward development and implementation of novel anticancer drugs. These are anticipated to have superior efficacy, increased selectivity for tumor tissue, reduced toxicity, a wider spectrum of activity, lack of tumor cell resistance, and improved pharmacological characteristics (e.g., possibility of oral administration) as compared to cisplatin. Still, of thousands of tested compounds, only a fraction (about 30) have entered clinical trials and merely three Pt drugs (cisplatin, carboplatin and oxaliplatin) have eventually been approved worldwide in 1978, 1993, and 2002, respectively (Wong et *al.*, 1999; Galansky *et al.*, 2003; Timerbaev *et al.*, 2006). The cytotoxicity of DDT is related to the amount of drug that enters the cell, the extent to which that drug reaches the nucleus and reacts with DNA, and the ability of the cell to repair or tolerate DDP adducts (Andrews *et al.*, 1990). Pt who becomes cationic species in the plasma and in the intracellular fluid, can form cross-links with DNA and acting as strong nucleophile links selectively amino acids containing sulfur, like cysteine and metionine. The major mechanisms of resistance that have been identified thus far involve reduced drug uptake, increased cytoplasmic detoxicification, and increased DNA repair (Perez *et al.*, 1993; Johnson *et al.*, 1997; Fink *et al.*, 1998). Among these, reduced cellular drug accumulation is the most universally identified correlate of acquired DDT resistance (Andrews *et al.*, 1990). DDT and its analogues are highly polar molecules and do not cross lipid bilayer membranes easily. It enters cells relatively slowly compared with most anticancer agents. Until short time ago, platinum-based

anticancer drugs were thought to enter the cell mainly by passive diffusion. However, recently it has been demonstrated that the Cu homeostasis system can regulate the uptake, intracellular compartmentalization and efflux of DDT, carboplatin and oxaliplatin. (Katano *et al.*, 2003; Samimi *et al.*, 2004; Safaei *et al.*, 2005).

Accumulation and export of these anticancer drugs can be regulated by two copper-transporting ATPases, the Menkes (ATP7A) and Wilson (ATP7B) proteins, respectively; thus suggesting that platinum drugs can be taken up, distributed into various intracellular compartments, and exported from tumor cells by the system of membrane transporters and soluble trasporters ("chaperones") that evolved to manage copper homeostasis. ATP7A and ATP7B are important constituents of the Cu homeostasis system that has evolved to deliver Cu to Cu-requiring proteins while protecting the cells from toxic effects of Cu (Culotta *et al*., 1999). ATP7A is expressed in most tissues other than liver, whereas ATP7B is expressed predominantly in the liver. Very little is known about the mechanism by which these copper-transporters shuffle the Pt drugs, while the copper transport mechanism has been extensively studied and clarified. The observation that ATP7A- and ATP7B-transfected cells accumulate high levels of DDP in their vesicular compartment after exposure to low concentrations of the drug suggests that DDP also may be a substrate for these transporters (Katano *et al.,* 2003; Samimi *et al*., 2003). In particular, consistent with a possible role for ATP7A in the export of DDP, ATP7A was found to be overexpressed in some ovarian carcinoma cell lines with acquired DDP resistance (Katano *et al.*, 2002).

Although several studies indicate that ATP7A and ATP7B are capable of transporting copper only in its reduced form [copper(I)], data from other P-type ATPases, such as Znt, indicate that this class of enzymes may be capable of transporting other heavy metals when the metals are present in high concentrations (Liu et al., 2006). DDP is a substrate for ATP7B but is transported at a much slower rate than copper (Safei *et al.*, 2008).

The major Cu uptake transporter is the copper transporter 1 (CTR1), which delivers Cu to pathway-specific chaperones such as ATOX1, CCS and COX17 for delivery to the secretory compartment, cytosol and mitochondria respectively (Culotta *et al.*, 1999). An important feature of Cu transporters and chaperones is the presence of specific histidine-, methionine-, and cysteine-rich metal binding domains that selectively bind Cu(I) and exchange it with other Cu homeostasis proteins (Huffman *et al.*, 2001).

It has been shown that most of the DDT injected in a patient is protein bound (Deconti *et al.*, 1973). Therefore the study of Pt-protein adducts is important both for drug's activity and undesired side effects (Espinosa *et al.*, 1995). Unraveling the interactions between DDT and metal ions with proteins allows to determine specific structural parameters and chemical features (effect of the

charge, steric hindrance, flexibility) that may influence the reactivity and modulate the metal binding properties of the complex to the transport proteins. A detailed description of the molecular architecture and metal-binding features of these macromolecular systems could help to shed light on the mechanisms of cellular transport of not essential metal ions and compounds, like platinum and may open new avenues for the design of potentially active anticancer agents with tailored uptake and efflux properties. Thus, these studies may represent an initial step towards the design of new anticancer drugs active towards tumors resistant to DDT (Timerbaev *et al.*, 2006). Moreover, through the optimisation of interactions with specific molecular targets, it could be also possible to minimise side effects, sometimes rather severe, that represent a big limitation in the use of these drugs and vary from individual to individual. Indeed, the diverse response of individuals, all subjected to the same chemotherapeutic treatment, originates from different cellular processing of loaded drug, which involve proteins interacting, and sometimes interfering with the drug itself.

4.1.1 Model proteins object of structural invastigation: The aim of our work has been the crystallisation and structure determination of adducts between model proteins and platinum-based anticancer drugs or, generally, metal ions. Proteins naturally involved in copper homeostasis have been used as model. Such proteins have also been shown to be responsible for platinum drugs transport (see section 4.1). Among these proteins we have used human Hah1 and CopC. Hah1 is a metallochaperonine protein implicated in copper delivery to the Menkes and Wilson disease proteins. CopC is a bacterial protein that transports copper and shows a methionine rich domain with a sequence similar to those observed in other proteins involved in copper homeostasis in cells.
It was planed to investigate by single crystal X-ray crystallography the interaction of Hah1 and CopC with selected platinum substrates. The aim was to characterise the sites of attack of the platinum drugs and the consequent conformational alteration of the protein.
Also human ubiquitin and superoxide dismutase (SOD) have been selected both for their biological relevance and their full characterisation in the native state.
The knowledge of the interaction between the metal and its transport protein represents an important step of the overall understanding of the metal trafficking through the cell.

4.1.1.1 Hah1: Hah1 is a 68-amino acid protein (Hung *et al.*, 1998). It is a copper transport protein, whose structure has been deeply studied. Hah1 is part of a family of copper-binding proteins that share a similar MT/CXXC Cu(I) binding motif that is also present in its target proteins**.**

The Hah1 metallochaperonine protein is implicated in copper delivery to the Menkes and Wilson disease proteins (ATP7A and ATP7B). This small protein has a sequence similar to the six copper (I)-binding domains present both in ATP7A and ATP7B (Werimont *et al*, 2000).

A sequence analysis of numerous metal-transporting ATPases by Arnesano and coworkers revealed sequence homology between Atx1 and Ccc2, the yeast homologs HAH1 and MNK, respectively. The primary structure similarity of the two proteins suggested that their complimentary tertiary structures could be important to inducing or facilitating Cu(I) transfer (Arnesano *et al*., 2001).

Furthermore, since no crystal structure of the donor-target complex exists, Larin *et al*. used the solution structure of MNK4 and the crystal structure of HAH1 to artificially create a complex whose structure was compared to the X-ray structure of the HAH1 homodimer by rmsd that showed a high level of structural homology to the HAH1:MNK4 heterodimer (Larin *et al.*, 1999). A similar docking study was undertaken by Arnesano in which the artificially docked Atx1:Ccc2 heterodimer was compared to available crystal structures of Atx1, Ccc2 and HAH1 (Arnesano *et al.*, 2004). In this study, it was noted that the Atx1:Ccc2 complex, the yeast homolog to the human HAH1:MNK4 complex, is remarkably similar to the crystal structure of the HAH1 dimer as a whole and with respect to the geometry of the Cu(I) binding region of the heterodimer. In light of these studies, the use of the HAH1 homodimer structure as a model of the HAH1:MNK4 heterodimer is considered valid.

Wernimont *et al*. elucidated the structure of Hah1 using X-ray crystallography (PDB ID 1FEE), and determined the protein to be dimeric in the crystalline state, with one Cu(I) ion bound per dimer in a near-tetrahedral configuration (Wernimon *et al.*, 2000). The crystal structure of Hah1 was determined in the presence of Cu(I), Hg(II), and Cd(II). The structure of CuHah1 revealed a copper ion coordinated by Cys residues from two adjacent Hah1 molecules. The CuHah1 crystal structure is the first of a copper chaperone bound to copper and provides structural support for direct metal ion exchange between conserved MT/HCXXC motifs in two domains. The structures of HgHah1 and CdHah1also revealed metal ion coordination by two MT/HCXXC motifs**.** Although it was clear that Cu was bound by residues from each monomer, the data from the crystal structure supported either a four-coordinate or three-coordinate Cu(I) state with a loosely-bound fourth residue (Rosenzweig *et al.*, 2001). A four-coordinate Cu(I) site would also produce an electrostatic environment with a net charge of -3 in the active site, which is unfavourable (Wernimon *et al.*, 2000). NMR studies performed by Anastassopoulou *et al*. concluded that Atx1, the yeast homolog of HAH1, exists as a monomer in solution, binding one Cu(I) ion per monomer in a nearly linear two-coordinate fashion (PDB ID 1TL4) (Anastassopoulou *et al.*, 2004).

We planed to investigate by single crystal X-ray crystallography the interaction of Hah1 with selected platinum substrates. The proposed crystallographic studies could allow to characterise the sites of attack of the platinum drugs and the consequent conformational alteration of the protein.

4.1.1.2 CopC: CopC is a small soluble protein consisting of 102 amino acids expressed in the periplasm of *Pseudomonas syringae* pathovar *tomato* as part of its copper resistance response (cop operon) (Zhang *et al.*, 2006). Bacterial resistance to copper conferred by plasmids has been described not only in *Pseudomonas* (Cooksey, 1994) but also in *Xanthomonas* (Lee *at al.*, 1994), and *E. coli* (Brown *et al.*, 1994; 1995). These systems are highly homologous (Brown *et al.*, 1994; Cooksey, 1993; 1994) and contain the same genes. The plasmid is able to confer copper resistance to the host strains of Gram-negative bacteria and protects the cells by sequestering the excess of copper in the periplasm and in the outer membrane (Cooksey, 1994).

For *Pseudomonas* sp., the two regulatory genes are called *copR* and *copS*, and the four structural genes *copABCD* (Fig. 42). The four structural proteins determining copper resistance are the inner membrane protein CopD, the outer membrane protein CopB, both membrane-bound copper pumps, and two soluble proteins CopA and CopC present in the oxidizing environment of the periplasm (Fig. 42). CopA and CopC are blue copper-binding proteins containing 11 and 1 Cu^{2+} ions, respectively (Cha *et al.*, 1991). The operon COP encoding the four proteins, CopABCD, acts under the control of a copper inducible promoter requiring CopR and CopS that form part of copper sensing and gene induction systems (Mills *et al.*, 1993). Storage of excess copper in the periplasmic space is considered to protect the cell from toxic copper. How the membrane proteins CopD and CopB are involved in movement of copper across the outer and inner membranes is not understood.

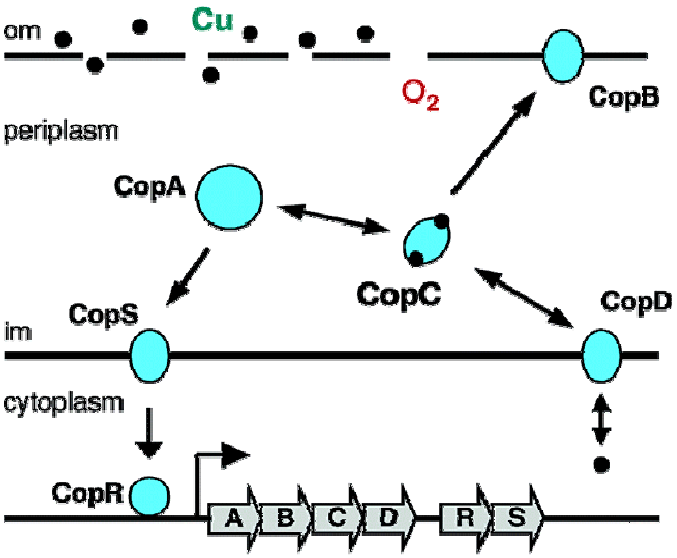

Figure 42. Copper transport and resistance in *Pseudomonas*. Om idicates outer membrane; im inner membrane.

CopC protein is proposed to be a copper carrier but in contrast to known cytoplasmic copper chaperones, it contains no cysteine residue (Zhang *et al.,* 2006). While Cys-rich sites are characteristic of copper(I) carriers in the reducing cytoplasm, His/Met-rich sites seem to be important in oxidizing environments (Huffman *et al.*, 2001; Tottey *et al.*, 2005). CopC shows a

region containing four methionine residues arranged as a $[M(X)_nM]_m$ motif, in analogy with other proteins involved in copper homeostasis in eukaryotic cell, like hCtr1 (Arnesano *et al.* 2003).

CopC can mimic the action of the copper transporter hCtr1 and the use of CopC as model is justified since hCtr1 is not a protein easily available, being its expression and purification very difficult.

NMR and EXAFS structural data revealed a β-barrel topology and two copper binding sites, separated by ~30 Å (Arnesano *et al.,* 2003; 2004). One site is specific for Cu(I) while the second is specific for Cu(II). A full solution structure analysis is reported for Cu(I)-CopC. The copper(I) site is constituted by His-48 and three of the four Met residues (40, 43, 46, 51), which are clustered in a Met-rich region. Oxidation of Cu(I)-CopC or reduction of Cu(II)-CopC causes migration of copper from one site to the other. This behavior indicates that CopC can exchange copper between two sites activated by a redox switch.

Since copper transport mechanisms have been studied and clarified , very little is known about the mechanisms by which copper-transporters shuttle platinum. We have investigated the interaction of CopC with selected platinum substrates to characterise the sites of attack of the platinum drugs and evaluate analogies/differences with the sites of interaction of copper.

4.1.1.3 Superoxide dismutase: There are three major families of superoxide dismutase, depending on the metal cofactor: Cu/Zn (which binds both copper and zinc), Fe and Mn types (which bind either iron or manganese), and finally the Ni type which binds nickel. In humans (as in all other mammals and most chordates), three forms of superoxide dismutase are present. SOD1 is located in the cytoplasm, SOD2 in the mitochondria and SOD3 is extracellular. The first is a dimer , while the others are tetramers. SOD1 and SOD3 contain copper and zinc, while SOD2 has manganese in its reactive centre.

Cytosolic Cu, Zn superoxide dismutase (SOD1; EC 1.15.1.1) is a critical component of the cellular defence against reactive oxygen species and catalyses the dismutation reaction of the superoxide radical anion to hydrogen peroxide and oxygen *via* the cyclic reduction and reoxidation of copper (Fridovich, 1975). On the other hand, SOD1 exhibits peroxidase activity and oxidizes various substrates in the presence of hydrogen peroxide (Hodgson *et al.*, 1975).

It is composed of two identical subunits, each containing 153 amino acids of known sequence (Barra *et al.,* 1980; Hallewell *et al.,* 1985) together with a Cu(II) and Zn(II) (Carrico *et al.,*, 1970). The recombinant human enzyme has been expressed at high levels, purified, and characterised from both Escherichia coli (Hallewell *et al.,* 1985) and yeast (Hallewell *et al.,* 1987). Both recombinant proteins have normal specific activity when compared to the enzyme purified from human

erythrocytes, but recombinant CuZn superoxide dismutase from *E. coli* lacks the N-acetylation found in the eukaryotic enzyme.

The overall fold in each SOD1subunit is described as an eight-stranded antiparallel β-barrel connected by three external loops (Tainer *et al.*, 1982; Rakhit *et al.*, 2006). Two of these loops, the Zn loop and the electrostatic loop, form the walls of a channel from the enzyme surface to the active site. The third loop region provides the Greek key connection across the β-barrel. Several charged residues within the electrostatic loop as well as the catalytically important Arg143 are involved in the electronic guidance of the substrate to the active site and so contribute to the high-level specificity of SOD1 for the superoxide substrate (Getzoff *et al.*, 1983). The Zn loop is so named because it contains ligands for the Zn ion. The metal ions in SOD1 are bridged by the imidazole ring of residue His63, which acts as a ligand to both metals. The catalytic copper is bound by four histidines, His 46, 48, 63 and 120, in a distorted tetrahedral binding geometry in the oxidised (Cu(II)) form and in a distorted trigonal planar geometry, bound by His 46, 48 and 120, in the reduced (Cu(I)) form, while the Zn is bound by His 63, 71, 80 and Asp 83 acting as a monodentate ligand, is thought to play a structural role and act as a positive charge sink. (Getzoff *et al.*, 1983; Rakhit *et al.*, 2006). There is structural evidence from crystallography and EXAFS that the Cu-His63-Zn-bridge in SOD1 is broken upon reduction to Cu(I), leaving an approximate trigonal planar Cu coordination (Strange *et al.*, 2003).

The first atomic-resolution structures for human SOD1, the first structure of a reduced SOD1, and the first structure of a fully Zn-substituted SOD1 enzyme have been solved by Strange *et al.* (Strange *et al.*, 2006).

Morover, crystals of cisplatin-treated bovin SOD were obtained by Calderone et al. (Calderone *et al.*, 2006). Structural data revealed a preference for platinum binding to His19 compared to Met115 or Cys6 residues. This preference was at least partially ascribed to the fact that the access to either Met115 or Cys6, the only free sulfur-containing groups of beSOD is somehow sterically hindered.

In SOD, both metal ions, Cu and Zn, can be selectively removed and replaced by other metals to obtain different metal ion derivatives which are useful for studying various aspects of metalloprotein chemistry (Valentine *et al.*, 1981). For this reason, human SOD1has been chosen as model protein to invastigate the interaction with cisplatin. In particular, SOD exhibits great stability under physiological-type condition and has several potential binding sites for platinum. Sulfur-containing side chains are known to represent preferred binding sites for platinum compounds. SOD1 has four cysteine residues, Cys6, Cys57, Cys111, and Cys146. An internal disulfide bond exists between Cys57 and Cys146 (Tainer *et al.,* 1982; Parge *et al.*, 1992), which contributes to the high stability of the SOD1 protein. This disulfide bond is highly conserved in SOD1s from various

organisms, including yeast, plants, flies, fishes, and mammals. In contrast, two free cysteines, Cys6 and Cys111, are not conserved: Only human and great ape SOD1s among mammals have the highly reactive free cysteine residue, Cys111, at the surface of the SOD1 molecule . Actually, yeast, fungi, and spinach (plants) have no free cysteines, and residue 6 is Ala and residue 111 is Ser in these organisms (Fink *et al.*, 2002). More evolved organisms, such as flies, fishes, and mammals, including the Japanese monkey, have only one free cysteine, Cys6.

It was demonstrated that Cys111 is a primary target for oxidative modification and plays an important role in oxidative damage to human SOD1, including familial amyotrophic lateral sclerosis mutants (Fujiwara *et al.*, 2007).

4.1.1.4 Ubiquitin: Ubiquitin (Ub) is a small protein of 76 residues (MW 8565 Da) folded in a compact globular structure in which a mixed parallel/anti-parallel β–sheet packs against an α-helix generating a hydrophobic core. Not found in bacteria, this protein is ubiquitous in eukaryotes and has highly conserved sequences, the human and the yeast proteins differing by only three residues (Vijay-Kumar *et al.*, 1987). The remarkable degree of sequence conservation underscores its important physiological role (Hershko *et al.*, 1998). Ub becomes attached to lysine residues of proteins to be degraded and targets them to the proteasome, the complex molecular machinery where the ATP-dependent process of degradation takes place. Besides protein degradation, Ub is known to activate cell signals in several pathways: tolerance to DNA damage, inflammatory response, protein trafficking, and ribosomal protein synthesis (Pickart *et al.*, 2004). The presence of Ub-positive protein aggregates is a biomarker of neurodegeneration (Ciechanover *et al.*, 2003), but the molecular mechanism underlying their accumulation is unknown. Protein aggregation is believed to be favored by metal ions, such as Cu(II) and Zn(II), whose levels are increased in brains of patients with Parkinson's and Alzheimer's diseases, the two most common neurodegenerative disorders (Sigel *et al.*, 2006). Ub has been widely used as model for stability, folding, and structural studies (Jackson *et al.*, 2006) and carefully characterized both in solution (Di Stefano *et al.*, 1987)and solid state (Vijay-Kumar *et al.*, 1987).

However, despite the plethora of structural investigations, only few studies concern the interaction with metal ions. Recently, binding of Cu(II) to Ub has been shown to destabilise the protein decreasing the thermal stability both in terms of unfolding temperature and enthalpy, while other metal ions, including Zn(II) and Cd(II), have no effect on the unfolding temperature (Milardi *et al.*, 2007). Crystallisation experiments with hUb and cisPt or Cu(II) have been carried out to investigate and compare the binding site(s). In the present study, also adduct formation between human ubiquitin (hUb) and group-12 metal ions Zn(II), Cd(II), and Hg(II) has been investigated by X-ray

crystallography. While Zn(II) is an essential element involved in several important cellular functions (Burdette *et al.*, 2003) Cd(II) and Hg(II) are toxic metal ions released into the environment by human activities, which may bind to adventitious sites, thus compromising protein functions (Valko *et al.*, 2005). The characterisation of metal-binding sites and the patterns of metal ion-induced crystallisation of human ubiquitin (hUb) can provide structural insights into the early aggregation mechanism of folded systems.

4.2 CRYSTALLISATION EXPERIMENTS

The aim of our work has been the crystallisation and structure determination of adducts between model proteins and platinum based anticancer drug or, generally, metal ions. Crystals of protein and cisplatin or other metal ions were preparated by co-crystallisation or soaking of already formed native crystals. The proteins are commercially available and human Hah1, CopC had been purchased by Protera srl while human SOD by Sigma-Aldrich. The cis-Pt based anticancer drugs had been supplied by the Laboratory of Prof. Natile, University of Bari, Italy.

4.2.1 Human Hah1: Hah1 cloned from human *c*DNA (residues 1-68, swissprot O00244), expressed in *E. Coli*, were used. Crystallisation experiments were performed in anaerobic conditions, being this protein sensitive to O_2. Crystallisation experiments were carried out at 293 K by the hanging drop method mixing 1.5 µl of protein with 1.5 µl of reservoir solution (750 µL in each well). To prepare metal- protein adducts, cisPt or Zeise 's salts ($K[PtCl_3(C_2H_4)]$), were used. In co-crystallisation experiments, the protein was dissolved at different concentrations in different metal solutions:

-5 mg/mL in 3.33 mM cisPt and milliQ water (protein-metal molar ratio 1:5).

-5 mg/mL in 3.33 mM cisPt and 20mM 2-[N-morpholino]ethanesulfonic acid (MES) pH 6.5 (protein-metal molar ratio 1:5).

-7.5 mg/mL in 1.92 mM cisPt and milli Q water (protein-metal molar ratio 1:2).

-7.5 mg/mL in 1.92 mM Sali di Zeiss and milli Q water (protein-metal molar ratio 1:2).

When Hah1 was tried to be co-crystallised with cisPt, the adduct was left to interact at least for 2 days before to set up crystallisation experiments, while only 1 day was enough for Zeise's salts being its hydrolysis time shorter than that of cisPt.

As reservoir solution, those reported in literature by Wernimont et al. and variation of them, including variation of precipitant concentration and/or buffer pH, were tested (Wernimont *et al.*, 2000):

a) 0.1 M MES pH 6.5, 1.8 M $(NH_4)_2SO_4$, 0.2 M $MgCl_2$, and 5 mM dithiothreitol (DTT).

b) 0.1 M MES pH 6.5, 0.1 M MES pH 6.5 and 1.5 M Li_2SO_4.

c) 1.0 M Li_2SO_4, and 5 mM DTT.

It was not possible to obtain any crystal of Hah1-metal adducts although dozen and dozen of co-crystallisation experiments were set up. Also attempts to obtain crystals of native protein were always unsuccessful.

4.2.2 CopC: Recombinant CopC, from *Pseudomonas syringae*, expressed in *Escherichia coli*, were used. It is in the apo form and consists of residues 25-126 (Swissprot accession C32018). Crystallisation experiments were carried out by the hanging drop method at room temperature by mixing the protein solution (1.0/2.0 µL) with an equal volume of reservoir solution (750 µl in each well). The tested reservoir solutions were those reported in literature and variations of them, including variation of precipitant concentration and/or buffer pH:

a) 2.0 M ammonium sulfate, 0.1 M sodium HEPES, pH 7.5, 2%(w/v) PEG 400 (Zhang *et al.*, 2006).

b) 4.4−5.2 M ammonium nitrate, 0.1 M sodium acetate, pH 4.6−4.8 (Zhang *et al.*, 2006).

c) 4.3 M NaCl, 0.1 M sodium HEPES, pH 7.5 (Wernimont *et al.*, 2003).

In the co-crystallisation experiments, to prepare metal- protein adducts, cisPt, transPt and Zeise's salts ($K[PtCl_3(C_2H_4)]$) were used: The adducts with cisPt or transPt were left to interact at least 2 days before to set up crystallisation experiments while those with Zeise's salts 1 day. The adducts were performed dissolving the protein in a metal aqueous solution containing the metal in molar ratio 1:3 with respect to the protein. The tested protein concentration ranged from 30 to 7 mg/mL. Co-crystallisations experiments did no produce crystals at all.

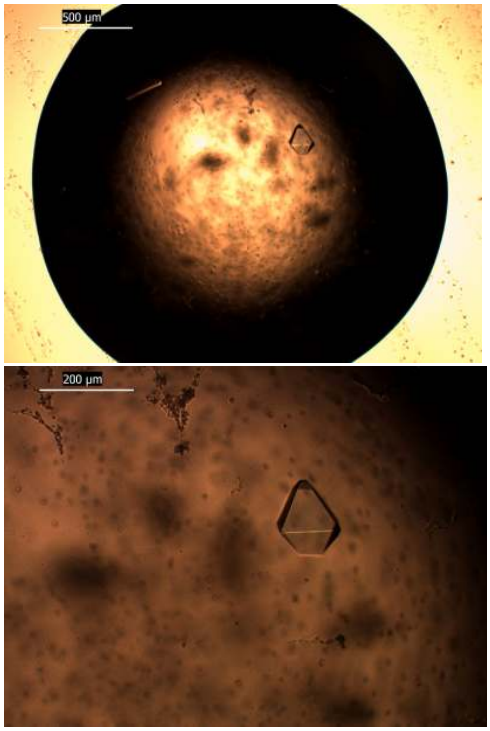

Figure 43. Optical micrographs at different magnifications of crystals of CopC grown in the presence of Cu(II).

Crystallisation experiments to obtain crystals of native protein were also unsuccessfully carried out.

In literature, the CopC was reported to be crystallised in the presence of Cu but not in the apo-form. So, we tried to dissolve the protein (14 mg/mL) in 2.66 mM $CuSO_4$ (protein-Cu(II) molar ratio 1:2) and we could obtain crystals (Fig. 43) in about one month, when 2.0 M Am_2SO_4, 0.1 M sodium HEPES, pH 7.5, 2% (w/v) PEG 400 were used as reservoir solution. Before to set up the crystallisation experiments, the CopC-Cu(II) adduct was left to interact one day.

4.2.3 Human superoxide dismutase: Superoxide dismutase from human erythrocytes (Catalog Number S9636) (hSOD) were crystallised either in hanging or sitting drop vapour diffusion at 293K. Crystallisation experiments to obtain native crystals of hSOD suitable for soaking experiments into solution containing cisPt and co-crystallisation metal-protein experiments were performed. The droplets (5µl or 10µl) contained protein and reservoir solution (750µL in each well)

in equal ratio. The conditions to grow single crystal were selected from those reported in literature for hSOD:

a) 2.2-2.4 M ammonium sulphate, 50 mM TRIS pH 7.5, 50 mM NaCl, 10^{-4} MEDTA, 0.01% (w/w) NaN_3 (Parge *et al.*, 1986).

b) 35-25% (v/w)PEG 8K, 50mM TRIS pH 7.5, 50mM NaCl, 10^{-4} MEDTA, 0.01% NaN_3 (Parge *et al.*, 1986).

c)15% (w/v) PEG 3350, 0.2 M calcium acetate, 0.1 M TRIS pH 8.0 (Strange *et al.*, 2003).

d) 2.1 M ammonium sulphate, 0.8 MNaCl, 50 mM TRIS pH 7.5 (DiDonato *et al.*, 2003).

e) 2.5 M ammonium sulphate, 0.1 M NaCl, 50 mM TRIS pH 7.5 (Strange *et al.*, 2006).

f) 3.0M ammonium sulphate, 0.1M NaCl, 50mM sodium acetate pH 4.75 (Strange *et al.*, 2006).

Hundreds of experiments were performed starting from those six conditions searching for the best one to growth single crystals. In each experiment, parameters such as precipitating concentration and pH of the buffer were changed one at the time or at the same time. The tested protein concentrations went from 20 to 8 mg/mL. When experiments to obtain crystals of native protein suitable for soaking into a platinum solution were set up, the protein was dissolved in 50 mM KH_2PO_4 pH 6.8.

In this case, the crystals generally always grew using condition a, b, d, e independently of the protein concentrations. In most case, aggregates of crystals were obtained (Fig. 44). When 2.1 M ammonium sulphate, 0.8 M NaCl, 50mM TRIS pH 7.5 or 2.5 M ammonium sulphate, 0.1 M NaCl, 50mM TRIS pH 7.5 were used as reservoir solution, after approximately 6 months single native crystals appeared (Fig. 45 a and b, c respectively):

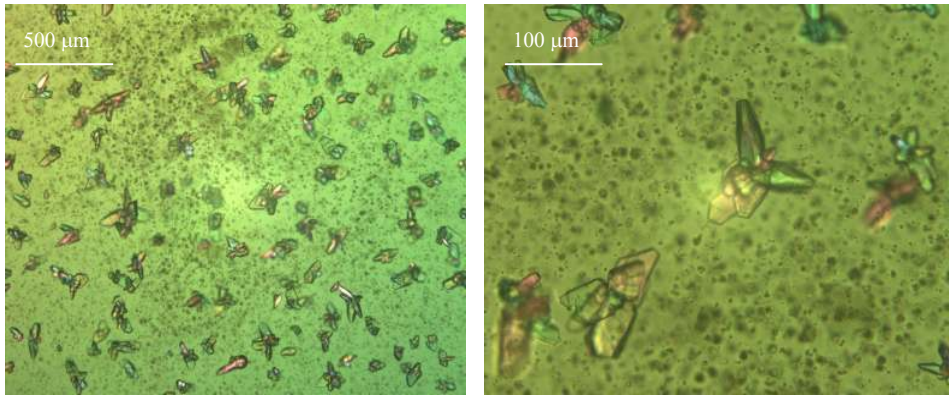

Figure 44. Optical micrographs at different magnifications of aggregated native human SOD crystals (20 mg/mL in 50 mM KH_2PO_4 pH 6.8) grown in the presence of ammonium sulphate.

All native crystals were used for soaking experiments: in these experiments crystals were soaked into a drop (5µl) containing the precipitating agent and the buffer in which they had grown, and cisPt.

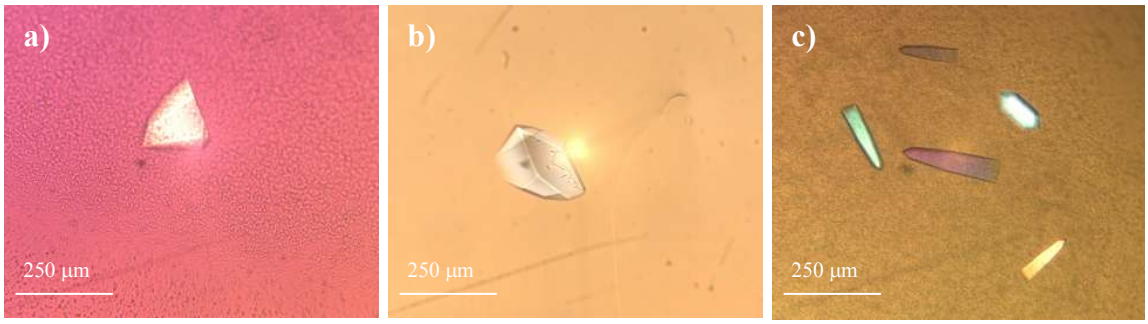

Figure 45. Optical micrographs at different magnifications of single native human SOD crystals (20 mg/mL in 50 mM KH_2PO_4 pH 6.8) grown in the presence of (a) 2.1 M ammonium sulphate, 0.8 MNaCl, 50 mM TRIS pH 7.5 and (b,c) 2.5 M ammonium sulphate, 0.1 M NaCl, 50 mM TRIS pH 7.5.

Because of the low solubility of cisPt, it was generally possible to prepare a soaking solution in which the concentration of cisPt corresponding at most to a protein-metal molar ratio 1:0.2. Although the low amount of cisPt, crystals dissolved in few minutes once introduced into the soaking solution.

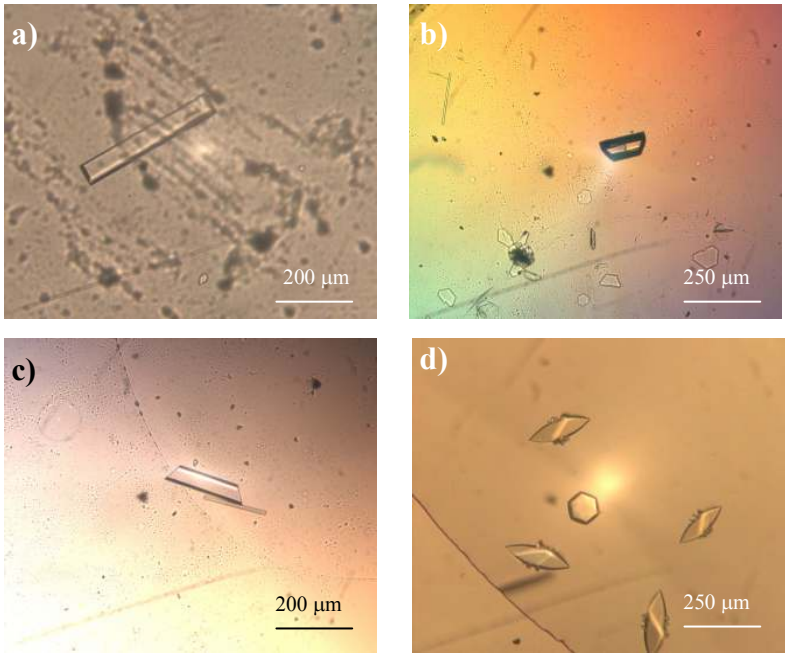

Figure 46. Optical micrographs of single human SOD crystals (20 mg/mL in 1.27 mM cisPt (protein-cisPt molar ratio 1:1) and 50 mM KH_2PO_4 pH 6.8) grown in the presence of (a) 15% (w/v) PEG 3350, 0.2 M calcium acetate, 0.1 M TRIS pH 8.0, (b) 2.2 M ammonium sulphate, 50 mM TRIS pH 7.5, 50 mM NaCl, 10^{-4} M EDTA, 0.01% (w/w) NaN_3, (c) 2.3 M ammonium sulphate, 50 mM TRIS pH 7.5, 50 mM NaCl, 10^{-4} M EDTA, 0.01% (w/w) NaN_3, (d) 2.4 M ammonium sulphate, 50 mM TRIS pH 7.5, 50 mM NaCl, 10^{-4} MEDTA, 0.01% (w/w) NaN_3.

Experiments of co-crystallisations were also tried. For these experiments hSOD-cisPt adducts were prepared dissolving protein and cisPt in 50 mM KH_2PO_4 pH 6.8 in molar ratio 1:1. The adducts

were left to interact 1 day before to set up crystallisation experiments. In 3/6 months, crystals generally grew in all the tested literature conditions.

Crystals tended to grow aggregated even if in the same drop also single crystals was possible to observe (Fig. 46a,b,c,d). In particular, in the same drop crystals with different morphology were often observed, especially when the used precipitating agent was ammonium sulphate (Fig. 46 b,c,d).

4.2.4 Human ubiquitin: Crystals of human ubiquitin and cisplatin or other metal ions such as Cd(II), Cu(II), Hg(II), and Zn(II) were prepared by co-crystallisation or soaking of already formed native crystals (Falini *et al.*, 2008). The crystallisation of metal ion-hUb adducts was carried out by the hanging drop method at 293 K. The drops (5µl) were formed by mixing equal ratio of protein and precipitating solution. The volume of the reservoir solution was 750 µl. The tested reservoir solution were those reported in literature:

a) 28% (w/v) PEG 4K 50 mM Na cacodylate pH 5.6 (Cook *et al.*, 1979).

b) 25% (w/v) PEG 1450K, 200 mM cadmium acetate, 50 mM HEPES pH 7.0 (Martin *et al.*, 2003).

c) 25% (w/v) PEG 8K, 200 mM cadmium acetate, 50 mM HEPES pH 7.0 (Martin *et al.*, 2003).

d) 60% (v/v) MPD, 20 mM Na citrate pH 4.0/4.2 (Igumenova *et al.*, 2004).

e) 31% (w/v) PEG 4K, 50 mM Na citrate pH 5.6 (Benitez-Cardoza *et al.*, 2004).

Hundreds of experiments were set up. The protein was dissolved in milliQ water at a concentration of 25 mg/mL. The metal ion was added to the protein solution up to a concentration close to that of precipitation. Hg-hUb crystals grew only in the presence of Hg-hUb molar ratio 1:1 and the reservoir was composed of 25% (w/v) PEG 1450, 50 mM HEPES pH 7.0, and 2.92 mM $Hg(CH_3COO)_2$. Orthorhombic crystals appeared within one month (Fig. 47).

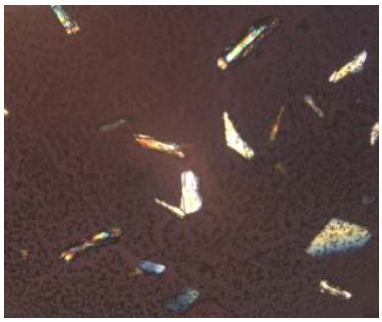

Figure 47. Optical micrographs of Hg-hUb crystals.

Single crystals of Zn-hUb were grown in the presence of 25% (w/v) PEG 1450, 50 mM HEPES pH 7.0, and $Zn(CH_3COO)_2$ at a concentration ranging from 200 to 25 mM. Orthorhombic crystals formed in about two weeks at the lowest zinc concentration (Fig. 48a), while cubic crystals formed in a week at the highest concentration (Fig. 48b,c). At intermediate concentrations around 75 mM both crystalline forms precipitated.

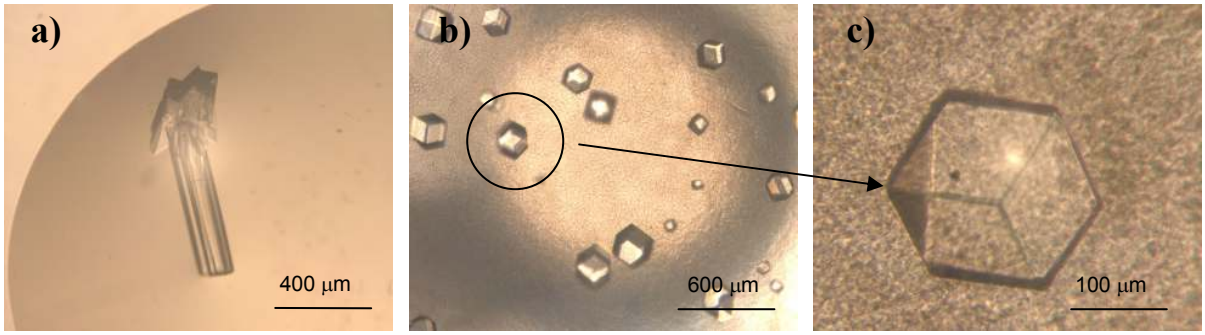

Figure 48. Optical micrographs of hUb crystals grown in the presence of (a) 75 mM $Zn(CH_3COO)_2$ and (b,c) 200 mM $Zn(CH_3COO)_2$.

Cd-hUb was crystallised using a precipitating solution composed of 25%(w/v) PEG 1450, 50mM HEPES pH 7.0 and 200mM $Cd(CH_3COO)_2$. Cubic crystals grew within two weeks (Fig. 49).

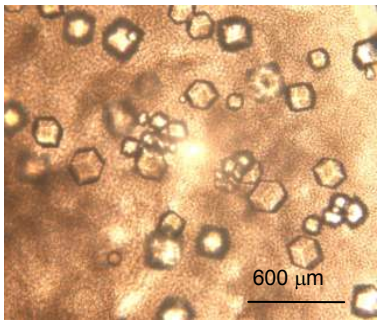

Figure 49. Optical micrographs of Cd-hUb crystals.

Crystals of native hUb were obtained in the presence of 30% (w/v) PEG 1450 in approximately 1 month (Fig. 50).

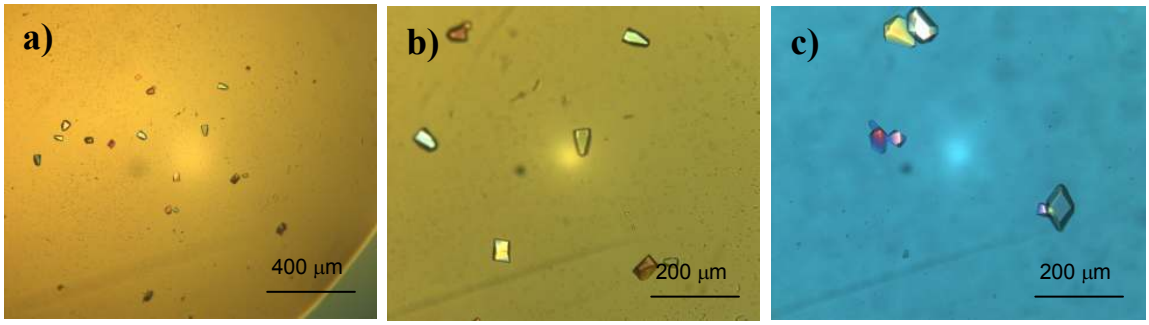

Figure 50. Optical micrographs of native hUb crystals.

Since any attempt of co-crystallisation cisPt-hUb or Cu-hUb failed, soaking experiments with native crystals grown in the absence of metal ions (the reservoir solution contained only PEG and the protein was dissolved in milliQ water) were tried. The hope was that cisPt or Cu(II) entered into crystals allowing to identify their binding site(s).

4.3 CRYSTALLOGRAPHIC STUDIES

4.3.1 Human Hah1: Since the crystallisation conditions of Hah1 have been reported in the literature (Wernimont *et al*., 2000), we were confident that Hah1 single crystals would be obtained. Although several crystallisation experiments were performed, no crystals were obtained neither of native protein nor of adducts with platinum. Currently, experiments have been performing to identify a reservoir solution that produces native crystals of Hah1 suitable for soaking experiments.

4.3.2 CopC: The crystals grown in the presence of Cu(II) were tested at Elettra (Trieste, Italy; beam line XRD1). They were soaked for two hours in a solution composed of 2.0 M ammonium sulphate, 10% (w/v) PEG 400, 6.65 mM Zeise's salts (protein-cisPt molar ratio 1:5) and positioned in the nitrogen stream at 100 K. Diffraction data were collected at Elettra (Trieste, Italy; beam line XRD1) and recorded at a wavelength of 1.0 Å, using an oscillation range of 1°, and a crystal-to-detector distance of 160 mm. The collected data have been elaborating to resolve the structure of the protein and verify if the platinum is entered in the crystal substituting the Cu(II) at the active site.

4.3.3 Human superoxide dismutase: A lot of crystals were tested at synchrotrons of Trieste (Elettra), Grenoble (ESRF) and Paris (Soleil). Although crystals , either of native protein or adducts with cisPt, diffracted at a good resolution (2-3Å), it was never possible to index the data.
Acrylamide gel electrophoresis revealed heterogeneity in their purity. A SOD1 modified form on Cys111 has been crystallised and the structure is under refinement.

4.3.4 Human ubiquitin: The crystallographic structures of ubiquitin and group-12 metal ions Zn(II), Cd(II), and Hg(II) have been resolved by X-ray crystallography (Falini *et al.*, 2008).
A single crystal of Hg-hUb was soaked for few seconds in a cryogenic solution composed of 25% (w/v) PEG 1450K, 2.92 mM $Hg(CH_3COO)_2$ and 20%(v/v) PEG 400 and positioned in the nitrogen stream at 100 K. Diffraction data were collected at Elettra (Trieste, Italy; beam line XRD1) and recorded at a wavelength of 1.2 Å, using an oscillation range of 1°, and a crystal-to-detector distance of 100 mm.
Prior to data collection Zn-hUb crystals were briefly transferred into a cryo-protectant solution (25% (w/v) PEG 1450, 200 mM or 25m M $Zn(CH_3COO)_2$, 15% (v/v) PEG 400). Data from Zn-hUb cubic and orthorhombic crystals were collected at Elettra (Trieste, Italy; beam line XRD1), at a wavelength of 1.0 Å, using an oscillation range of 1°, and a crystal-to-detector distance of 130 mm.

Cd-hUb data were collected from single crystals at 100 K at beam line ID21, ESFR (Grenoble, France) using a wavelength of 0.997 Å, an oscillation range of 1°, and a crystal-to-detector distance of 150mm.All data were processed and scaled using DENZO/SCALEPACK package (Otwinowski *et al.*, 1997) and the statistics are reported in Table 17.

The structure of orthorhombic Hg-hUb and orthorombic crystals of Zn-hUb were solved at 1.8 Å resolution. Cubic crystals of Zn-hUb adduct were also obtained in the presence of high concentration of Zn(II). They diffracted at the maximum resolution of 3.6 Å with cell parameters $a = b = c$= 105.143 Å. Data collection statistics gave R_{sym} = 0.154 and mosaicity equal to 1. These data did not allow a resolution of the structure with the required accuracy.

The crystal structure of Cd-hUb was solved at 3.0 Å resolution in a cubic form.

The structures were solved by molecular replacement, using the structure of native ubiquitin (1UBQ) as probe. The metal ions were added in the regions with high electronic density (contoured more than 5σ on the ($2F_o$ - F_c) map) in the electron density maps, having a distance from the protein donor atom(s) shorter than the sum of the Van der Waals radii and a correct geometry. The refinements were performed with CNS (Brunger *et al.*, 1998) with a starting σ cut-off on amplitudes of 2.0, which was later decreased to 0. A 5% of the total data was randomly selected for R_{free} calculations. The models were rebuilt with the graphic program XtalView (McRee, 1999). In the final stage of the refinement of Hg-hUb and Zn-hUb the solvent network was built. Water molecules were automatically added, and after a visual inspection they were conserved in the model only if contoured at 0.8σ on the ($2F_o$ - F_c) map and if they fell into an appropriate hydrogen bonding environment. Only few water molecules were manually added to the Cd-hUb structure. The high thermal factors of this structure (Table 18) with respect to those of Zn-hUb and Hg-hUb are probably due to the low data resolution and to an intrinsic crystal disorder enhanced by the high crystal symmetry. All the refinement statistics are listed in Table 18.

The Ramachandran plots of the solved structures, obtained using PROCHECK (Laskowski *et al.*, 1993), show the majority of the residues lying in the most favored and allowed regions, and the remaining in the additional allowed regions. The C-terminal region of the protein showed a high degree of disorder, only the amino acids clearly visible in the electron density maps were included in the structure and refined.

For Cu(II), the best results were obtained when native crystals were soaked for not more than 1 hour into a solution composed of 25% (w/v) PEG 1450, 50 mM HEPES pH 7.0, 7 mM Cu acetate (hUb-Cu(II) molar ratio 1:2). Data from one crystal were collected at Soleil (Paris, France, beamline PROXIMA1) and recorded at a wavelength of 1.377 Å, using an oscillation range of 1°, and a crystal-to-detector distance of 199 mm. Crystal diffracted at 2.0 Å. Data have been elaborating.

Table 17. Cell parameters and data collection statistics for ubiquitin crystallised in the presence of metal ions.

	Zn-hUb	**Cd-hUb**	**Hg-hUb**
Space group	$P2_12_12_1$	$P4_332$	$P2_12_12_1$
Unit cell *a*, *b* ,*c*, (Å)	44.36, 50.95, 93.32	105.253	28.02, 42.83, 50.37
N° molecules in a.u.	3	2	1
Resolution range*	32.5-1.8(1.84-1.80)	74.5-3.0 (3.1-3.0)	24.5-1.8 (1.85-1.80)
Measured reflections	70229	348 734	29 818
Unique reflections	19140	4357	5484
Completeness (%)*	94.8	100 (100)	93.7 (58.8)
Redundancy	3.7	80	5.4
R_{sym}*	0.114(0.513)	0.078 (0.70)	0.074 (0.162)
$I/\sigma(I)$*	11.7(1.3)	76.5 (10.4)	32.5 (15.0)

*Value in parenthesis refers to the last resolution shell

Table 18. Refinement statistics for ubiquitin crystallised in the presence of metal ions.

	Zn-hUb	**Cd-hUb**	**Hg-hUb**
No. protein atoms	1706	1166	575
No. metal atoms	1	12	1
No. water molecules	127	7	105
R (%)	22.2	27.9	23.5
R_{free} (%)	27.1	30.1	29.3
B mean (Å^2)	25.8	74.1	20.9
B (Wilson Plot, Å^2)	17.2	73.8	20.1
B protein atoms (Å^2)	24.0	74.3	19.3
B metal atoms (Å^2)	44.1	64.2	28.4
B solvent atoms (Å^2)	45.4	58.7	29.8
rmsd bond length (Å)	0.005	0.012	0.005
rmsd bond angles (°)	1.2	1.9	1.2

For the experiments with platinum, two soaking solutions were tested:
1) 25% (w/v) PEG 1450, 10% (v/v) glycerol, 1 mM cisPt (hUb-Pt molar ratio 1:0.5).
2) 30% (w/v) PEG1450, 50 mM HEPES pH 7.0, 7 mM Zeise's salts (hUb-Pt molar ratio 1:2.5).
Crystals were left into soaking solution in both cases 1 hour before to collect data.
Data were collected at Soleil (Paris, France, beamline PROXIMA1). For the crystal soaked into cisPt solution, data were recorded at a wavelength of 1.071 Å, using an oscillation range of 1°, and a crystal-to-detector distance of 120 mm. Orthorhombic primitive crystal diffracted at the maximum resolution of 2.0 Å with cell parameters a = 28.31, b =42.68, c= 50.82 Å. The structure of adducts has been resolving. Preliminary data suggest the possible presence of cisPt ions close to His68.
For the crystal soaked into Zeise's salts solution, data were recorded at a wavelength of 1.071 Å, using an oscillation range of 1°, and a crystal-to-detector distance of 195 mm. Crystal diffracted at the maximum resolution of 1.8 Å. At the status of art, those collect data have been not processed yet.

4.3.4.1 Characterisation of human ubiquitin-metals adducts: Crystals of hUb were grown in the presence of different concentrations of Zn(II), Cd(II) or Hg(II) acetate. Zn-hUb adducts crystallize in orthorhombic or cubic form depending upon the metal/protein molar ratio used (8:1 and 70:1, respectively). Crystallisation of a Cd-hUb adduct takes place only at high metal/protein molar ratio (70:1), while crystals of Hg-hUb were obtained only at very low Hg(II)/protein molar ratio (1:1).
The structure of orthorhombic Hg-hUb was solved at 1.8 Å resolution. The asymmetric unit contains one protein molecule and one Hg(II) ion. Inspection of the electron density maps shows other regions which could host metal ions with low occupancy factors (i.e. the fraction of sites occupied by metal ions) and high thermal factors, these ill-defined metal sites were not considered. His68 binds Hg(II) through NE2 of the imidazole ring. The metal ion completes its linear coordination geometry by binding NE2 of Gln31* of a symmetry-related molecule (Fig. 52a and Table 19). This site has an occupancy factor of 0.77 and the bond distances for Hg1–NE2 His68 and Hg1–NE2 Gln31* are 2.2 and 2.4 Å, respectively.
Orthorombic crystals of Zn-hUb (1.8 Å resolution) contain, in the asymmetric unit, three hUb molecules (A, B, and C) and one Zn(II) ion, which interacts with two protein molecules (A and B) by coordination to NE2 of His68 residues (Fig. 51B). This site has an occupancy factor of 0.50 and the bond distances for Zn–NE2 His68A and Zn–NE2 His68B are 2.5 and 2.4 Å, respectively. The Zn(II) ion interacts weakly also with two water molecules. His68 of the third protein molecule (C) in the asymmetric unit does not appear to have metal ions in its proximity.

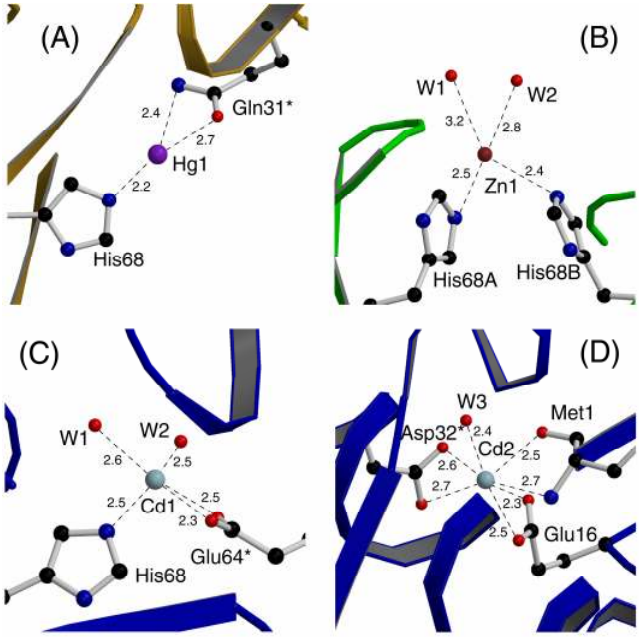

Figure 51. hUb metal binding sites Me1 **(A, B, C)** and Me2 **(D).** (**A**) Structure of the Hg-hUb adduct; (**B**) structure of the orthorhombic Zn-hUb adduct; (**C**, **D**) structure of the cubic Cd-hUb adduct. The distances are reported in Å.

The crystal structure of Cd-hUb has been solved at 3.0 Å resolution in a cubic form. In the asymmetric unit there are two protein molecules (A and B), each one interacting with several Cd(II) ions. The metal binding sites are the same for the two protein molecules, but the occupancy factors are different (Table 20). One cadmium ion (Cd1) is anchored to NE2 of His68 and completes its quasi-tetrahedral geometry by binding the carboxylate group of Glu64* of a symmetry-related protein molecule and two water molecules (Fig 51c). A second Cd(II) ion (Cd2) is anchored to the carboxylate group of Glu16, which undergoes a remarkable displacement from its position in native hUb (PDB code: 1UBQ (Vijay-Kumar *et al.*, 1987), Fig. 52a). Cd2 also binds the NH_2 and CO of Met1, the carboxylate group of Asp32* of a symmetry-related molecule, and a water molecule (Fig. 51d).

Binding of Cd2 appears to weaken the hydrogen bond between CO of Met1 and NH of Val17, the distance between these two groups increasing from 2.5 Å in the native form to 3.4 Å in the adduct (Fig. 52A); however, the local fold of hUb does not change significantly, due to the persistence of the hydrogen bond between NH_2 of Met1 and CO of Val17. Donor atoms for the third Cd(II) ion (Cd3) are the carboxylate oxygens of Glu18 and of Asp21* and Glu18* of a symmetry-related molecule (Fig. 52B).

Table 19. Metal ion – protein donor atom distances below 3.5 Å in the most relevant metal binding sites of hUb.

Me-hUb adduct	Metal ion sites	Chain A			Chain B		
		Protein residues		Dist. (Å)	Protein residues		Dist. (Å)
Hg-hUb	Hg1	His68	NE2	2.2			
		Gln31*	NE2	2.4			
		Gln31*	OE1	2.7			
Zn-hUb	Zn1	His68	NE2	2.5	His68	NE2	2.4
		W1	O	3.2			
		W2	O	2.8			
Cd-hUb	Cd1	Glu64	OE1	2.3	Glu64*	OE1	2.6
		Glu64	OE2	2.5	Glu64*	OE2	2.3
		His68*	NE2	2.5	His68	NE2	2.3
		W1		2.6			
		W2		2.5			
	Cd2	Glu16	OE1	2.5	Glu16	OE1	2.5
		Glu16	OE2	2.3	Glu16	OE2	2.4
		Asp32*	OD1	2.6	Asp32*	OD2	2.6
		Asp32*	OD2	2.7			
		Met1	NH	2.7	Met1	NH	2.8
		Met1	CO	2.5	Met1	CO	2.6
		W3		2.4	W5		2.3
	Cd3	Glu18	OE1	2.7	Glu18*	OE1	2.8
		Glu18	OE2	2.3	Glu18*	OE2	2.4
		Asp21*	OD1	2.6	Asp21	OD1	2.6
		Asp21*	OD2	2.6	Asp21	OD2	2.5
		Glu18*	OE1	2.7	W6		2.9
		W4		3.4	W7		2.5

*indicates that the residue belongs to a symmetric molecule

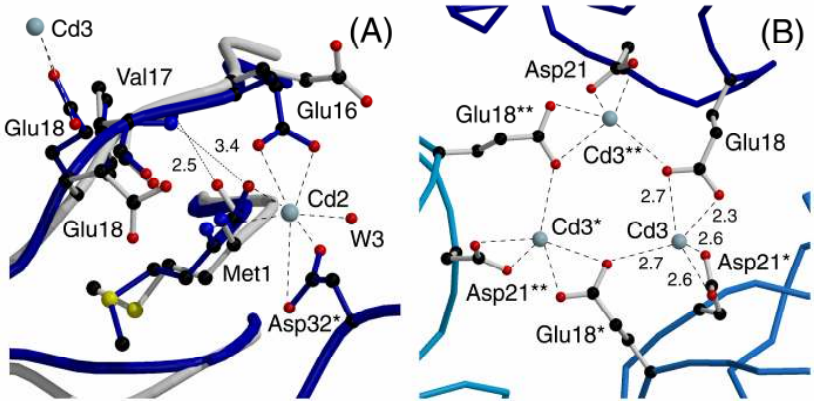

Figure 52. (**A**) Superposition of the structures of native hUb (white) and Cd-hUb (blue) in the region of the binding sites Cd2 and (only partially) Cd3. The interactions between the metal ions (Cd2 and Cd3) and donor atoms are indicated by dashed lines. The Met1 CO — Val17 NH and Met1 NH_2— Val17 CO interactions are indicated by dotted lines. (**B**) Cd3 metal binding sites in Cd-hUb. The three symmetry-related hUb molecules (coloured in different blue tones) are linked by a bond network involving three Cd2 and three Cd3 ions (light blue spheres).

Table 20. Occupancy and thermal factors of Hg(II), Zn(II), and Cd(II) ions in the binding sites of Me-hUb adducts.

Me-hUb adduct	Metal ion sites	Chain A		Chain B	
		occupancy factor*	thermal factor (B)	occupancy factor*	thermal factor (B)
Hg-hUb	Hg1	0.77	28.4		
Zn-hUb	Zn1	0.50	44.1		
Cd-hUb	Cd1	0.70	67.1	0.20	63.9
	Cd2	0.85	59.4	0.45	64.5
	Cd3	0.85	58.4	0.75	61.2

* Occupancy factor defines the fraction of crystallographic sites occupied by metal ions

Similarly to Glu16, also Glu18 undergoes a remarkable displacement from its position in native hUb (Fig. 52a). Cd2 and Cd3 bridge, in pairs, three protein molecules of different asymmetric units (Fig. 53a), thus playing a crucial role in the molecular packing. Other Cd(II) ions are localized on the protein surface and bound to carboxylate groups, however their occupancy factors are generally low.

Cubic crystals of Zn-hUb adduct were also obtained in the presence of high concentration of Zn(II). Unfortunately, their low quality prevented an accurate determination of the crystallographic structure which, however, appeared to be similar to that one of cubic Cd-hUb.

In general, the observed metal ion–protein donor atom distances are slightly larger than the average for

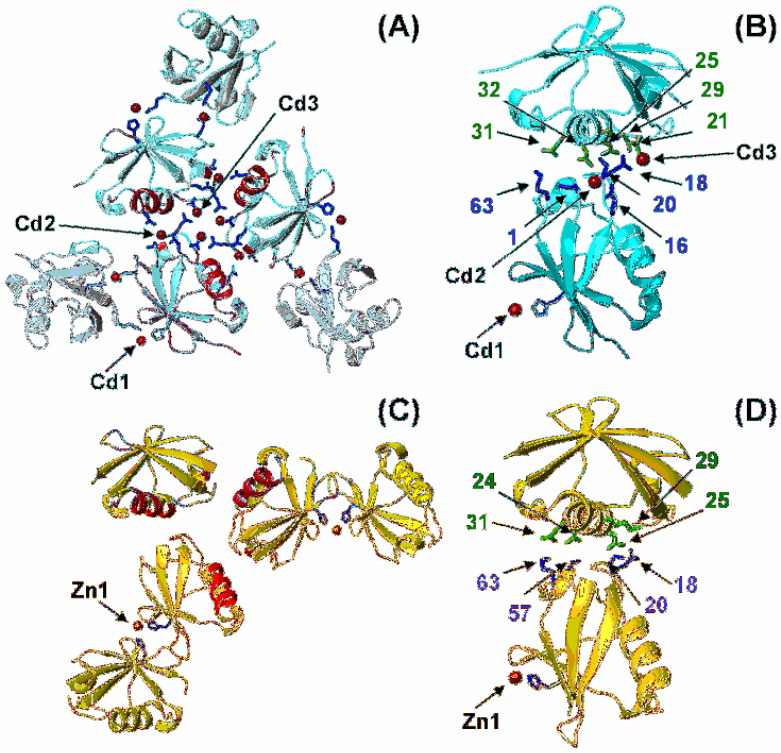

Figure 53. Packing of molecules in cubic Cd-hUb (A, B) and orthorhombic Zn-hUb (C, D) crystals. hUb molecules are coloured in cyan and yellow, respectively. In (A) and (B) hUb molecules forming one trimer are shown in more intense colour; Zn(II) or Cd(II) ions are shown as red spheres, while the Zn(II) or Cd(II) ligands are shown as blue sticks. Regions containing poorly wrapped backbone hydrogen bonds (*dehydrons*) are shown in red. Conserved contacts between two hUb molecules within the trimer are shown in detail in (B) and (D). Residues at the interface are shown as green and blue sticks and pointed out by arrows. The metal binding sites are indicated for one hUb molecule.

inorganic compounds. This is not unexpected since the donor atoms are linked to the protein frame and thus are more subject to spatial constraints.

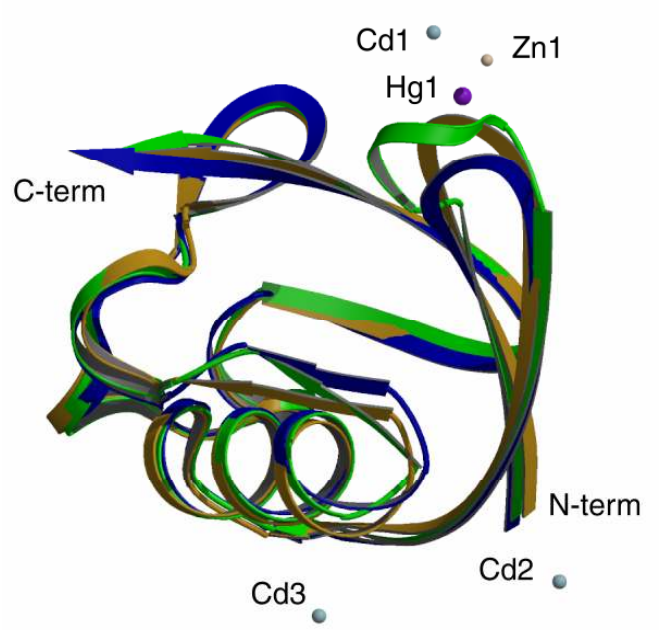

Figure 54. Superposition of the three Me-hUb adduct structures. Only the C□ trace of the protein molecules is shown in different colours. Zn-hUb is shown in green, Cd-hUb is shown in blue and Hg-hUb is shown in gold. Metal ions are shown as spheres of different colours: brown indicates Zn(II), light blue indicates Cd(II) and violet indicates Hg(II). The N-terminal (N-term) and C-terminal (C-term) regions of the protein are also indicated.

The three structures (superimposed in Fig. 54) allow a hierarchy among protein metallation sites to be established.

At low metal/protein ratio the surface exposed His68 appears to be the dominant anchoring site. By increasing the metal ion concentration, the carboxylate side chains of Glu16 and Glu18, located near the N-terminus of hUb, can also load a metal ion. Binding to His68 and to the N-terminus has been already observed, respectively, in a Ub variant crystallised in the presence of Cd(II) ions (Bang *et al.*, 2006) and in a Ub-like protein crystallised in the presence of Zn(II) ions (Rao *et al.*, 1998). His68 and Met1 are also the sites of copper ion binding. Specifically, Met1 was found to be the primary site of attack by Cu(II) ion, which attains a tetragonal geometry by coordinating the nitrogen of Met1 and three oxygen donor ligands (Milardi *et al.*, 2007). In contrast, when three copper coordination positions are held by a tridentate ligand (such as iminodiacetate, IDA), the imidazole nitrogen of His68 becomes the preferential site of attack (Nomura *et al.*, 2004).

Hg-hUb and Zn-hUb show preferential coordination to His68, thus resembling the hUb-Cu(IDA) system. It is most likely that, in the solid state, an adjacent hUb molecule plays a similar role like the IDA ligand in solution experiments, that is to provide additional donor atoms to the metal ion. Binding of Cu(II) to Met1 of hUb was shown to cause a destabilization of the protein, such a destabilization is not observed in the case of Cd(II) in agreement with previous calorimetric determinations (Milardi *et al.*, 2007) This could be a consequence of the different coordination mode of Cu(II) with respect to Cd(II). While Cu(II) is bound to a single hUb molecule, Cd(II) binds to Met1 and Glu16 of one hUb molecule and completes its coordination shell by binding to Asp32* of a symmetry-related molecule and to water molecules of crystallisation. Moreover, the coordination geometry of Cd(II) is generally tetrahedral or octahedral, but not tetragonal as for Cu(II). It is also worthnoting that, notwithstanding the several attempts, all trials to crystallize hUb

in the presence of copper were unsuccessful, even when using very small amounts of Cu(II). This could be a consequence of Cu(II) destabilizing the protein structure and hampering crystallisation.

At NMR studies, the primary binding of Cu(II) ions was identified to be a specific site at the N terminus of Ub, involving the Met1 nitrogen and three oxygen donor ligands in a tetragonal geometry (Milardi *et al.*, 2007). Potential oxygen donor ligands are Met1 and Val17 (carbonyl groups), and Glu16 and Glu18 (carboxylate groups). At physiological pH the N-terminal group ($pK_a \approx 9$) of uncomplexed Ub is completely protonated and Cu(II) has to compete strongly with protons for coordination to this site. Since the residues close to the N terminus are involved in the formation of a βstrand, Cu(II) binding may destabilize the protein starting from its N-terminal region. Furthermore, in native Ub, the first residue, Met1, is involved in two key hydrogen bonds (Vijay-Kumar *et al.*, 1987): one occurring between the N-terminal group and the CO of Val17 and the other between the side chain sulphur atom of Met1 and the amide NH of Lys3. Therefore Cu(II) binding to Ub might hamper the proteins' turnover and other in vivo signalling events regulated by Lys63-linked polyubiquitination (Pickart *et al.*, 2004; Eddins *et al.*, 2006).

The Cu(II) affinity of the primary site of Ub appears to be competitive with that of amyloidogenic proteins involved in prion, Alzheimer's, and Parkinson's diseases. In all cases the affinity is in the submicromolar range, a fact that may have important biological implications (Rasia *et al.*, 2005).

The analysis of molecular packing shows that, in cubic crystals of Cd-hUb, helix α1 (residues 23-31) of one hUb molecule packs against the N-terminal region of another molecule and comes in contact with residues 18-20 (located in the loop between β2 and α1) and with the side chain of Lys63. Each of the two hUb molecules, in turn, establishes complementary contacts with a third molecule, thus giving rise to a symmetric trimer stabilized by three Cd2 and three Cd3 ions (Fig. 53a).

Interestingly, a similar trimeric arrangement of hUb molecules is also found in orthorombic crystals of Zn-hUb, where Me2 and Me3 ions are missing, thus suggesting that such an intermolecular interaction involving helix α1 of one hUb and the N-terminal region of another hUb does not necessarily require support from metal ions (Fig. 53c).

Instead, a series of electrostatic intermolecular interactions (H-bonds and salt bridges) are established (Glu18/Lys29, Ser20/Asn25, Ser57/Glu24, and Lys63/Gln31; Fig. 53b and d). Helix α1 of native hUb contains a large number of poorly wrapped backbone hydrogen bonds (Fernandez *et al.*, 2007) called dehydrons, which are generally correlated to the aggregation propensity of a protein (Fernandez *et al.*, 2003). Mapping on the Zn-hUb and Cd-hUb structures reveals that dehydrons are clustered in the core of the trimer (Fig. 53a and c). Therefore, such "structural defects" in isolated hUb molecules may be partially offset in the crystals by intermolecular

interactions at the trimeric core. From this analysis it is also inferred that bridging metal ions may enhance the aggregation propensity of surface regions of hUb, thus shifting the equilibrium towards the formation of oligomeric species.

In conclusion, we have shown that hUb can bind group 12 metal ions at different sites, His68, Glu16/Met1, and Glu18 being, in the given order, the preferred anchoring residues. Metal binding to the second and third site causes a polymorphic transition and stabilizes a trimeric arrangement of hUb molecules characterized by the clustering of dehydrons.

4.4 REFERENCES

- Anastassopoulou, A., Banci, L., Bertini, I., Cantini, F., Katsari, E., Rosato, A. Solution structure of the apo and copper(I)-loaded human metallochaperone HAH1. (2004) *Biochem.* **43,** 13046-13053.
- Andrews, P.A., Howell, S.B. Cellular pharmacology of DDT: perspectives on mechanisms of acquired resistance. (1990) *Cancer Cells* **2**, 35-43.
- Arnesano, F., Banci, L., Bertini, I., Huffman, D.L., O'Halloran, T.V. Solution structure of the Cu(I) and apo forms of the yeast metallochaperone, Atx1. (2001) *Biochem.* **40**, 1528-1539.
- Arnesano, F., Banci, L., Bertini, I., Thompsett, A.R. Solution structure of CopC: a cupredoxin-like protein involved in copper homeostasis. (2002) *Structure* **10,** 1337-1347.
- Arnesano, F., Banci, L., Bertini, I., Mangani, S., Thompsett, A.R. A redox switch in CopC: An intriguing copper trafficking protein that binds copper(I) and copper(II) at different sites. (2003) *PNAS* **100(7)**, 3814-3819.
- Arnesano, F., Banci, L., Bertini, I., Bonvin, A.M.J.J. A docking approach to the study of copper trafficking proteins: Interaction between metallochaperones and soluble domains of copper ATPases. (2004) *Struct.* **12**, 669-676.
- Arnesano, F., Banci, L., Bertini, I., Ciofi-Baffoni, S. Perspectives in inorganic structural genomics: a trafficking route for copper. (2004) *Eur. J. Inorg. Chem.*, 1583-1593.
- Bang, D., Gribenko, A.V., Tereshko, V., Kossiakoff, A.A., Kent S.B., Makhatadze, G.I. Dissecting the energetics of protein α-helix C-cap termination through chemical protein synthesis. (2006) *Nat. Chem. Biol.* **2**, 139-143.
- Barra, D., Martini, F., Bannister, J.V., Schinina, M.E., Rotilio, G., Bannister, W.H., Bossa, F. The complete amino acid sequence of human Cu/Zn superoxide dismutase. (1980) *FEBS Lett.* **120,** 53-56.
- Benítez-Cardoza, C.G., Stott, K., Hirshberg, M., Went, H.M., Woolfson, D.N., Jackson, S.E. Exploring sequence/folding space: folding studies on multiple hydrophobic core mutants of ubiquitin. (2004) *Biochem.* **43(18)**, 5195-5203.
- Brown, N.L., Lee, B.T.O., Silver, S. Bacterial transport of and resistance to copper. (1994) In *Metal Ions in Biological Systems* **30**, ed. H Sigel, A Sigel. New York: Dekker, 405-434.
- Brown, N.L., Barrett, S.R., Camakaris, J., Lee, B.T.O., Rouch, D.A. Molecular genetics and transport analysis of the copper-resistance determinant (*pco*) from *Escherichia coli* plasmid pRJ1004. (1995) *Mol. Microbiol.* **17**, 1153-1166.
- Brünger, A.T., Adams, P.D., Clore, G.M., DeLano, W.L., Gros, P., Grosse-Kunstleve, R.W., Jiang, J.S., Kuszewski, J., Nilges, N., Pannu, N.S., Read, R.J., Rice, L.M., Simonson, T., Warren, G.L. Crystallography and NMR system: a new software suite for macromolecular structure determination. (1998) *Acta Crystallogr. Sect. D: Biol. Crystallogr.* **54**, 905-921.

- Burdette, S.C., Lippard, S.J. Meeting of the minds: Metalloneurochemistry. (2003) *Proc. Natl. Acad. Sci. U.S.A* **100**, 3605-3610.
- Calderone, V., Casini, A., Mangani, S., Messori, L., Orioli, P.L. Structural investigation of cisplatin-protein interactions: selective platination of His19 in a cuprozinc superoxide dismutase**.** (2006) *Angew. Chem. Int. Ed Engl.* **45(8)**, 1267-1269.
- Carrico, R.J., Deutsch, H.F. The presence of zinc in human cytocuprein and. some properties of the apoprotein. (1970) *J. Biol. Chem.* **245,** 723-727.
- Cha, J.S., Cooksey, D.A. Copper resistance in Pseudomonas syringae mediated by periplasmic and outer membrane proteins. (1991) *PNAS* **88(20)**, 8915-8919.
- Ciechanover, A., Brundin, P. The ubiquitin protease system in neurodegenerative dieases. Sometimes the chicken, sometimes the egg. (2003) *Neuron* **40**, 427-446.
- Cook, W.J., Suddath, F.L., Bugg, C.E., Goldstein, G. Crystallisation and preliminary x-ray investigation of ubiquitin, a non-histone chromosomal protein. (1979) *J. Mol. Biol.* **130(3)**, 353-355.
- Cooksey, D.A. Copper uptake and resistance in bacteria. (1993) *Mol. Microbiol.* **7**, 1-5.
- Cooksey, D.A. Molecular mechanisms of copper resistance and accumulation in bacteria. (1994) *FEMS Microbiol Rev.* **14(4)**, 381-386.
- Culotta, V.C., Lin, S.J., Schmidt, P., Klomp, L.W., Casareno, R.L., Gitlin, J. Intracellular pathways of copper trafficking in yeast and humans. (1999) *Adv Exp Med Biol* **448,** 247-254.
- DeConti, R.C., Toftness, B.R., Lange, R.C., Creasey, W.A. Clinical and Pharmacological Studies with *cis*-Diamminedichloroplatinum(II). (1973) *Cancer Research* **33**, 1310-1315.
- DiDonato, M., Craig, L., Huff, M.E., Thayer, M.M., Cardoso, R.M., Kassmann, C.J., Lo, T.P., Bruns, C.K., Powers, E.T., Kelly, J.W., Getzoff, E.D., Tainer, J.A. ALS mutants of human superoxide dismutase form fibrous aggregates via framework destabilization. (2003) *J. Mol. Biol.* **332(3)**, 601-615.
- Di Stefano, D.L., Wand, A.J. Two-dimensional 1H NMR study of human ubiquitin: at main-chain directed assignment and structure analysis. (1987) *Biochem.* **26**, 7272-7281.
- Eddins, M.J., Carlile, C.M., Gomez, K.M., Pickart, C.M., Wolberger, C. Mms2/Ubc13 covalently bound to ubiquitin: structural basis of linkage-specific polyubiquitin chain formation. (2006) *Nat. Struct. Mol. Biol.* **13**, 915-920.
- Espinosa, E., Feliu, J., Zamora, P., Baron, M.G., Sanchez, J.J., Ordonez, A., Espinosa, J. Serum albumin and other prognostic factors related to response and survival in patients with advanced non-small cell lung cancer. (1995) *Lung. Cancer* **12(1)**, 67-76.
- Falini, G., Fermani, S., Tosi, G., Arnesano, F., Natile, G. Structural probing of Zn(II), Cd(II) and Hg(II) binding to human ubiquitin. (2008) *Chem. Commun.*, 5960-5962.
- Fernandez, A., Kardos, J., Scott, L.R., Goto, Y., Berry, R.S. Structural defects and the diagnosis of amyloidogenic propensity. (2003) *Pro.c Natl. Acad. Sci. U.S.A* **100**, 6446-6451.
- Fernandez, A., Chen, J., Crespo, A. Solvent-exposed backbone loosens the hydration shell of soluble folded proteins. (2007) *J. Chem. Phys.* **126,** 245103.

- Fink, D., Aebi, S., Howell, S.B. The role of DNA mismatchrepair in drug resistance. (1998) *Clin. Cancer Res.* **4**, 1-5.
- Fink, R.C., Scandaliios, J.G. Molecular evolution and structure–function relationships of the superoxide dismutase gene families in angiosperms and their relationship to other eukaryotic and prokaryotic superoxide dismutases. (2002) *Arch. Biochem. Biophys.* **399,** 19-36.
- Fridovich, I. Superoxide dismutase. (1975) *Annu. Rev. Biochem.* **44**, 147-159.
- Fujiwara, N., Nakano, M., Kato, S., Yoshihara, D., Ookawara, T., Eguchi, H., Taniguchi, N., Suzuki, K. Oxidative modification to cysteine sulfonic acid of Cys^{111} in human copper-zinc superoxide dismutase. (2007) *Biol. Chem.* **282(49),** 35933-35944.
- Galanski, M., Arion, V.B., Jakupec, M.A., Keppler, B.K. Recent developments in the field of tumor-inhibiting metal complexes. (2003) *Curr. Pharm. Des.* **9**, 2078-2089.
- Getzoff, E.D., Tainer, J.A., Weiner, P.K., Kollman, P.A., Richardson, J.S., Richardson, D.C. Electrostatic recognition between superoxide and copper, zinc superoxide dismutase. (1983) *Nature* **306**, 287-290.
- Hallewell, R.A., Masiarz, F.R., Najarian, R.C., Puma, J. P., Quiroga, M.R., Randolph, A., Sanchez-Pescador, R., Scandella, C.J., Smith, B., Steimer, K.S., Mullenbach, G.T. Human Cu/Zn superoxide dismutase cDNA: isolation of clones synthesising high levels of active or inactive enzyme from an expression library. (1985) *Nucleic Acids Res.* **13,** 2017-2034.
- Hallewell, R.A., Mills, R., Tekarmp-Olson, R.P., Blacher, R., Rosenbar, S., Ottng, F., Scandella, D.J. Amino terminal acetylation of authentic human Cu,Zn-superoxide dismutase produced in yeast. (1987) *Biotechnol.* **5**, 363-366.
- Hershko, A., Ciechanover, A. The ubiquitin system. (1998) *Annu. Rev. Biochem*. **67**, 425-479.
- Huffman, D.L., O'Halloran, T.V. Function, structure, and mechanism of intracellular copper trafficking proteins. (2001) *Annu. Rev. Biochem.* **70**, 677-701.
- Hodgson, E.K., Fridovich, I. The interaction of bovine erythrocyte superoxide dismutase with hydrogen peroxide: chemiluminescence and peroxidation. (1975) *Biochem.* **14,** 5299-5303.
- Hung, I.H., Casareno, Ruby, L.B., Labesse, G., Mathews, F.S., Gitlin, J.D. HAH1 is a copper-binding protein with distinct amino acid residues mediating copper homeostasis and antioxidant defense. (1998) **273(3)**, 1749-1754.
- Igumenova, T.I, Wand, A.J., McDermott, A.E. Assignment of the backbone resonances for microcrystalline ubiquitin. (2004) *J. Am. Chem. Soc.* **126(16)**, 5323-5331.
- Jackson, S.E. Ubiquitin: a small protein folding paradigm. (2006) *Org. Biomol. Chem*., **4**, 1845-1853.
- Johnson, S.W., Laub, P.B., Beesley, J.S., Ozols, R.F., Hamilton, T.C. Increased platinum-DNA damage tolerance is associated with DDT resistance and cross-resistance to various chemotherapeutic agents in unrelated human ovarian cancer cell lines. (1997) *Cancer Res.* **57,** 850-856.

- Katano, K., Kondo, A., Safaei, R., Holzer, A., Samimi, G., Mishima, M., Kuo, Y.M., Rochdi, M., Howell, S. Acquisition of resistance to cisplatin is accompanied by changes in the cellular pharmacology of copper. (2002) *Cancer Res.* **62**, 6559-6565.
- Katano, K., Safaei, R., Samimi, G., Holzer, A., Rochdi, M., Howell, S.B. The copper export pump ATP7B modulates the cellular pharmacology of carboplatin in ovarian carcinoma cells. (2003) *Mol. Pharmacol.* **64,** 466-473.
- Larin, D, Mekios, C, Das, K, Ross, B, Yang, A, Gilliam, T.C. Characterisation of the interaction between the Wilson and Menkes disease proteins and the cytoplasmic copper chaperone, HAH1. (1999) *J Biol Chem.* **274**, 28497-28504.
- Laskowski, R.A., MacArthur, M.W., Moss, D.S., Thornton, J.M. PROCHECK: A program to check the stereo chemical quality of protein structure. (1993) *J. Appl. Crystallogr.* **26**, 283-291.
- Lee, Y.A., Hendson, M., Panopoulus, N.J., Schroth, M.N. Molecular cloning, chromosomal mapping, and sequence analysis of copper resistance genes from *Xanthomonas campestris* pv. juglandis: homology with blue copper proteins and multicopper oxidase. (1994) *J. Bacteriol.* **176**, 173-188.
- Liu, J., Dutta, S.J., Stemmler, A.J., Mitra, B. Metal-binding affinity of the transmembrane site in ZntA: implications for metal selectivity. (2006) *Biochem.* **45,** 763-772.
- Martin, R.W., Zilm, K.W. Preparation of protein nanocrystals and their characterisation by solid state NMR. (2003) *J. Magn. Reson.* **165(1)**, 162-174.
- McRee, D.E. XtalView/Xfit-A versatile program for manipulating atomic coordinates and electron density. (1999) *J. Struct. Biol.* **125**, 156-165.
- Milardi, D., Arnesano, F., Grasso, G., Magri, A., Tabbi, G., Scintilla, S., Natile, G., Rizzarelli, E. Ubiquitin stability and the Lys63-linked polyubiquitination site are compromised on copper binding. (2007) *Angew. Chem. Int. Ed Engl.* **46**, 7993-7995.
- Mills, S.D., Jasalavich, C.A., Cooksey, D.A. A two-component regulatory system required for copper-inducible expression of the copper resistance operon of *Pseudomonas syringae*. (1993) *J. Bacteriol.* **175(6)**, 1656-1664.
- Nomura, M., Kobayashi, T., Kohno, T., Fujiwara, K., Tenno, T., Shirakawa, M., Ishizaki, I., Yamamoto, K., Matsuyama, T., Mishima, M., Kojima, C. Paramagnetic NMR study of Cu(2+)-IDA complex localization on a protein surface and its application to elucidate long distance information. (2004) *FEBS Lett*. **566**, 157-161.
- Otwinowski, Z., Minor, W. Processing of X-ray diffraction data collected in oscillation mode. (1997) *Methods Enzymol.* **276**, 307-326.
- Parge, H.E., Getzoff, E.D., Scandella, C.S., Hallewell, R.A., Tainer, J.A. Crystallographic characterisation of recombinant human CuZn superoxide dismutase. (1986) **261(34),** 16215-16218.
- Parge, H.E., Hallewell, R.A., Tainer, J.A. Atomic structures of wild-type and thermostable mutant recombinant human Cu,Zn superoxide dismutase. (1992) *Proc. Natl. Acad. Sci. U. S. A.* **89,** 6109-6113.

- Perez, R.P., Hamilton, T.C., Ozols, R.F., Young, R.C. Mechanisms and modulation of resistance to chemotherapy in ovarian cancer. (1993) *Cancer (Phila.)* **71**, 1571-1580.
- Pickart, C.M., Fushman, D. Polyubiquitin chains: polymeric protein signals**.** (2004) *Curr. Opin. Chem. Biol*. **8**, 610-616.
- Rakhit, R., Chakrabartty, A. Structure, folding, and misfolding of Cu,Zn superoxide dismutase in amyotrophic lateral sclerosis. (2006) *Biochim. Biophys. Acta Mol. Basis Dis.* **1762(11-12)**, 1025-1037.
- Rao-Naik, C., DelaCruz, W., Laplaza, J.M., Tan, S., Callis, J., Fisher, A.J. The rub family of ubiquitin-like proteins crystal structure of Arabidopsis rub1 and expression of multiple rubs in Arabidopsis. (1998) *J. Biol. Chem.* **273**, 34976-34982.
- Rasia, R.M., Bertoncini, C.W., Marsh, D., Hoyer, W., Cherny, D., Zweckstetter, M., Griesinger, C., Jovin, T.M., Fernández, C.O. Structural characterisation of copper(II) binding to alpha-synuclein: Insights into the bioinorganic chemistry of Parkinson's disease. (2005) *Proc. Natl. Acad. Sci. USA* **102**, 4294-4299.
- Rosenberg, B. In *Cisplatin. Chemistry and Biochemistry of a Leading Anticancer Drug*; Lippert, B., Ed.; Helvetica Chimica Acta: Zu¨rich, 1999.
- Rosenzweig, A.C. Copper delivery by metallochaperone proteins. (2001) *Acc Chem Res.* **34,** 119-128.
- Safaei, R., Howell, S.B. Copper transporters regulate the cellular pharmacology and sensitivity to Pt drugs. (2005) *Crit. Rev. Oncol. Hematol*. **53(1)**, 13-23.
- Safaei, R., Otani, S., Larson, B.J., Rasmussen, M.L., Howell, S.B. Transport of Cisplatin by the Copper Efflux Transporter ATP7B. (2008) *Mol. Pharmacol.* **73**, 461-468.
- Samimi, G., Varki, N.M., Wilczynski, S., Safaei, R., Alberts, D.S., Howell, S.B. Increase in expression of the copper transporter ATP7A during platinum drug-based treatment is associated with poor survival in ovarian cancer patients. (2003) *Clin. Cancer Res.* **9**, 5853-5859.
- Samimi, G., Safaei, R., Katano, K., Holzer, A.K., Rochdi, M., Tomioka, M., Goodman, M., Howell, S.B. Increased expression of the copper efflux transporter ATP7A mediates resistance to DDT, carboplatin, and oxaliplatin in ovarian cancer cells. (2004) *Clin. Cancer Res.* **10(14)**, 4661-4669.
- Samimi, G., Katano, K., Holzer, A.K., Safaei, R., Howell, S.B. Modulation of the cellular pharmacology of cisplatin and its analogs by the copper exporters ATP7A and ATP7B. (2004) *Mol. Pharmacol.* **66,** 25-32.
- Sigel, A., Sigel, H., R.K.O., Sigel (editors). Neurodegenerative diseases and metal ions: Metal ions in life sciences. (2006) ed. Wiley **Vol. 1**, 1-488.
- Strange, R.W., Antonyuk, S., Hough, M.A., Doucette, P.A., Rodriguez, J.A., Hart, P.J., Hayward, L.J., Valentine, J.S., Hasnain, S.S. The structure of holo and metal-deficient wild-type human Cu, Zn superoxide dismutase and its relevance to familial amyotrophic lateral sclerosis**.** (2003) *J. Mol. Biol.* **328(4)**, 877-891.

- Strange, R.W., Antonyuk, S.V., Hough, M.A., Doucette, P.A., Valentine, J.S., Hasnain, S.S. Variable metallation of human superoxide dismutase: atomic resolution crystal structures of Cu-Zn, Zn-Zn and as-isolated wild-type enzymes. (2006) *J. Mol. Biol.* **356(5)**, 1152-1162.
- Tainer, J.A., Getzoff, E.D., Beem, K.M., Richardson, J.S., Richardson, D.C. Determination and analysis of the 2 Å structure of copper, zinc superoxide dismutase. (1982) *J. Mol. Biol.* **160,** 181-217.
- Timerbaev, A.R., Hartinger, C.G., Aleksenko, S.S., Keppler, B.K. Interactions of antitumor metallodrugs with serum proteins: Advances in characterisation using modern analytical methodology. (2006) *Chem. Rev.* **106(6)**, 2224-2248.
- Tottey, S., Harvie, D.R., Robinson, N.J. Understanding how cells allocate metals using metal sensors and metallochaperones (2005) *Acc. Chem. Res.* **38**, 775-783.
- Valentine, J.S., Pantoliano, M.W. Protein-metal ion interactions in cuprozinc protein (Superoxide Dismutase) (1981), 291−358. *In: Copper proteins*, **Vol**. **III**. Spiro, T. G. (ed.), John Wiley & Sons, NY.
- Valko, M., Morris, H., Cronin, M.T. Metals, toxicity and oxidative stress. (2005) *Curr. Med. Chem*. **12**, 1161-1208.
- Vijay-Kumar, S., Bugg, C.E., Cook, W.J. Structure of ubiquitin refined at 1.8 A resolution**.** (1987) *J. Mol. Biol.* **194**, 531-544.
- Vijay-Kumar, S., Bugg, C.E., Wilkinson, K.D., Vierstra, R.D., Hatfield, P.M., Cook, W.J. Comparison of the three-dimensional structures of human, yeast, and oat ubiquitin. (1987) *J. Biol. Chem.* **262**, 6396-6399.
- Wernimont, A.K., Huffman, D.L., Lamb, A.L., O'Halloran, T.V., Rosenzweig, A.C. Structural Basis for copper transfer by the metallochaperone for the Menkes/Wilson disease proteins. (2000) *Nat. Struct. Biol.* **7**, 766-771.
- Wong, E., Giandomenico, C.M. Current status of platinum-based antitumor drugs. (1999) *Chem. Re*v. **99**, 2451-2466.
- Zhang, L., Koay, M., Maher, M.J., Xiao, Z., Wedd, A.G. Intermolecular transfer of copper ions from the CopC protein of *Pseudomonas syringae*. Crystal structures of fully loaded Cu(I)Cu(II) forms. (2006) *J. Am. Chem. Soc.* **128**, 5834-5850.

CURRICULUM VITAE

Giovanna Tosi was born in Bologna in 1979. In 2004 she got her degree in Biology *cum laude* from the University of Bologna discussing a thesis on the theme "Crystalline Structure of Ribosome Inactivating Proteins" (adviser Prof. N. Roveri). Since 2005 her research activity is mainly addressed in the design and developing of nucleant surfaces and substrates able to control and favor the crystallization of biological macromolecules. Since 2007, in order to do it, she has been collaborating with the Spanish group of Prof. JM Garzia Ruiz (Granada). In January 2006 she has begun her PhD in Chemistry in the Chemistry Department of Bologna University with the project "Macromolecular Crystallography: Crystallisation and Structural Determination". She is focalizing her activity on the crystallography studies of different proteins, ribosome-inactivating proteins (RIPs) extracted from plants, amelogenin (major protein involved in enamel eukaryotes formation), crystallization of biological macromolecules using engineered surfaces and structural studies of adducts between macromolecules involved in copper trafficking and platinum based anti-cancer drugs.

The research activities of Giovanna Tosi is carried out through the use of several experimental techniques. She has had access to sources of synchrotron light (in Trieste, Grenoble and Paris) for the study by X-ray diffraction of the crystalline structure of biological macromolecules.

She has attended several national and international conferences and in the International School on Biological Crystallization held in Granada (Spain) in 2006, she won the prize for the best poster. She is co-author of several papers published on international scientific journals (see following list).

LIST OF PUBLICATIONS

1. Simona Fermani, Giuseppe Falini, Alberto Ripamonti, Giovanna Tosi, Francesca Sparla, Paolo Pupillo, Paolo Trost**. "The crystal structure of photosynthetic A_2B_2-glyceraldehyde-3-phosphate dehydrogenase discloses the mechanism of thioredoxin regulation"**. (2007) *Elettra highlights* 2006-07, 30-31.

2. Giuseppe Falini, Giovanna Tosi, Simona Fermani, Norberto Roveri. **"Influence on the SBA-3 structure by alkaline or alkaline earth ions"**. (2008) *Chem Lett.* 37(4), 414-5. doi:10.1246/cl.2008.414.

3. Giovanna Tosi, Simona Fermani, Giuseppe Falini, Jose Antonio Gavira Gallardo, Juan Manuel Garcia Ruiz. "**Crystallisation of proteins on functionalised surfaces**". (2008) *Acta Cryst. D* 64 (10), 1054-1061. doi:10.1107/S0907444908025079.

4. Giuseppe Falini, Simona Fermani, Giovanna Tosi, Fabio Arnesano, Giovanni Natile. **"Probing Zn(II), Cd(II) and Hg(II) Binding to Human Ubiquitin"**. (2008) *Chem. Comm.* 5960-5962. doi: 10.1039/b813463d.

5. Giuseppe Falini, Simona Fermani, Giovanna Tosi, Enrico Dinelli. **"Calcium carbonate morphology and structure in the presence of sea water ions and humic acids".** (2009) *Cryst.Growth Des.* In press.

6. Simona Fermani, Giovanna Tosi, Valentina Farini, Letizia Polito, Giuseppe Falini, Alberto Ripamonti, Norberto Roveri, Luigi Barbieri, Angela Chambery, and Andrea Bolognesi. **"Structure/function studies on two type 1 Ribosome Inactivating Proteins"**. (2009) *J. Struct. Biol.* Submitted.

7. Giovanna Tosi, Simona Fermani, Giuseppe Falini, Jose Antonio Gavira Gallardo, Juan Manuel Garcia Ruiz. **"Merging strategies in proteins crystallisation: functionalised surfaces in the crystallisation mushroom"**. (2009) *Cryst. Growth Des.* Submitted.

APPENDIX

During her PhD, Giovanna Tosi has collaborated in research regarding the study of biomineralization processes. These collaboration is documented by the following articles:

1. Giuseppe Falini, Giovanna Tosi, Simona Fermani and Norberto Roveri
"Influence on the SBA-3 Structure by Alkaline or Alkaline Earth"
Chem. Lett. **37(4)**, 414-415. (2008)

Alkaline and alkaline earth cations have been used in the synthesis of SBA-3, a silica mesoporous materials. These cations can not substitute silicon in the silica structure. However, we found that SBA-3 surface area, pore size and thickness, periodic order and microporosity were affected by the presence of lithium, magnesium or calcium ions. Chemical interactions among these ions and silica species are supposed to occur on the SBA-3 pore surface.

2. Giuseppe Falini, Simona Fermani, Giovanna Tosi, Enrico Dinelli.
Cryst. Growth Des., cg-2008-002959.R1. (2009)
"Calcium carbonate morphology and structure in the presence of sea water ions and humic acids"
The effectiveness of some sea water components, such as magnesium, potassium, sodium, sulphate and chloride ions and humic acid, in the control of calcium carbonate composition, morphology and phase distribution has been studied. These components were tested singularly, in pairs and all together. It has been observed that magnesium ions phase distribution control is influenced by the presence of other ions and that in the presence of high content of magnesium ions monohydrocalcite precipitates. Moreover, in the presence of magnesium or potassium ions the calcite crystals show modified rhomohedral morphologies, while the presence of sulphate ions favours their aggregation. Humic acids have an inhibition effect on calcium carbonate precipitation, induce the formation of empty spheres of vaterite and modify the calcium carbonate phase distribution. The isomorphic substitution of magnesium to calcium in the calcite structure is favoured by some sea water ions and

KNOWLEDGMENTS:

Sono molte le persone che devo ringraziare per aver creduto in me e per avermi sostenuto in questa "avventura". Vorrei ringraziare il Prof. Norberto Roveri, mio relatore di tesi. Un sentito ringraziamento va al Prof. Alberto Ripamonti i cui consigli sono stati un prezioso sostegno ed un valido aiuto scientifico.

Ma le persone a cui devo di più sono due: il Prof. Giuseppe Falini e la Dott.ssa Simona Fermani. Mi hanno spronato giorno dopo giorno a migliorare, a crescere professionalmente, consigliandomi costantemente. Col Prof. Falini l'interazione non è sempre stata delle più facili essendo lui una persona che pretende moltissimo da chi gli sta accanto. Devo ringraziarlo per la rigidità e la severità con cui talune volte mi ha trattata perché mi hanno incoraggiata a non accontentarmi mai ed a cercare di raggiungere livelli sempre più alti. Simona mi ha insegnato tutto ciò che so, ma sinceramente la cosa più preziosa che mi ha dato in questi anno è stata un'amicizia che va oltre l'essere colleghi.

I would like to express my deep gratitude to Prof. Garcia Ruiz who has contributed to the develop of a part of this thesis.

I extremely thank Dr. José Antonio Gavira Gallardo, Dr. Jaime Gómez Morales, Dr. Luis Antonio González Ramírez, Dr. María Angeles Hernández y Hernández, Dr. Alexander Van Driessche and all the other people of the Spanish group for making my stay in their laboratory a wonderful and fruitful experience (at the same time both scientific and human).

Un grazie di cuore a tutti coloro che in questi anni mi hanno aiutata, sopportata ed incoraggiata.